AD-A135 836 DEVELOPMENT OF A STRESS-DEPENDENT FINITE ELEMENT SLAB MODEL(U ILLINOIS UNIV AT URBANA DEPT OF CIVIL ENGINEERING M R THOMPSON ET AL. MAY 83 1/2

UNCLASSIFIED AFOSR-TR-83-1061 AFOSR-82-0143 F/G 13/2 NL

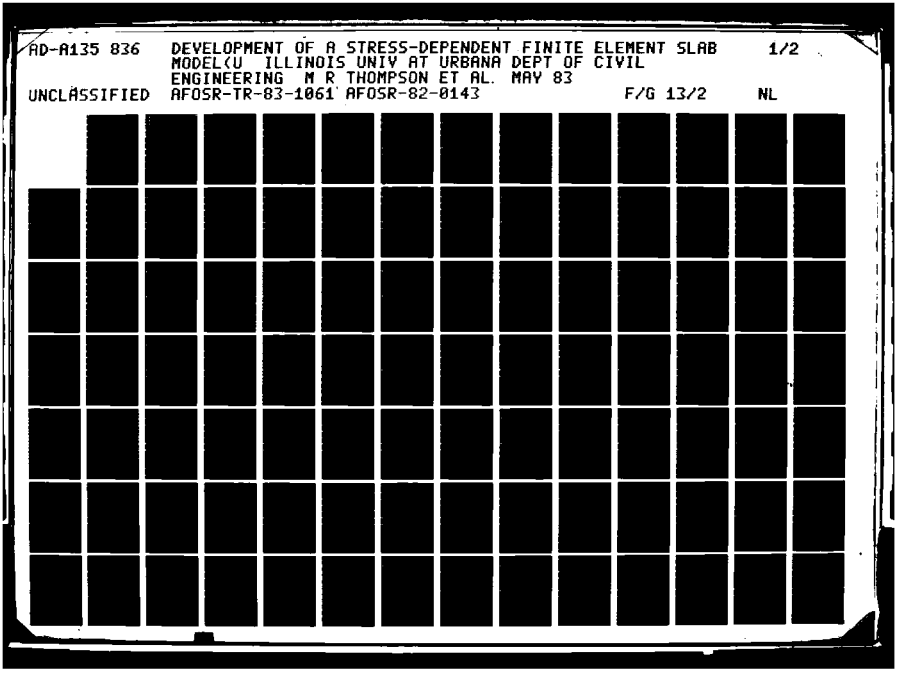

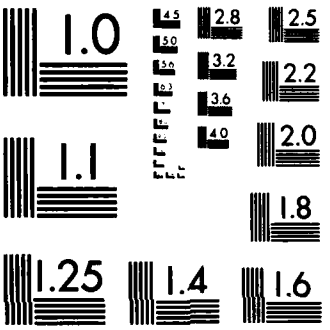

MICROCOPY RESOLUTION TEST CHART
NATIONAL BUREAU OF STANDARDS-1963-A

DEVELOPMENT OF A STRESS-DEPENDENT FINITE ELEMENT SLAB MODEL

(AFOSR-82-0143)

Submitted to

Air Force Office of Scientific Research (AFOSR)
Air Force Systems Command
United States Air Force
Bolling AFB, DC 20332

by

Department of Civil Engineering
University of Illinois at Urbana-Champaign
Urbana, Illinois 61801

Project Staff

Project Investigators: Dr. M. R. Thompson - Dr. E. J. Barenberg
Research Assistants: A. M. Ioannides - J. A. Fischer

Program Manager

Lt. Col. J. J. Allen

May, 1983

Qualified requestors may obtain additional copies from the Defense Technical Information Service.

UNCLASSIFIED

SECURITY CLASSIFICATION OF THIS PAGE *(When Data Entered)*

REPORT DOCUMENTATION PAGE		READ INSTRUCTIONS BEFORE COMPLETING FORM
1. REPORT NUMBER **AFOSR-TR- 83-1061**	2. GOVT ACCESSION NO. AD-A135836	3. RECIPIENT'S CATALOG NUMBER
4. TITLE *(and Subtitle)* DEVELOPMENT OF A STRESS-DEPENDENT FINITE ELEMENT SLAB MODEL		5. TYPE OF REPORT & PERIOD COVERED ANNUAL 6 Jan 82 - 30 Apr 83 6. PERFORMING ORG. REPORT NUMBER
7. AUTHOR(s) M R THOMPSON A M IOANNIDES E J BARENBERG J A FISCHER		8. CONTRACT OR GRANT NUMBER(s) AFOSR 82-0143
9. PERFORMING ORGANIZATION NAME AND ADDRESS UNIVERSITY OF ILLINOIS AT URBANA-CHAMPAIGN DEPARTMENT OF CIVIL ENGINEERING URBANA, IL 61801		10. PROGRAM ELEMENT, PROJECT, TASK AREA & WORK UNIT NUMBERS 61102F 2307/C1
11. CONTROLLING OFFICE NAME AND ADDRESS AIR FORCE OFFICE OF SCIENTIFIC RESEARCH/NA BOLLING AFB, DC 20332		12. REPORT DATE May 1983 13. NUMBER OF PAGES 179
14. MONITORING AGENCY NAME & ADDRESS*(if different from Controlling Office)*		15. SECURITY CLASS. *(of this report)* Unclassified 15a. DECLASSIFICATION DOWNGRADING SCHEDULE

16. DISTRIBUTION STATEMENT *(of this Report)*

Approved for Public Release; Distribution Unlimited.

17. DISTRIBUTION STATEMENT *(of the abstract entered in Block 20, if different from Report)*

18. SUPPLEMENTARY NOTES

19. KEY WORDS *(Continue on reverse side if necessary and identify by block number)*

PAVEMENTS, SLAB MODEL, FINITE ELEMENT SLAB MODEL, SUBGRADE SUPPORT, RESILIENT MODULUS OF SUBGRADE REACTION, PAVEMENT ANALYSIS

20. ABSTRACT *(Continue on reverse side if necessary and identify by block number)*

The concept of the Resilient Modulus of Subgrade Reaction, K_R, is developed to account for the stress dependent behavior of typical fine-grained subgrade soils. This new subgrade support parameter is defined as plate pressure/resilient deflection in an impulse plate load test simulated using finite element program ILLI-PAVE. The resilient modulus of subgrade reaction, K_R, is expressed in the same units as the standard static modulus of subgrade reaction, k, but the value of the former is significantly higher. This indicates increased stiffness in response to rapidly moving loads.

CONTINUED --OVER

DD FORM 1 JAN 73 1473 EDITION OF 1 NOV 65 IS OBSOLETE

UNCLASSIFIED

SECURITY CLASSIFICATION OF THIS PAGE *(When Data Entered)*

ABSTRACT CONTINUED

Factors influencing K_R include plate size, deflection level and subgrade type. A 30-in. diameter plate was chosen in this study, in conformity with general practice. Equations relating K_R and deflection level are developed for four broad cohesive subgrade soil types: very soft, soft, medimum and stiff. The effect of a granular subbase on K_R is also examined. The introduction of a granular layer increases K_R substantially. The importance of this effect, however, diminishes rapidly as subbase thickness exceeds 8 inches. The beneficial effect of a granular subbase is consistent over the range of plate pressures investigated (c, 2c, and πc psi - c is subgrade cohesion).

The finite element model presented in this report is a modified and expanded version of ILLI-SLAB, developed in 1977 for the study of jointed, slab-on-grade pavements. A number of modifications to the original code are described. The most important of these is the incorporation, through an iterative procedure, of the deflection dependent Resilient Modulus of Subgrade Reaction (K_R). This parameter is considered more appropriate in modeling nonlinear subgrade response to rapidly moving loads. Other changes include: generation of contour plots of system response; introduction of lines of symmetry; correction of the uniform subgrade stiffness matrix; specification of loaded areas in terms of global coordinates; and, free-form input capability. To illustrate the impact of these innovations, results from several demonstration runs are summarized. The major effect of the proposed model is due to the higher values of K_R, compared to the commonly used static k.

ACKNOWLEDGMENTS

This report was prepared as part of a Project entitled, "DEVELOPMENT OF A STRESS-DEPENDENT FINITE ELEMENT SLAB MODEL". The Project is sponsored (Grant No. AFOSR-82-0143) by the Air Force Office of Scientific Research (AFOSR), Air Force Systems Command, Bolling AFB, DC.

Lt. Col. J. J. Allen is the Program Manager.

DISCLAIMER

The contents of this report reflect the views of the authors who are responsible for the facts and the accuracy of the data presented herein. The contents do not necessarily reflect the official views or policies of the U. S. Air Force. This report does not constitute a standard, specification, or regulation.

CONDITIONS OF REPRODUCTION

TABLE OF CONTENTS

CHAPTER			PAGE
1.	INTRODUCTION		1
2.	PAVEMENT SUPPORT CHARACTERIZATION		5
	2.1	LITERATURE REVIEW	5
	2.2	RESILIENT, SEMI-INFINITE HALF-SPACE	17
		2.2.1 General	17
		2.2.2 Fine-Grained Soils	18
		2.2.3 Granular Materials	22
		2.2.4 Other Materials	26
3.	DEVELOPMENT OF STRESS DEPENDENT SUPPORT MODELS FOR ILLI-SLAB		27
	3.1	THE ILLI-PAVE MODEL	27
	3.2	SIMULATION OF REPEATED PLATE LOAD TESTS	29
	3.3	ALGORITHM DEVELOPMENT	31
	3.4	SUBBASE EFFECTS	40
		3.4.1 Effect of a Granular Subbase	40
		3.4.2 Effect of a Stabilized Subbase	45
4.	THE FINITE ELEMENT METHOD AS APPLIED TO SLAB-ON-GRADE DESIGN		46
	4.1	GENERAL	46
	4.2	THREE-DIMENSIONAL MODELS	48
	4.3	THE DISCRETE ELEMENT MODEL	53
	4.4	KENTUCKY	55
	4.5	WESLIQID	57
	4.6	FINITE	59

CHAPTER PAGE

4.7 ILLI-SLAB 60

4.8 TYPICAL RESULTS AND COMPARISONS 63

4.8.1 Objectives 63

4.8.2 Problems Investigated 64

4.8.3 Comparison of Present Version of ILLI-SLAB to That Developed by A. Tabatabaie 66

4.8.4 Effect of Load Representation 71

4.8.5 Effect of Load Placement with Respect to Finite Element Mesh 75

4.8.6 Convergence Characteristics of ILLI-SLAB upon Mesh Refinement 80

4.8.7 Convergence Characteristics of ILLI-SLAB upon Slab Size Expansion 87

4.8.8 Effect of Element Aspect Ratio 95

4.8.9 Effect of Size of Loaded Area 95

4.8.10 Preliminary Recommendations 101

5. MODIFICATION OF ILLI-SLAB 104

5.1 AIMS OF MODIFICATIONS 104

5.2 STRESS DEPENDENT SUBGRADE 105

5.3 CONTOURING CAPABILITY 108

5.4 TOWARD MORE EFFICIENT MEMEORY CORE UTILIZATION 110

5.5 CORRECTION OF SUBGRADE STIFFNESS MATRIX 112

5.6 SPECIFICATION OF LOADED AREAS IN TERMS OF GLOBAL COORDINATES 113

5.7 FREE-FORM INPUT CAPABILITY 115

5.8 MISCELLANEOUS CHANGES 117

CHAPTER PAGE

6. TYPICAL EFFECTS USING MODIFIED ILLI-SLAB 120

6.1 CASES CONSIDERED 120

6.2 DISCUSSION OF RESULTS 133

6.2.1 Effect of Load Transfer 133

6.2.2 Effect of Resilient Modulus Characterization ... 135

6.2.3 Effect of Stress Dependence -- Iterative Scheme 137

7. CONCLUDING REMARKS 141

REFERENCES 145

APPENDIX: INPUT GUIDE FOR ILLI-SLAB

(REVISED VERSION: FEB. 1983) A-1

LIST OF TABLES

TABLE		PAGE
2.1	Typical Resilient Property Data	25
3.1	Materials Property Summary	30
3.2	Models Considered	38
3.3	Regression Equation Parameters and Statistics	41
4.1	(a) Revalidation of ILLI-SLAB	67
	(b) Comparison with Westergaard Solutions	68
4.2	Effect of Load Placement with Respect to F.E. Mesh	79
4.3	(a) Effect of F.E. Mesh Fineness	83
	(b) Comparison Between ILLI-SLAB, 'SPRINGS' and WESLIQID	84
4.4	Theoretical and Empirical Size Limitations for the Westergaard Solution	90
4.5	Effect of Slab Size	92
4.6	Effect of Element Aspect Ratio	96
4.7	Effect of Size of Loaded Area	100
5.1	Free-Form Data Groups and Key Words	116
6.1	Parameters for Demonstration Runs	121
6.2	Demonstration Runs Results	132
6.3	Effect of Load Transfer	134
6.4	Effect of Resilient Modulus	136
6.5	Effect of Stress Dependence	138
6.6	Combined Effect of Proposed Changes	140

LIST OF FIGURES

FIGURE		PAGE
2.1	Plate Load Test	7
	(a) Typical Setup for Plate Load Test	7
	(b) Typical Plate Load Test Results	7
2.2	(a) Hyperbolic Model for Nonlinear Subgrade	9
	(b) Hyperbolic Model with Transformed Axes	9
2.3	Ramberg-Osgood Model for Loading and Unloading	10
2.4	Parameters for Butterfield and Georgiadis Empirical Equation	12
2.5	Filonenko-Borodich Foundation	15
2.6	Idealized Foundation Model According to Butterfield and Georgiadis	15
2.7	Arithmetic Model for Stress Dependent Resilient Behavior of Fine-Grained Soils	19
2.8	Typical Stress Dependent Resilient Behavior of a Fine-Grained Soil [AASHTO A-7-6(36)]	20
2.9	Semi-Log Model for Stress Dependent Resilient Behavior of a Fine-Grained Soil [AASHTO A-7-6(36)]	21
2.10	Subgrade Soil Material Models for ILLI-PAVE Analyses	23
2.11	Resilient Modulus - θ Relation for a Sandy Gravel [AASHTO A-1-b(0)]	24
3.1	Axisymmetric Solid Representation Used in ILLI-PAVE	28
3.2	Plate Pressure-Resilient Displacement Relations for Medium and Very Soft Subgrades	32
3.3	Plate Pressure-Resilient Displacement Relations for Stiff and Soft Subgrades	33
3.4	K_R - Deflection Relations for Various Plate Sizes (Very Soft Subgrade)	34
3.5	K_R - Deflection Relations for Various Plate Sizes (Soft Subgrade)	35

FIGURE		PAGE
3.6	K_R - Deflection Relations for Various Plate Sizes (Medium Subgrade)	36
3.7	K_R - Deflection Relations for Various Plate Sizes (Stiff Subgrade)	37
3.8	K_R - Granular Subbase Thickness Effects	43
3.9	K_R - Granular Subbase Effects for Variable Plate Pressures	44
4.1	A Typical F. E. Mesh Used for 3-Dimensional Analysis (After Tabatabaie, et al, 1979 - Ref. 1)	51
4.2	Discrete Element Model of a Plate or Slab	54
4.3	Revalidation of ILLI-SLAB	69
4.4	F. E. Mesh Used for Revalidation of ILLI-SLAB (Mesh I)	70
4.5	Effect of Load Placement (Mesh II)	76
4.6	Effect of Load Placement (Mesh III)	77
4.7	Effect of Mesh Fineness: Number of Elements = 144	82
4.8	Effect of F. E. Mesh Fineness (Revised ILLI-SLAB)	85
4.9	Effect of F. E. Mesh Fineness on Deflection Bowl (WESLIQID)	88
4.10	Effect of F. E. Mesh Fineness on Stresses (WESLIQID)	89
4.11	Effect of Slab Size: F. E. Mesh	91
4.12	Effect of Slab Size (ILLI-SLAB)	93
4.13	Effect of Element Aspect Ratio on Deflection Bowl (WESLIQID)	97
4.14	Effect of Element Aspect Ratio on Stresses (WESLIQID)	98
4.15	Effect of Size of Loaded Area	102
5.1	Sample Contour Plots	109
5.2	Comparison of Free-form and Fixed-form Input Data Files for Run DR003 (See Table 6.2; Fig. 6.1)	118

FIGURES PAGE

6.1 F. E. Mesh for F-4 at Edge of PCC Pavement 123

6.2 F. E. Mesh for C-130 at Edge of PCC Pavement 124

6.3 F. E. Mesh for F-111 at Edge of PCC Pavement 125

6.4 F. E. Mesh for F-4 at Interior of PCC Pavement 126

6.5 F. E. Mesh for C-130 at Interior of PCC Pavement 127

6.6 F. E. Mesh for F-111 at Interior of PCC Pavement 128

6.7 F. E. Mesh for F-4 at Edge of ALRS Pavement 129

6.8 F. E. Mesh for C-130 at Edge of ALRS Pavement 130

6.9 F. E. Mesh for F-111 at Edge of ALRS Pavement 131

CHAPTER 1

INTRODUCTION

When loaded by ordinary traffic, Portland Cement Concrete (PCC) pavements as well as flexible pavements with high strength base materials (eg. soil-cement, econocrete, lime-flyash aggregate, etc.), display a slab-type behavior. This behavior is characterized by the development of significant flexural stresses and relatively low subgrade stresses. These pavements may have longitudinal construction joints and/or transverse joints. Transverse joints are typically sawed or constructed for PCC pavements, but may also occur as transverse cracks in the case of stabilized base courses. The presence of joints and cracks makes it important to consider such factors as load placement (ie. interior, edge, or corner), multiple wheel loading, load transfer, etc. and their overall impact on pavement response and performance.

In the calculation of stresses in slab-on-grade pavements, it is necessary to idealize the characteristics of the supporting medium. In general, one of two fundamentally different hypotheses concerning the

properties of the subgrade is used. In the first of these theories, the soil is regarded as an elastic, isotropic and homogeneous semi-infinite body. The term 'elastic solid' is often used to describe this idealization. The majority of current analyses which treat the subgrade as a semi-infinite, elastic half-space, employ axisymmetric models. Thus, they are only applicable to the interior condition -ie. where the load is away from any edge. Furthermore, most such analyses can only handle a single-wheel load; exceptions include MWELP (61), BISAR (62), as well as certain Pickett and Ray Charts (52). Accommodation of multiple-wheel loads has not yet been achieved in the case of ILLI-PAVE (16), a stress dependent (nonlinear), elastic model, described in Chapter 3.

In the other support characterization theory, the subgrade is regarded as a flexible bed, with surface pressure proportional to surface deflection at each point, while adjacent unloaded areas are not at all affected. This idealization is commonly termed as a 'dense liquid' or a Winkler subgrade. Finite element program ILLI-SLAB (1,2) employs a Winkler-type subgrade and can be used to study two-layer, cracked pavement sections, load transfer by aggregate interlock and/or dowels, variable slab thickness, variable subgrade support and complex multi-wheel loading, at any position on the pavement. This model has been validated and extensively utilized in various University of Illinois studies (1,25,54).

In the original version of ILLI-SLAB, the modulus of subgrade reaction, k, obtained from the plate load test, is used for subgrade characterization. This is in conformity with general engineering practice, as well as several other finite element models. The value of k can be varied from node to node according to a pattern specified by the user at the beginning of the analysis. Note that k is independent of stress/deflection level, being essentially a linear, low stress modulus. Most subbase-subgrade support systems, however, display a stress-level dependent load-deflection response. Typically, a softer (lower k) response is exhibited at higher magnitudes of stress/deflection.

The purpose of this study is to develop deflection dependent support relations and incorporate these into ILLI-SLAB to accommodate deflection dependent subgrade behavior. Various models previously proposed are reviewed in Chapter 2, with special attention paid to those that can be used to simulate nonlinear subgrade response. Thompson and Robnett (13) have proposed a resilient modulus characterization for the 'elastic solid' foundation. This not only introduces soil nonlinearity, but also -perhaps more importantly- accounts for the apparent increase in subgrade stiffness, produced by rapidly moving, repeated loads. The aim of this study is to develop a similar resilient modulus characterization for the 'dense liquid' foundation.

Data for the development of the necessary algorithms are obtained using ILLI-PAVE to simulate repeated plate loading tests, as described in Chapter 3. Equations are derived relating the resilient modulus of

subgrade reaction, K_R, and deflection. Note that this is no longer the modulus, k, derived from the static plate load test, but a modulus characterizing subgrade response to a repeated (impulse-type) test. The latter loading condition is considered more appropriate for the type of moving loads applied by modern-day aircraft traffic.

Chapter 4 examines in more detail computer program ILLI-SLAB currently used in pavement design and analysis, as well as several other finite element programs. By comparing ILLI-SLAB results with those from other programs and from Westergaard's theory, the validity of the ILLI-SLAB model is confirmed. A number of recommendations are also made for its most efficient utilization.

The stress dependent subgrade algorithms developed in Chapter 3 are incorporated into ILLI-SLAB through an iterative scheme. This change is described, together with several other improvements, in Chapter 5. Finally, typical results from the revised version of ILLI-SLAB are presented in Chapter 6, where the effects of the proposed changes are evaluated.

CHAPTER 2

PAVEMENT SUPPORT CHARACTERIZATION

2.1 LITERATURE REVIEW

In this section, several models proposed for the characterization of subgrade support systems --other than that of the semi-infinite, elastic half-space-- are reviewed. The emphasis is on models that could be used to simulate stress dependent (nonlinear) subgrade response. The resilient, semi-infinite half-space characterization developed by Thompson and his co-workers (13), is discussed separately in Section 2.2.

The simplest representation of an elastic soil medium is the Winkler Foundation (3). Winkler assumed the elastic foundation to be represented by a bed of closely spaced, independent, linear springs. The stiffness of the springs, generally referred to as the modulus of subgrade reaction, is usually denoted by the symbol k (psi/in.). The modulus of subgrade reaction relates the reaction pressure (q) to the deflection (w) at a given location in the subgrade through the equation:

$$q(x) = kw(x).$$

Most current rigid pavement design procedures are based on the Winkler model.

The subgrade modulus, k, is calculated using data from 30-in. diameter plate load tests (Fig. 2.1a). ASTM standards (4) include non-repetitive (ASTM D1196) and repetitive (ASTM D1195) static plate load tests. The Corps of Engineers (CE), however, only uses a non-repetitive static plate load test (5). The Air Force Engineering and Services Center routinely conducts plate bearing tests in its airfield pavement evaluation activities. Correlations between k, CBR and soil classification have been suggested by various agencies. These correlations are widely used, since plate load tests are expensive and time consuming.

A typical plate pressure - plate deflection relation for a fine-grained soil shows a nonlinear, stress softening trend (Fig. 2.1b). The modulus of subgrade reaction is usually calculated using either the CE or the PCA procedure. In the CE procedure (5), k is determined for a plate pressure of 10 psi and the corresponding deflection. Using the PCA procedure (6), k is evaluated at a plate pressure corresponding to a 50-mil (0.050-in.) plate deflection.

A more sophisticated representation of an elastic soil medium would consider the nonlinearity of the springs and more accurately approximate the stress softening behavior of a fine-grained subgrade. Two of the

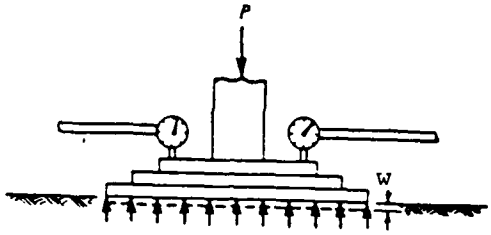

(a) Typical setup for Plate Load Test

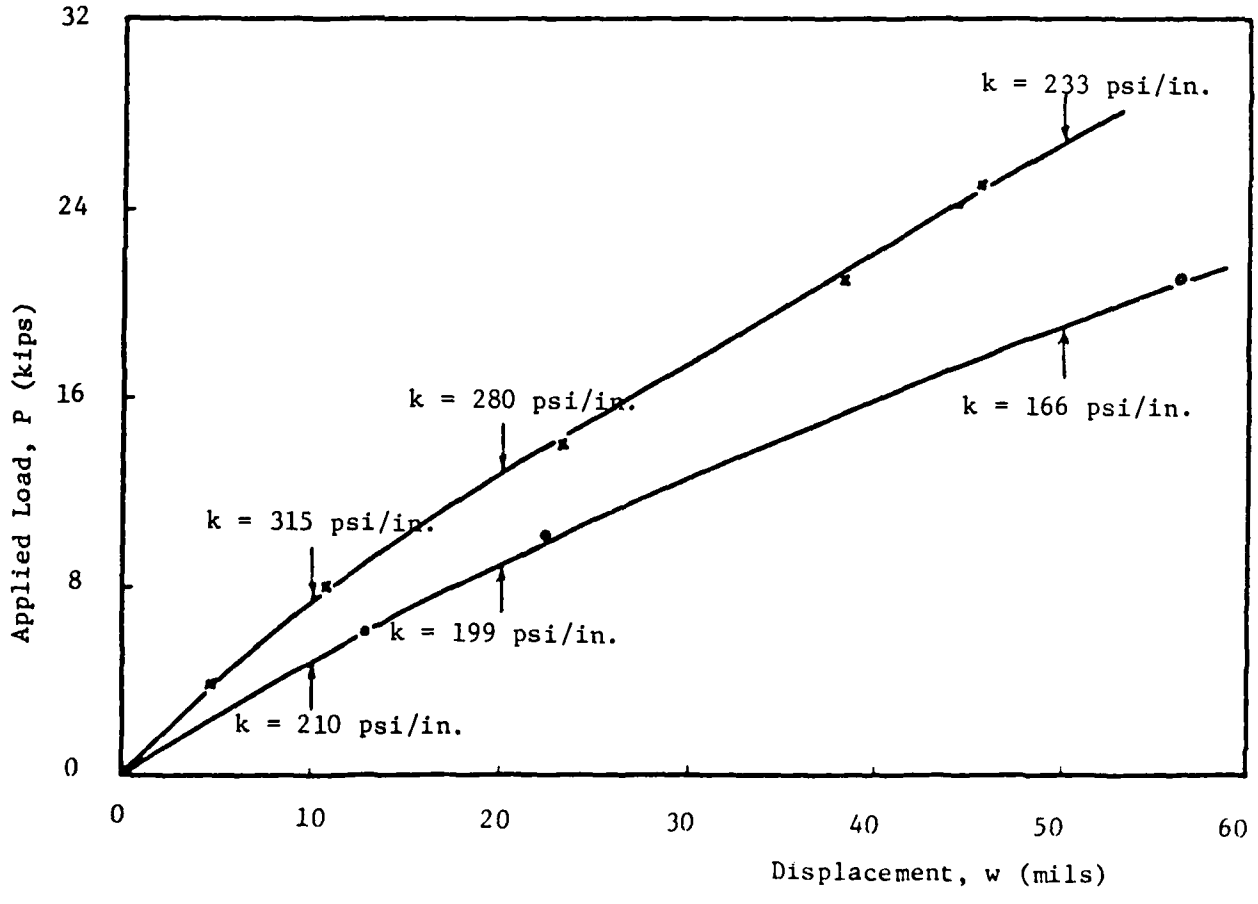

(b) Typical Plate Load Test Results (After Ref. 63)

Fig. 2.1 Plate Load Test

more widely used nonlinear models in geotechnical engineering are the hyperbolic and Ramberg-Osgood models. Both models were originally developed to reconstruct stress-strain curves, but are easily adapted to pressure-deflection data.

The hyperbolic model (7) assumes the plate pressure-deflection (p-w) plot is a hyperbola (Fig. 2.2a). The equation has the form:

$$p = \frac{w}{b + aw}$$

where 'a' and 'b' are empirical constants.

If the equation is rearranged, a relationship of the form:

$$\frac{1}{k} = \frac{w}{p} = b + aw$$

can be obtained. On transformed axes (Fig. 2.2b), this equation plots as a straight line with a slope of 'a' and an intercept of 'b'. The term (1/b) is equivalent to the initial stiffness, k_o.

The Ramberg-Osgood function (7) is usually expressed in the following form (Fig. 2.3):

$$\frac{w}{w_y} = \frac{p}{p_y} + a \left| \frac{p}{p_y} \right|^r \qquad \text{for first loading}$$

$$\frac{w - w_o}{2\, w_y} = \frac{p - p_o}{2\, p_y} + a \left| \frac{p - p_o}{2\, p_y} \right|^r \qquad \text{for reloading}$$

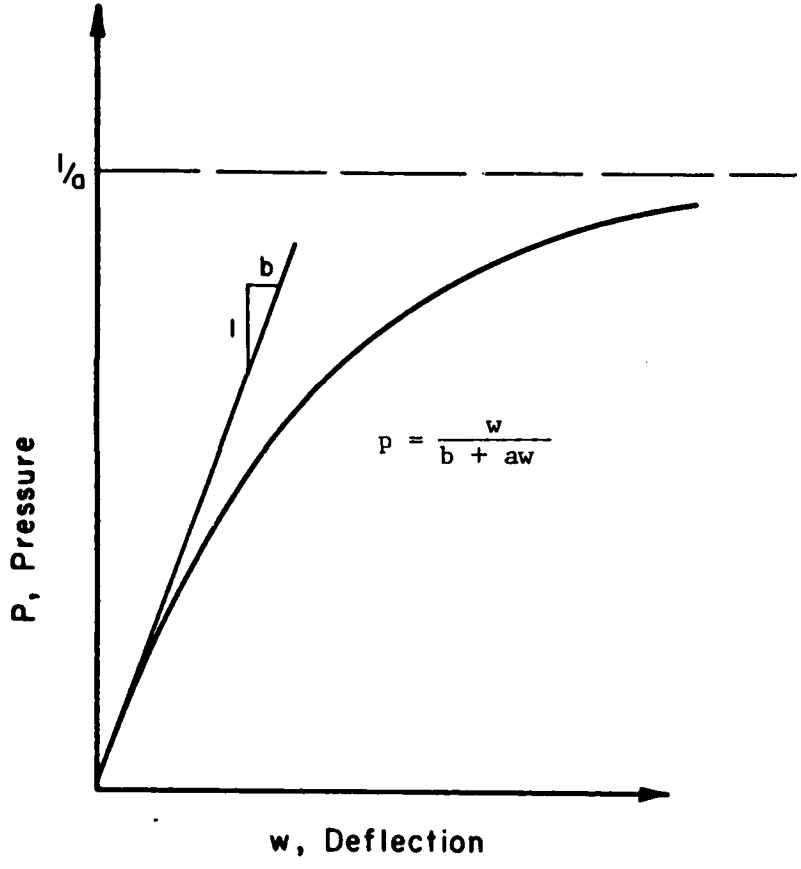

Fig. 2.2a Hyperbolic Model for Nonlinear Subgrade

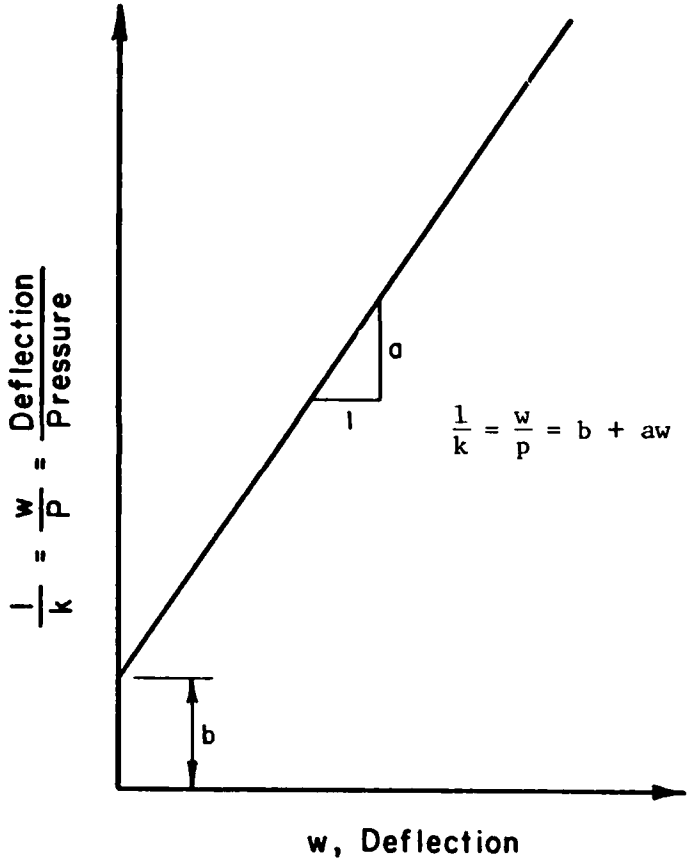

Fig. 2.2b Hyperbolic Model with Transformed Axes

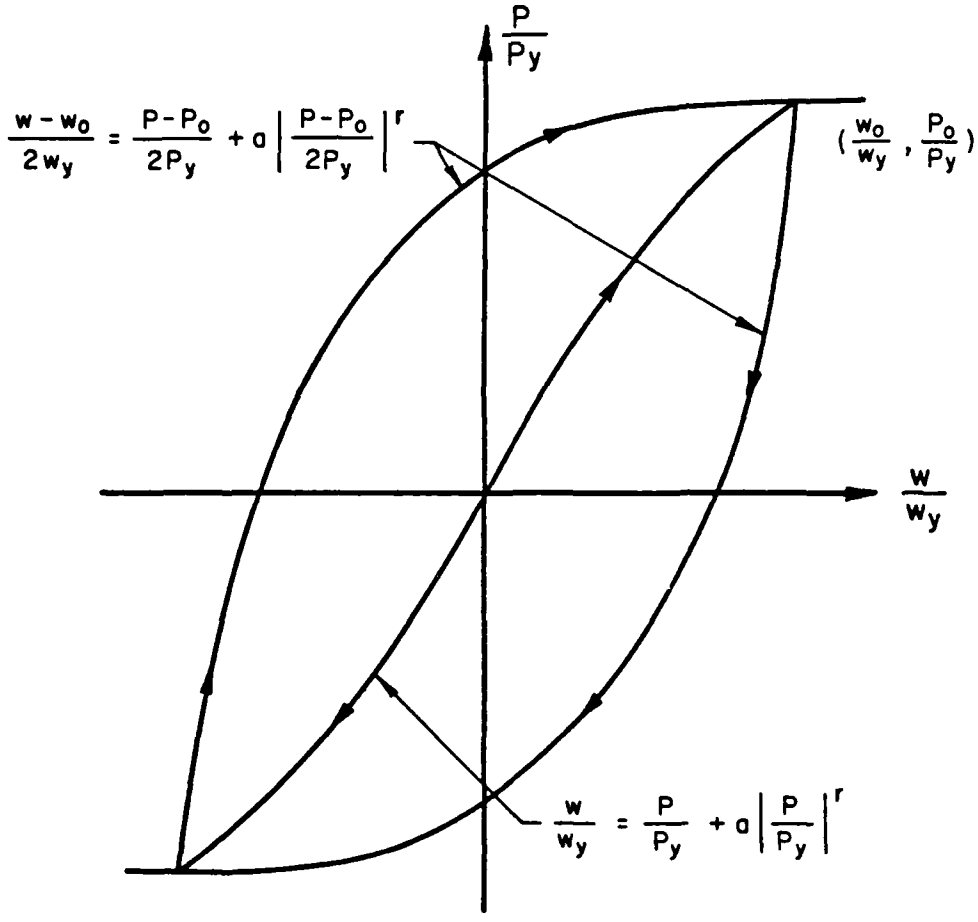

Fig. 2.3 Ramberg-Osgood Model for Loading and Unloading

where w_y and p_y are the deflection and plate pressure at yielding, respectively, and w_o and p_o are the extreme values of w and p for the cycle. The values of the constants 'a' and 'r' must be determined experimentally. The Ramberg-Osgood model is especially suited for cyclic loading situations, where both the loading and unloading curves are of interest.

A third model used to account for the nonlinearity of the subgrade springs is an empirical equation developed by Butterfield and Georgiadis (8). The basis of the equation is an idealization proposed by Burland and Lord (9). The equation is characterized by three parameters: an initial stiffness k_o, a final stiffness k_f and a pressure axis intercept q_u (Fig. 2.4). The form of the equation is:

$$q = q_u \left(1 - \exp \{ - (k_o - k_f)\, w/q_u \} \right) + k_f\, w$$

A major drawback of one-parameter models (including the Winkler and nonlinear spring models) is their inability to adequately describe the behavior of a half-space. In a physical sense, this means that no deflection is possible outside the loaded area, as deflection at any point is only a function of pressure at that point. In reality, some deflection inevitably occurs outside the loaded area. It is this inaccuracy that led researchers to look for a second parameter to describe elastic foundation response (10).

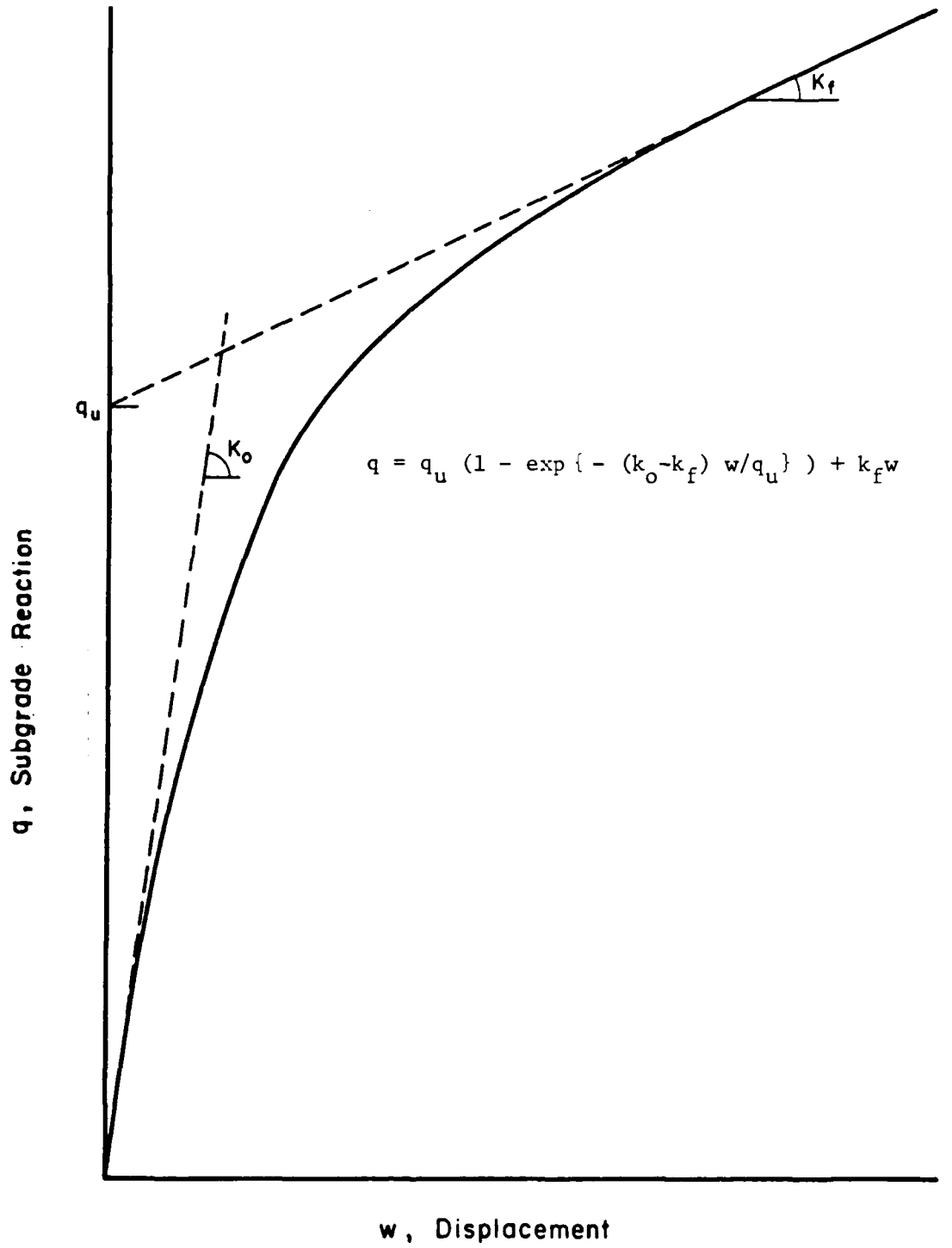

Fig. 2.4 Parameters for Butterfield and Georgiadis Empirical Equation

One of the earliest two-parameter models was the Filonenko-Borodich Foundation (3). In addition to the vertical springs which are common to the one-parameter models, this foundation includes a stretched elastic membrane (Fig. 2.5). The elastic membrane which is subjected to a constant tension field of T is connected to the top end of the springs to develop some interaction among them. The amount of interaction is a direct function of T. The relation between subgrade stress (q) and deflection (w) is of the form:

$$q = kw - T\nabla^2 w$$

where ∇^2 is the Laplace operator in x and y.

Another two-parameter model is the Pasternak Foundation (3). Pasternak considered the existence of shear interactions between the spring elements by tying the springs together at the top with a plate consisting of incompressible vertical elements that deform only by transverse shear. The relation between pressure and deflection is very similar to that of the Filonenko-Borodich Foundation, with T replaced by G (the plate shear modulus) so that:

$$q = kw - G\nabla^2 w$$

Butterfield and Georgiadis (8), expanding on an idealization first proposed by Engesser (11) and using the Pasternak Foundation, developed a loading equation using two stiffness parameters, one for the compression springs and one for the shear springs. Engesser (11) proposed that for

the case of a beam on an elastic foundation, the modulus of subgrade reaction could be represented by an equation of the form:

$$k = a + (b/B)$$

where 'a' and 'b' are constants and B is the breadth of the beam. Butterfield and Georgiadis (8) suggested that the pressure applied on a rigid square plate (BxB) is balanced by two sets of forces. The first is the pressure due to the displacement of the vertical springs directly beneath the plate and the second the shear force around the edge of the plate, which is a direct function of the deflection of the springs in the unloaded region (Fig. 2.6). The equation derived is:

$$q = kw_o + (4g^{0.5}/B) \int_o^{w_o} [p\ dw/\sqrt{2 \int p\ dw}\ ]$$

where q is the subgrade stress , w_o is the displacement of the plate, k is the compression spring stiffness and g is the shear spring stiffness. Note that the second term is dependent on B, while the first term is not. The parameters k and g are nonlinear functions of w_o and are independent of the plate size.

For a given displacement, the above equation can be reduced to the form:

$$q = a + \frac{b}{B}$$

with constants 'a' and 'b' directly dependent on k, g, and w_o. Butterfield and Georgiadis (8) showed that the values of 'a' and 'b' could be calculated for a given displacement from two different size

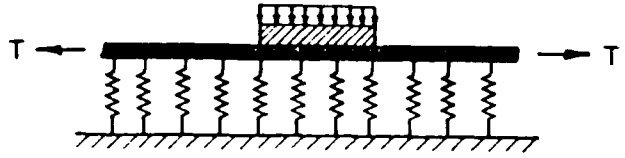

Fig. 2.5 Filonenko-Borodich Foundation

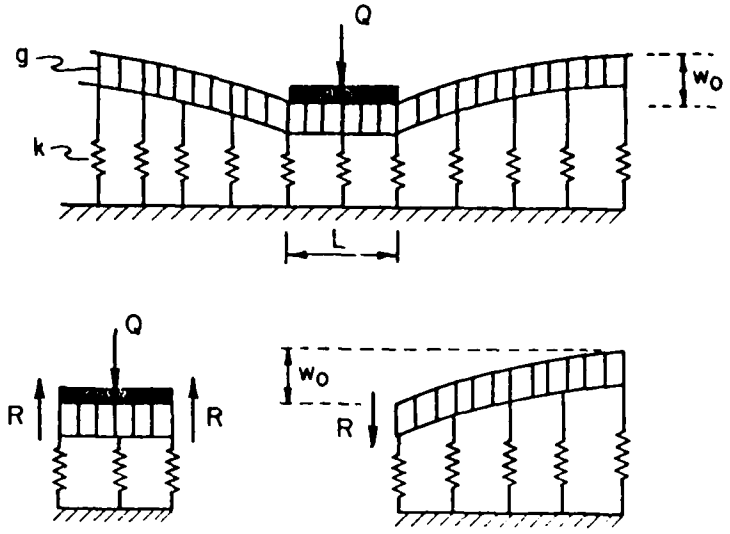

Fig. 2.6 Idealized Foundation Model According to Butterfield and Georgiadis

plate tests. The values of k and g can then be back-calculated from 'a' and 'b'.

All of the models discussed previously, with the exception of the Ramberg-Osgood model, were developed for static loading conditions. However, it appears that these models may also be applicable for the resilient subgrade response to repeated loading, since the pressure-deflection plots for both loading conditions are very similar in shape. Butterfield and Georgiadis (12) proposed a model that could predict the cyclic load behavior of plates of any size from two in-situ tests: a conventional plate bearing test and a single-load level cyclic plate test. From these two tests, the following empirical equations were developed:

$$k_u = k_o - C_2 \frac{Q_c}{Q_u} \left[1 + C_3 \log \{ N/(Q_c/Q_u) \}\right] \quad \text{for unloading}$$

$$k_r = k_o - C_1 \frac{Q_c}{Q_u} \quad \text{for reloading}$$

where k_o: initial stiffness;

k_f: final stiffness;

Q_u: load axis intercept;

Q_c: cyclic load;

k_r: reloading stiffness;

k_u: unloading stiffness;

C_1, C_2, C_3: experimentally determined constants;

N :number of cycles.

These equations can be used to predict the nonlinear response of a plate for any number of cycles at any load level.

2.2 RESILIENT, SEMI-INFINITE HALF-SPACE

2.2.1 General

The resilient behavior of a soil or material is an important property for pavement analysis and design. A commonly used measure of resilient response is the "resilient modulus", defined by:

$$E_R = \frac{\sigma_D}{\varepsilon_R}$$

where:

E_R: resilient modulus;

σ_D: repeated deviator stress;

ε_r: recoverable axial strain.

Repeated unconfined compression or triaxial testing procedures are often used to evaluate the resilient moduli of fine-grained soils and granular materials. Resilient moduli are stress dependent: fine-grained soils experience resilient modulus decreases with increasing stress, while granular materials stiffen with increasing stress level.

2.2.2 Fine-Grained Soils

Two stress dependent behavior models have been proposed for describing the stress softening behavior of fine-grained soils. The arithmetic model is demonstrated in Figures 2.7 and 2.8, and the semi-log model is shown in Fig. 2.9. Extensive resilient laboratory testing, nondestructive testing, and pavement analysis and design studies at the University of Illinois have indicated that the arithmetic model (Fig. 2.7) is adequate for pavement analysis activities.

In the arithmetic model, the value of the resilient modulus at the break-point in the bilinear curve, E_{Ri} (Fig. 2.7), is a good indicator of a soil's resilient behavior. The slope values, K_1 and K_2, display less variability and influence pavement structural response to a smaller degree than E_{Ri}. Thompson and Robnett (13) developed procedures for predicting the resilient behavior of fine-grained soils based on soil classification, soil properties, and moisture content. They suggested the following regression equations relating E_{Ri} with static soil modulus, E, and unconfined compressive strength, q_u:

$$E_{Ri} = 3.36 + 1.9\ E$$

where:

$$E_{Ri} = 0.86 + 307\ q_u$$

E_{Ri}, E : Moduli, ksi

q_u: Unconfined compressive strength, psi

It is seen that E_{Ri} is substantially greater than static E, due to the stiffer soil response to repeated, short-duration loads. The E_{Ri}-deviator stress relations developed for Illinois soils

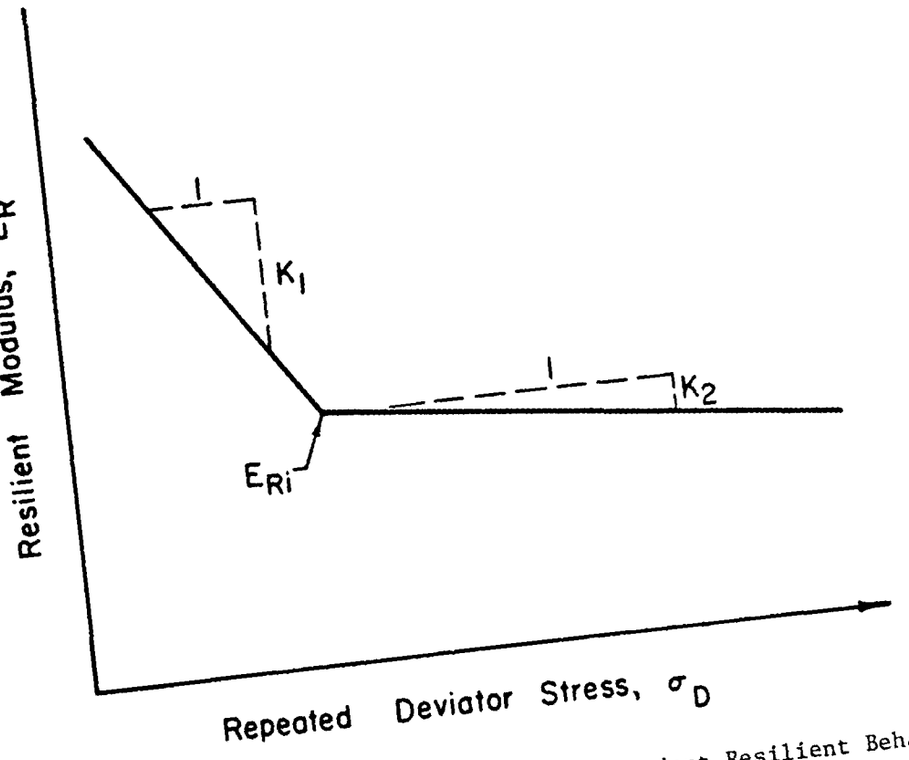

Fig. 2.7 Arithmetic Model for Stress Dependent Resilient Behavior of Fine-Grained Soils.

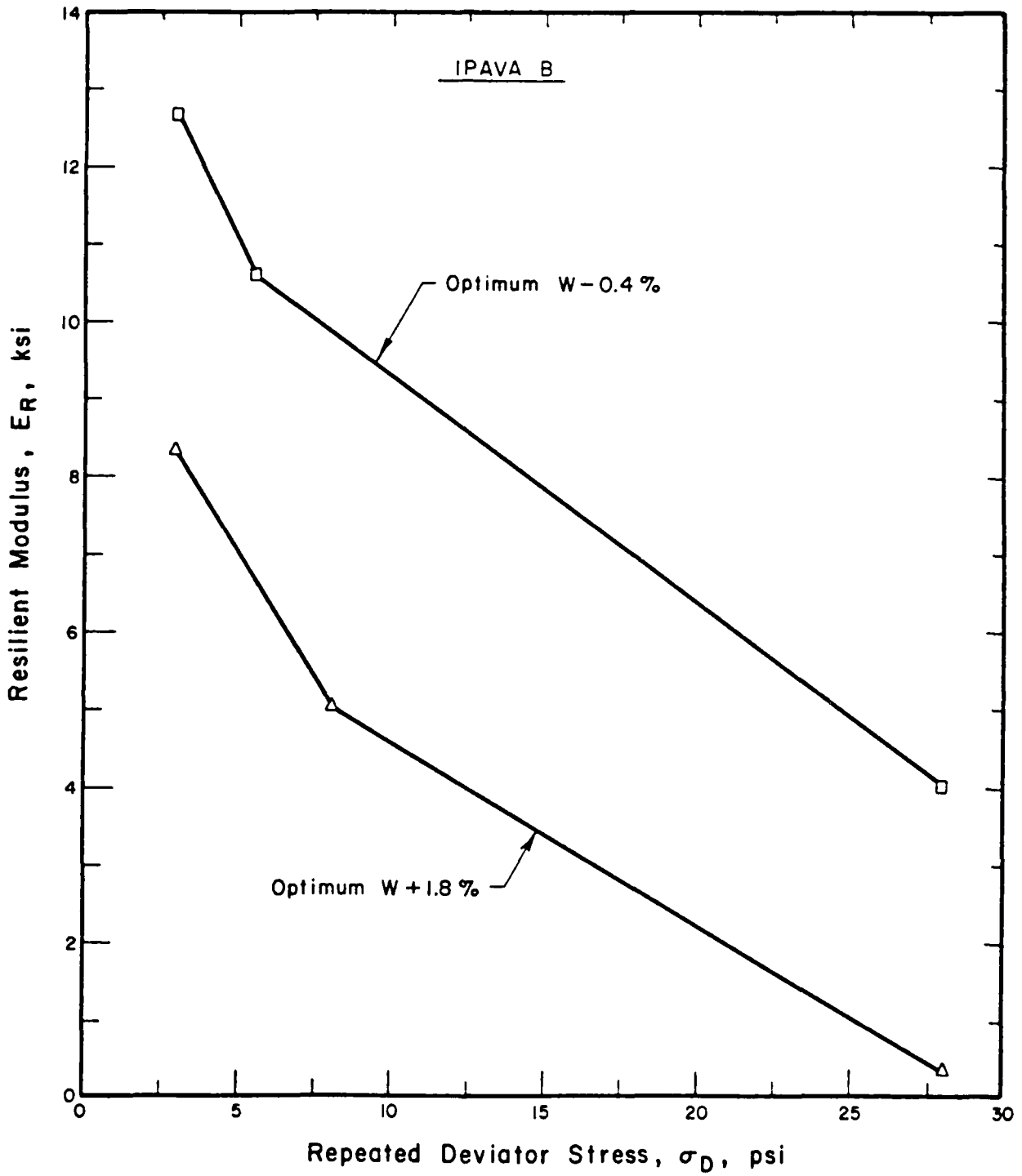

Fig. 2.8 Typical Stress Dependent Resilient Behavior of a Fine-Grained Soil [AASHTO A-7-6(36)].

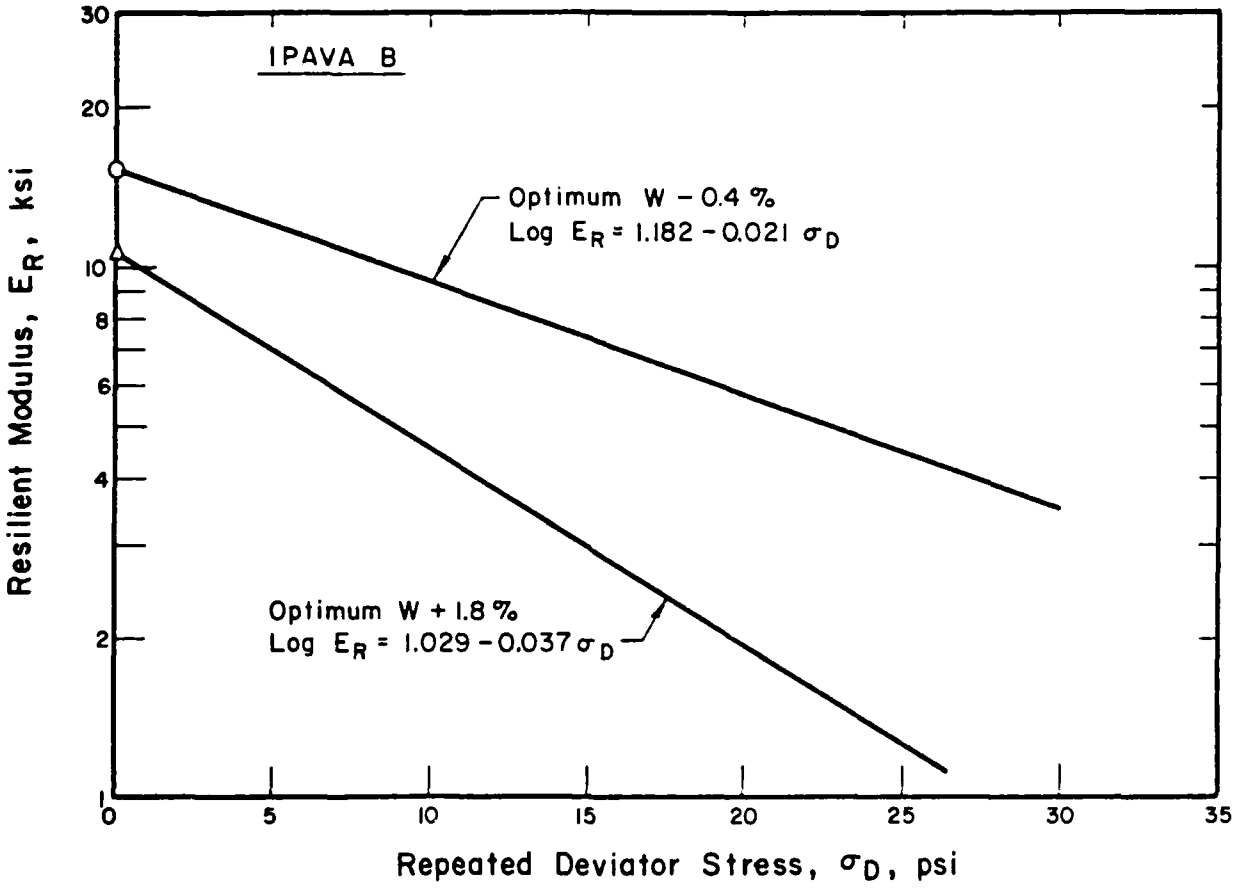

Fig. 2.9 Semi-Log Model for Stress Dependent Resilient Behavior of a Fine-Grained Soil [AASHTO A-7-6(36)].

(Fig. 2.10), are representative of soils exhibiting stress softening behavior (13).

2.2.3 Granular Materials

In contrast to fine-grained soils, granular materials stiffen as the stress level increases. Repeated load triaxial testing is used to characterize the resilient behavior of granular materials. The resilient modulus is a function of the applied stress state, as follows:

$$E_R = K\theta^n$$

where:

E_R = resilient modulus

K , n = experimentally derived factors

θ = first stress invariant = $\sigma_1 + 2\sigma_3$

(Note: $\sigma_2 = \sigma_3$ in a standard triaxial compression test)

Figure 2.11 is an E_R-θ relation for a sandy-gravel (GW in the Unified System).

Rada and Witczak (14) have summarized and analyzed statistically extensive published resilient moduli data for a broad range of granular materials. The average values and ranges for K and n are presented in Table 2.1 for several granular materials and coarse-grained soils.

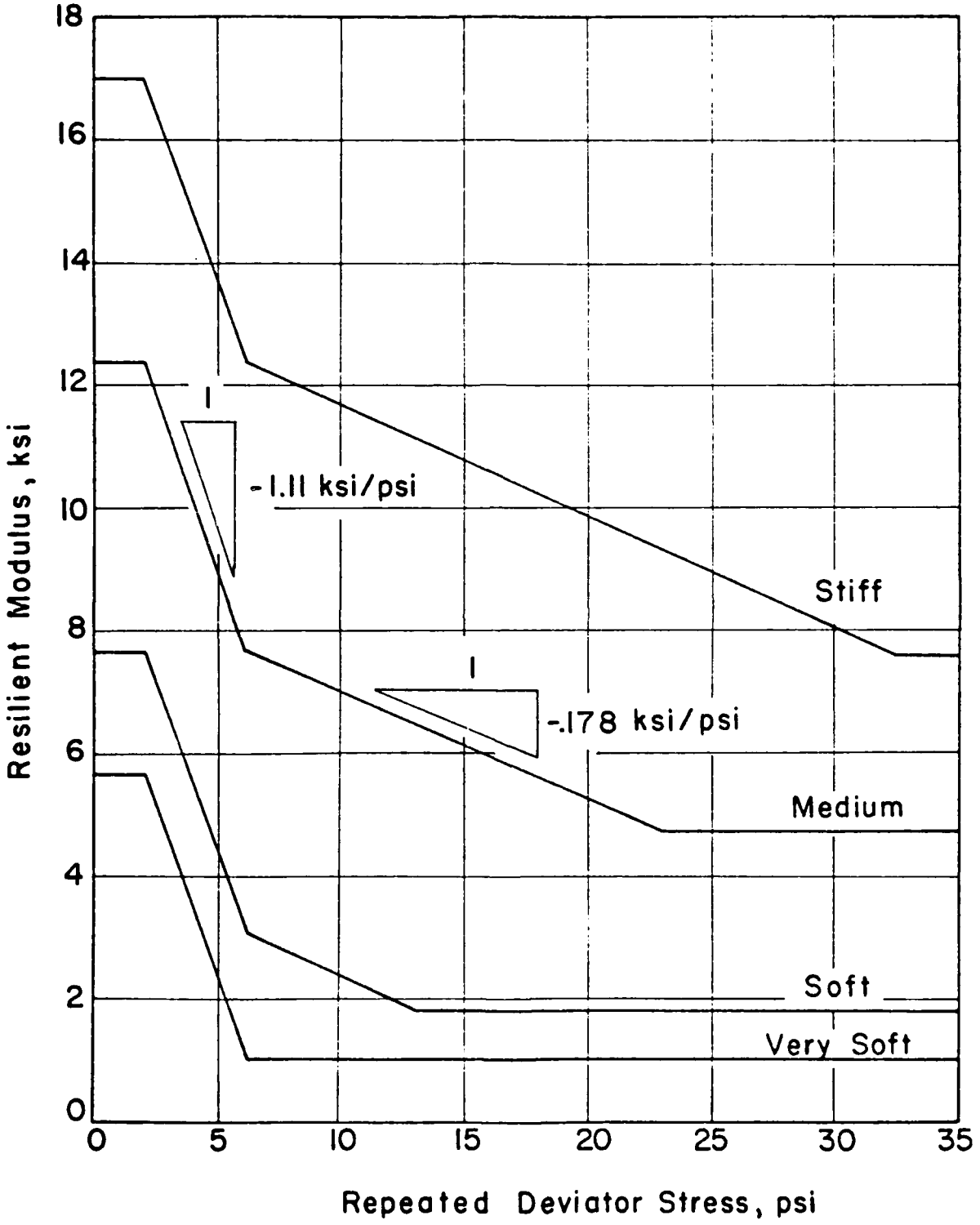

Fig. 2.10 Subgrade Soil Material Models for ILLI-PAVE Analyses

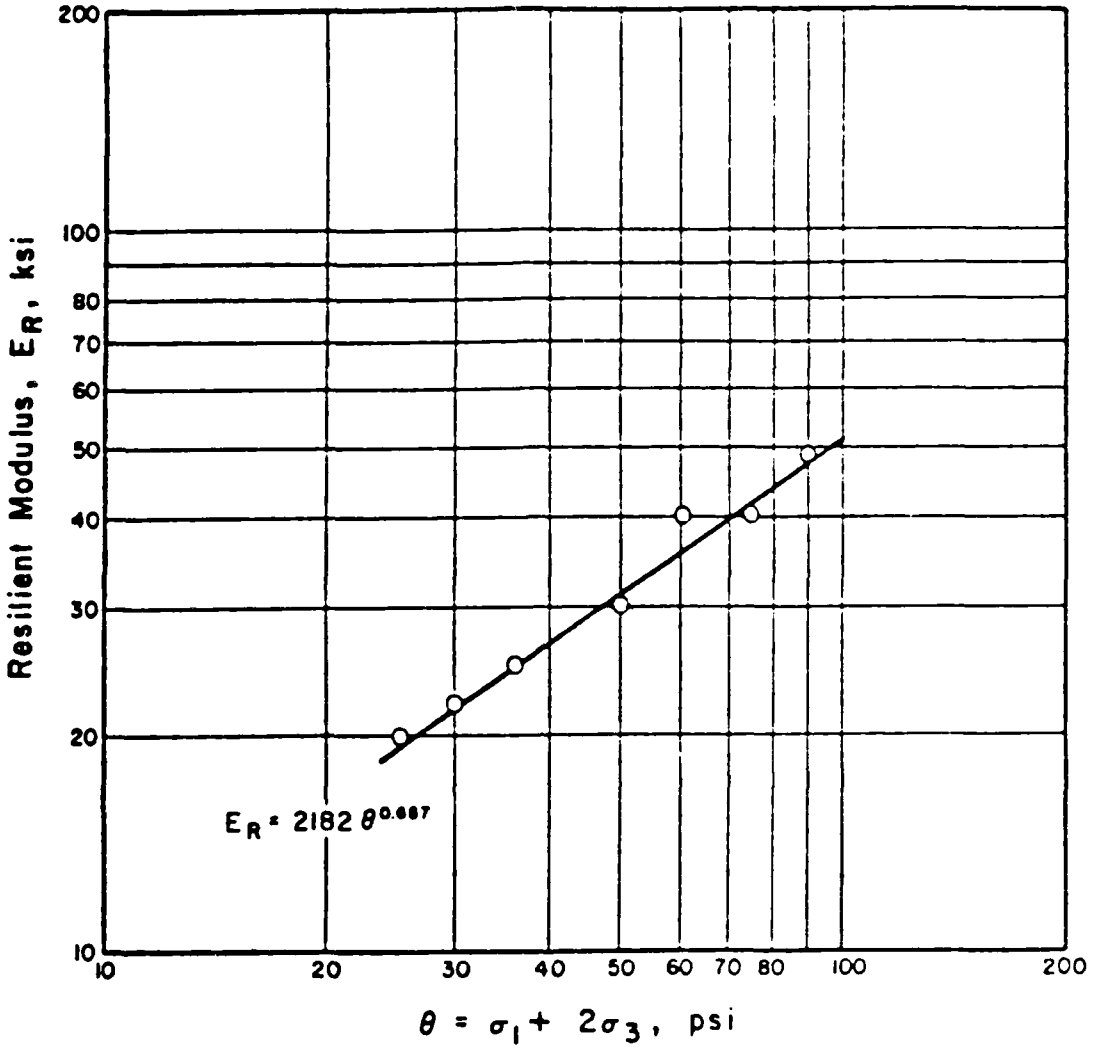

Fig. 2.11 Resilient Modulus - θ Relation for a Sandy Gravel [AASHTO A-1-b(0)].

TABLE 2.1

TYPICAL RESILIENT PROPERTY DATA (14)

Granular Material Type	Number of Data Points	K* (psi)		n*	
		Mean	Standard Deviation	Mean	Standard Deviation
Silty Sands	8	1620	780	0.62	0.13
Sand-Gravel	37	4480	4300	0.53	0.17
Sand-Aggregate Blends	78	4350	2630	0.59	0.13
Crushed Stone	115	7210	7490	0.45	0.23

* $E_R = K\theta^n$ where

E_R = resilient modulus, psi

K,n = experimentally derived factors from repeated triaxial testing data

2.2.4 Other Materials

Stabilized materials such as soil-cement, cement-aggregate mixtures, soil-lime mixtures, lime-flyash-aggregate mixtures and similar high strength--high modulus materials are frequently used as base and subbase layers. These materials are normally characterized as constant modulus materials.

CHAPTER 3

DEVELOPMENT OF STRESS DEPENDENT SUPPORT MODELS FOR ILLI-SLAB

3.1 THE ILLI-PAVE MODEL

The data required for the development of an algorithm which would be incorporated into ILLI-SLAB to account for stress dependent response of typical subgrade soils, were derived by simulating repeated plate load tests using finite element program ILLI-PAVE (16). This considers an axisymmetric solid of revolution as shown in Fig. 3.1. The program employs nonlinear, stress dependent material models (see Section 2.2) and failure criteria for granular materials and fine-grained soils (15,16,17). The principal stresses in the granular and subgrade layers are modified at the end of each iteration so that they do not exceed the strength of the materials as defined by the Mohr-Coulomb theory of failure.

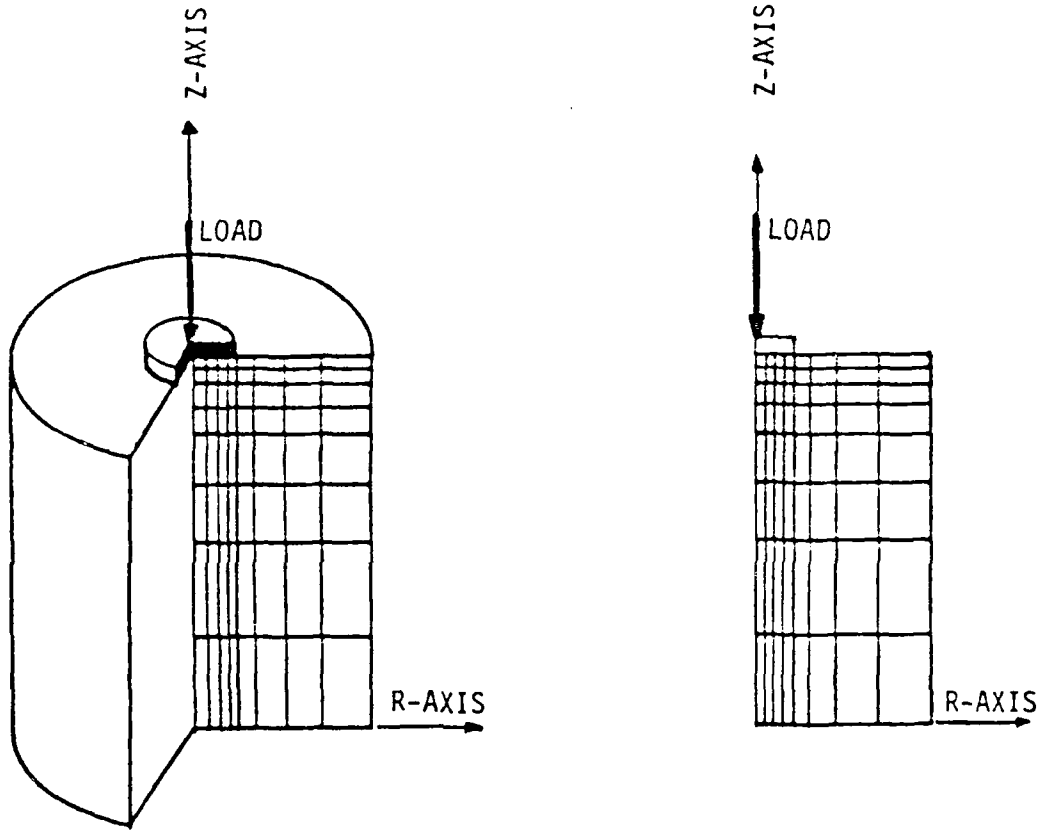

Fig. 3.1 Axisymmetric Solid Representation Used in ILLI-PAVE

Studies comparing measured and ILLI-PAVE predicted load-deformation responses, reported by Raad and Figueroa (16), Suddath and Thompson (18), Traylor (19), and Hoffman and Thompson (20), yielded favorable results. The ILLI-PAVE approach has been successfully utilized in developing a highway flexible pavement overlay design procedure based on nondestructive testing data analyses (21), as well as mechanistic thickness design procedures for secondary road flexible pavements (22) and soil-lime layers (23).

3.2 SIMULATION OF REPEATED PLATE LOAD TESTS

ILLI-PAVE was used to simulate repeated plate loading tests on various subgrades. The rigid plate condition was represented by a 4-in. thick steel loading plate ($E_s = 30 \times 10^6$ psi). Plate diameters of 30, 21, and 15 in. were considered. Various plate pressures were applied. For each loading condition, a resilient (recoverable) deflection was determined from the ILLI-PAVE analysis. The resilient modulus of subgrade reaction (K_R) is analogous to k, but is calculated by dividing the plate pressure by the calculated resilient plate deflection.

The four subgrade types introduced earlier (very soft, soft, medium, and stiff) were investigated. Pertinent subgrade properties and characteristics are summarized in Table 3.1. Resilient moduli-repeated stress level relations for these subgrades are shown in Fig. 2.10.

TABLE 3.1

MATERIALS PROPERTY SUMMARY

	Subgrade				
	Very Soft	Soft	Medium	Stiff	Gravel
Unit Weight (pcf)	110.0	115.0	120.0	125.0	135.0
Coefficient Earth Pressure at Rest	0.82	0.82	0.82	0.82	0.6
Poisson's Ratio	0.45	0.45	0.45	0.45	0.38
E_{Ri} (ksi)	1.00	3.02	7.68	12.34	--
E_R - Model (psi)*	--	--	--	--	$5000\theta^{.50}$
Friction Angle (degree)	0.0	0.0	0.0	0.0	40.0
Cohesion, psi	3.1	6.5	11.4	16.4	0.0

* $E_R = K\theta^n$ (E_R, K, and θ in psi)

Applied plate pressures ranged from 2 psi to πc psi (c is the subgrade cohesion). Pressures larger than πc are not of practical interest, since at higher pressures significant permanent deformation (rutting) will occur in the subgrade.

Plate pressure versus resilient displacement data are presented in Figures 3.2 and 3.3. Resilient modulus of subgrade reaction (K_R) versus plate deflection relations for the various subgrades are shown in Figures 3.4 through 3.7. The subgrades show a definite softening behavior (reduced K_R) with increasing pressures. The softening behavior is most pronounced for the soft subgrade (Fig.3.5), where K_R at a pressure of πc is approximately 60% of K_R at 2 psi. For a given plate pressure and subgrade type, a decrease in plate size results in a stiffer plate response (K_R increases).

3.3 ALGORITHM DEVELOPMENT

The ILLI-PAVE plate pressure-deflection data were analyzed using different theories and empirical equations described in Section 2.1, above (Table 3.2). The Ramberg-Osgood model and Butterfield and Georgiadis' cyclic plate-bearing model may be better suited for the case where both the loading and unloading pressure-deflection curves are of interest. However, these models did not provide a good fit for ILLI-PAVE resilient data. The hyperbolic model and Butterfield and Georgiadis' two parameter model did not adequately describe the ILLI-PAVE resilient pressure-deflection data either.

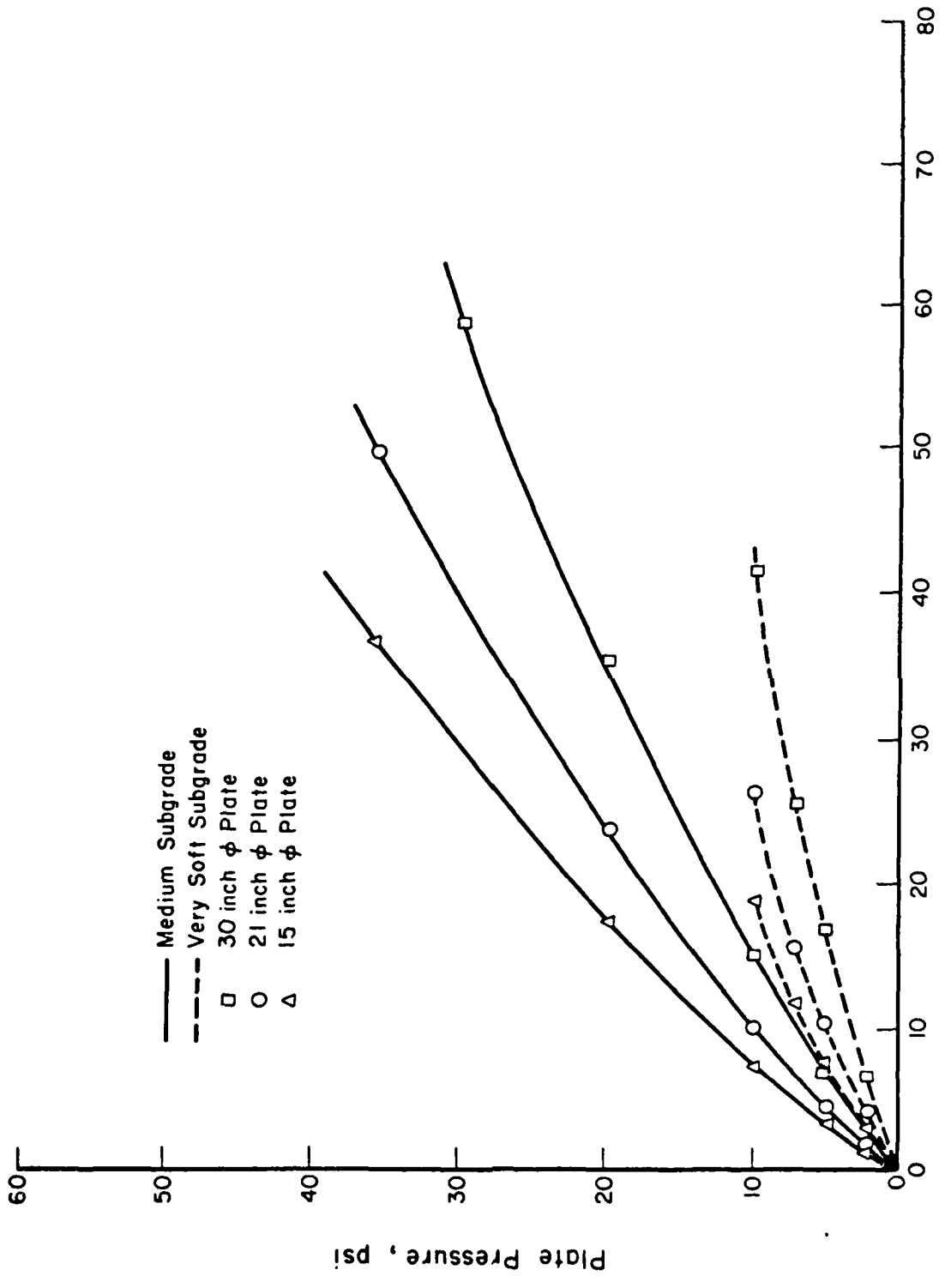

Fig. 3.2 Plate Pressure-Resilient Displacement Relations for Medium and Very Soft Subgrades

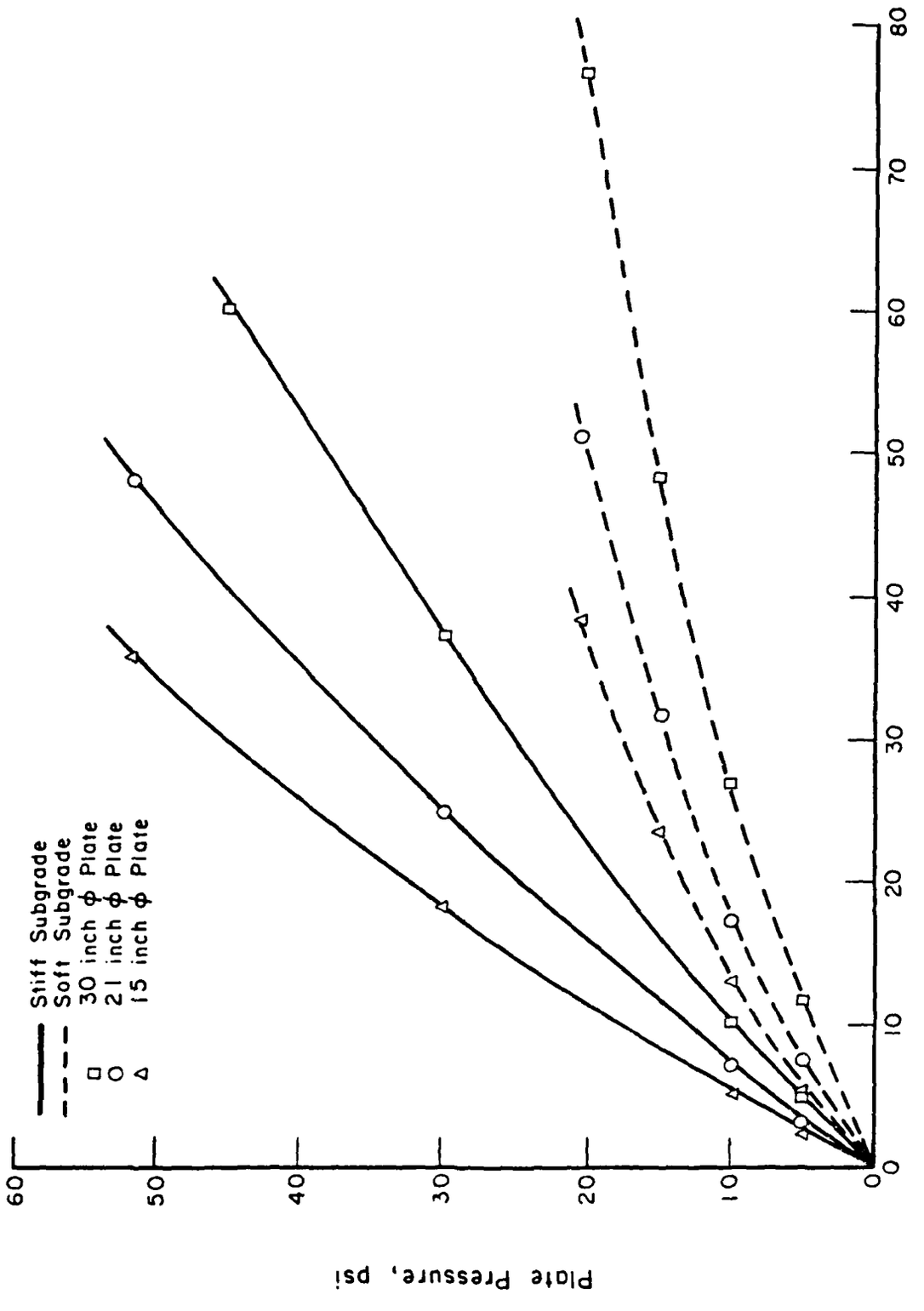

Fig. 3.3 Plate Pressure-Resilient Displacement Relations for Stiff and Soft Subgrades

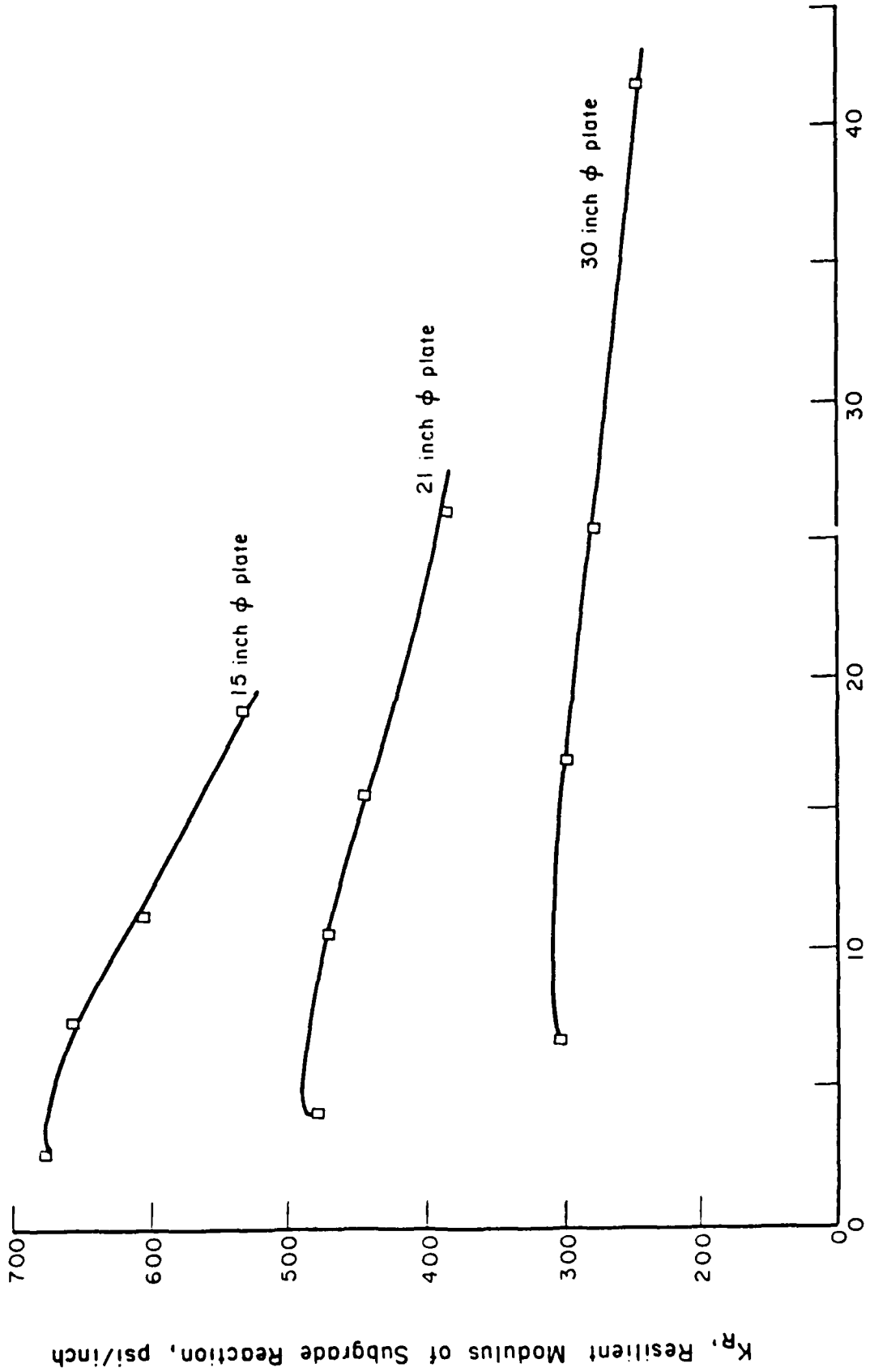

Fig. 3.4 K_R - Deflection Relations for Various Plate Sizes (Very Soft Subgrade)

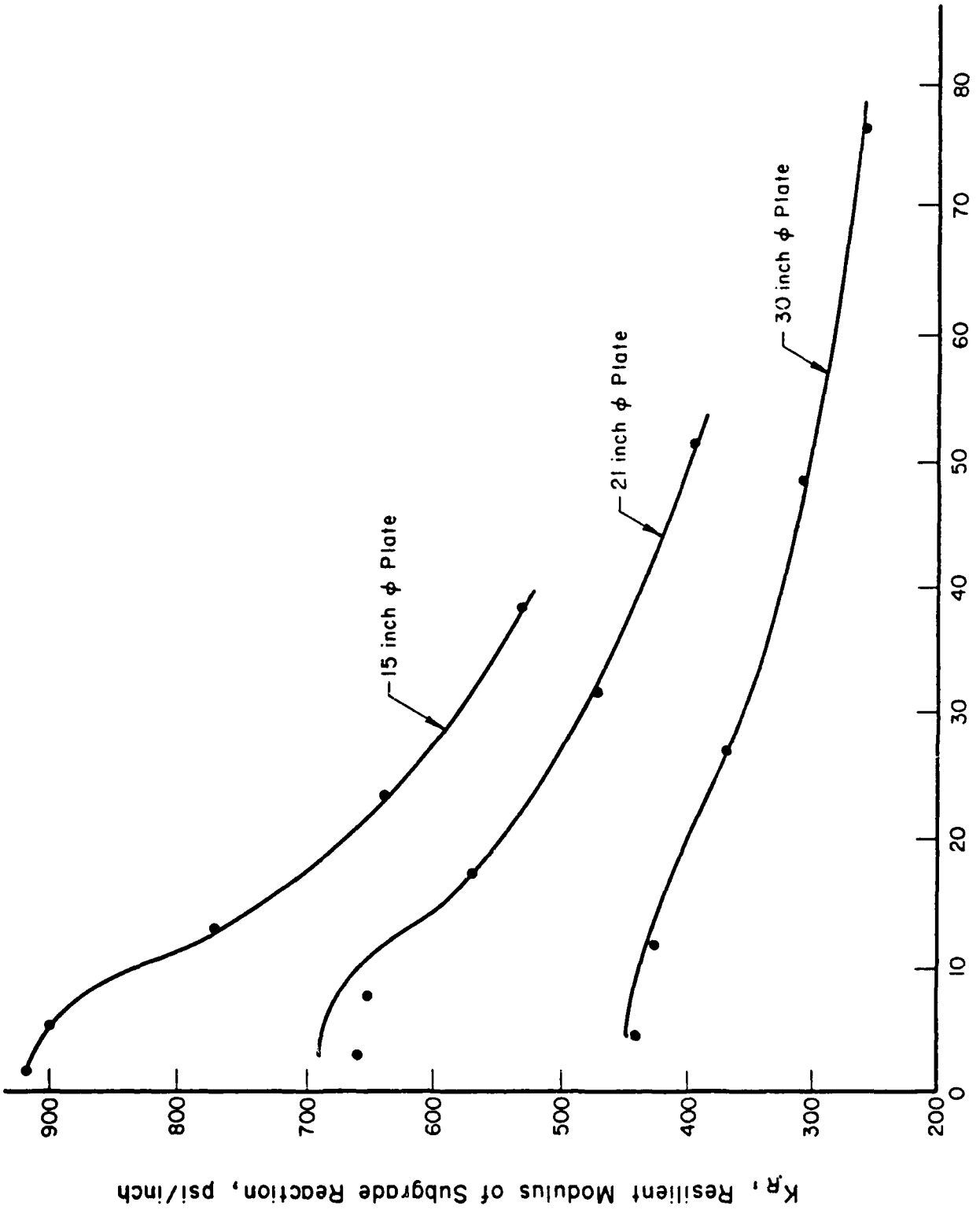

Fig. 3.5 K_R - Deflection Relations for Various Plate Sizes (Soft Subgrade)

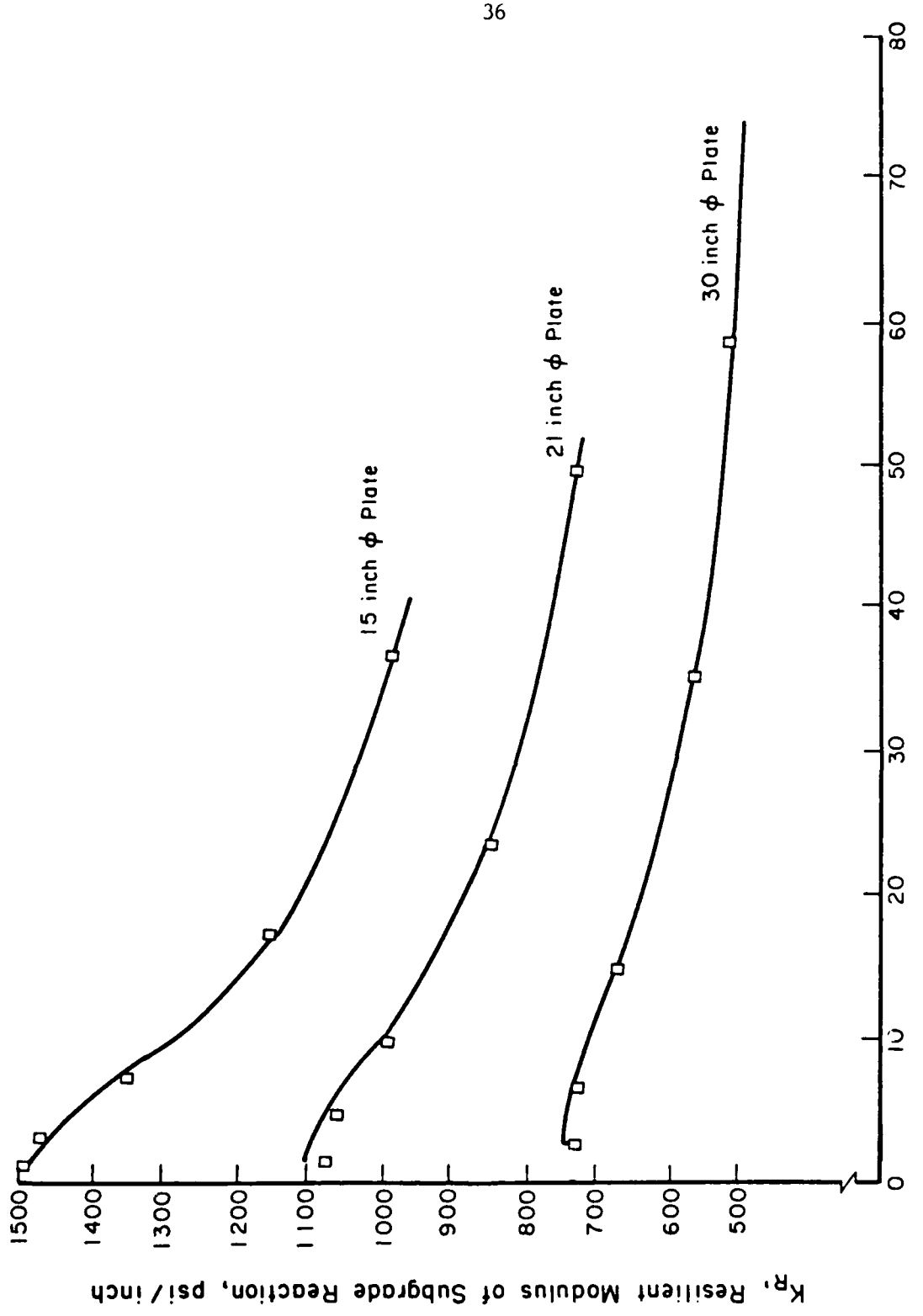

Fig. 3.6 K_R - Deflection Relations for Various Plate Sizes (Medium Subgrade)

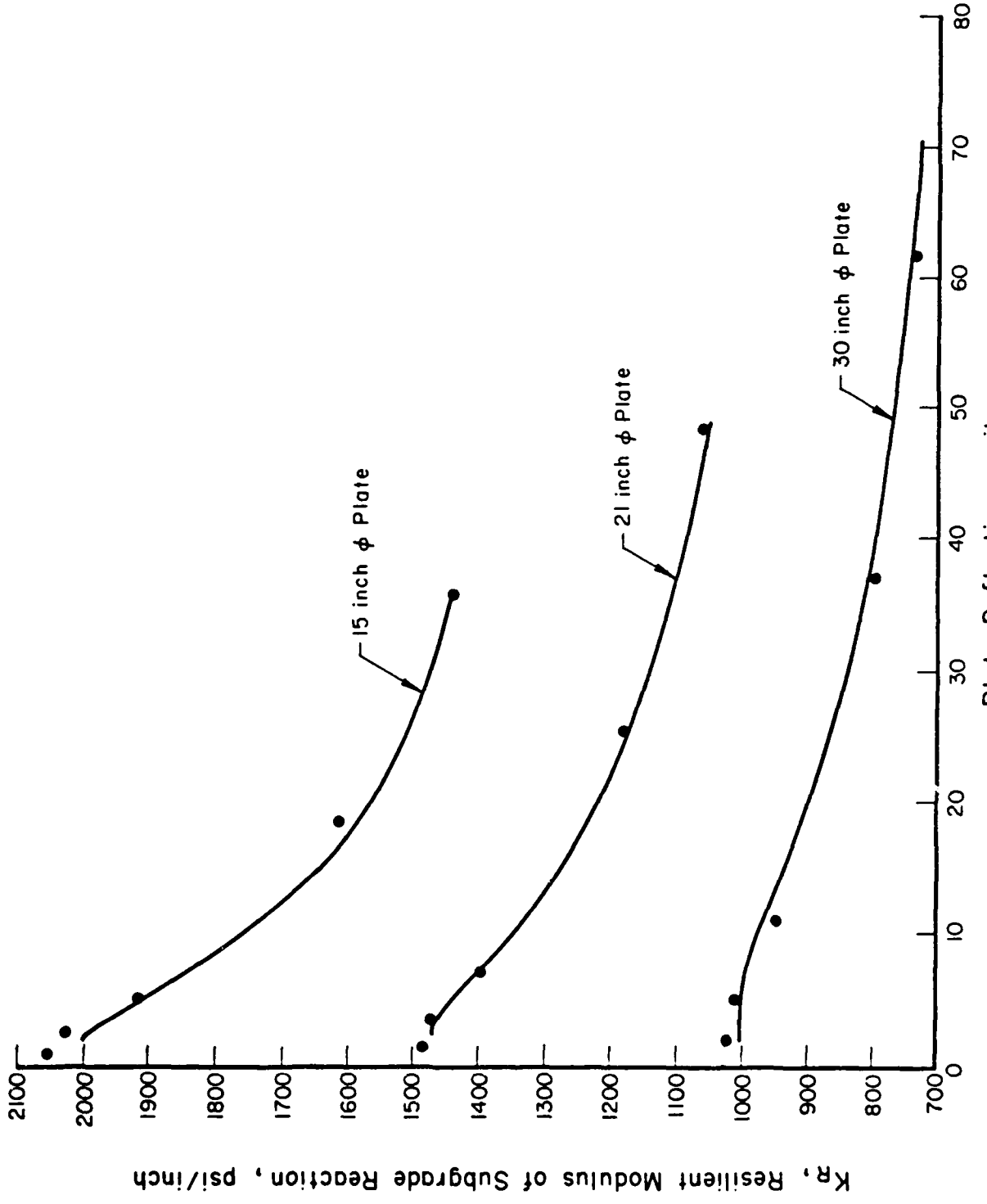

Fig. 3.7 K_R - Deflection Relations for Various Plate Sizes (Stiff Subgrade)

TABLE 3.2

MODELS CONSIDERED

MODEL	EQUATIONS		SYMBOLS
Ramberg-Osgood (7)	$\frac{w}{w_y} = \frac{p}{p_y} + a \left\lvert \frac{p}{p_y} \right\rvert^{r}$	for first loading	w : plate deflection p : plate pressure w_y, p_y: values of w and p at yield a, r : experimentally determined constants w_o, p_o: extreme values of w and p for any cycle
	$\frac{w - w_o}{2w_y} = \frac{p - p_o}{2p_y} + a \left\lvert \frac{p - p_o}{2p_y} \right\rvert^{r}$	for reloading	
Butterfield and Georgiadis Cyclic Model (12)	$k_u = k_o - C_2 \frac{Q_c}{Q_u} [1 + C_3 \log \{N/(Q_c/Q_u)\}]$	for unloading	k_o: initial stiffness k_f: final stiffness Q_u: load axis intercept Q_c: cyclic load k_r: reloading stiffness k_u: unloading stiffness C_1, C_2, C_3: experimentally determined constants N : number of cycles
	$k_r = k_o - C_1 \frac{Q_c}{Q_u}$	for reloading	
Hyperbolic Model (7)	$p = [\frac{1}{b+aw}]\ w$		a, b : experimentally determined constants
Butterfield and Georgiadis Two-parameter Model (8,11)	$q = k\, w_o + (4g^{0.5}/B) \int_o^{w_o} [p\, dw / \sqrt{2 \int p\, dw}]$		q : subgrade stress w_o : central deflection g : shear spring stiffness B : side length of rigid square plate
Butterfield and Georgiadis Empirical Equation (8,9)	$q = q_u (1 - \exp\{-(k_o - k_f)\, w / q_u\}) + k_f w$		q_u: pressure axis intercept

The empirical equation proposed by Butterfield and Georgiadis provided the best fit with the ILLI-PAVE data. This equation was modified for presenting the ILLI-PAVE plate pressure-resilient displacement data. A normalized deflection parameter (w/D_y) was substituted into the equation in place of w, where D_y represents the deflection at a plate pressure of πc psi (πc corresponds to the upper bound for plate pressures considered in the ILLI-PAVE analyses). The resulting equation is:

$$p = A_1 \left[1 - \exp \left\{ -A_2 \left(\frac{w}{D_y} - A_3\right) \right\} \right] + A_4 \left(\frac{w}{D_y} - A_3\right) + 2$$

where:

p : plate pressure;

w : plate deflection;

D_y : deflection factor for a given subgrade type (very soft; soft; medium; stiff);

A_1, A_2,... : subgrade constants.

If this equation is divided through by the plate deflection, w, the p/w term is K_R, the resilient modulus of subgrade reaction. The final K_R algorithm is:

$$K_R = \frac{A_1 \left[1 - \exp \left\{ - A_2 \left(\frac{w}{D_y} - A_3\right) \right\} \right] + A_4 \left(\frac{w}{D_y} - A_3\right) + 2}{w}$$

Regression analyses were used to develop four equations (one for each type of subgrade). The equation parameters for a 30-in. diameter plate are summarized in Table 3.3. Values of the correlation coefficient, R, standard error of estimate and coefficient of variation for the equations are also presented in Table 3.3. To be consistent with the subgrade resilient modulus-stress level relations (see Fig. 2.10), K_R is assumed to be a constant for pressures less than 2 psi.

Note that the resilient modulus of subgrade reaction, K_R, obtained from these algorithms, has values much greater than the corresponding static subgrade modulus, k, for any given soil. This is consistent with the observation that soils exhibit a much stiffer response when loaded by rapidly moving loads, rather than static loads. A similar observation was made earlier in relation to the values of E_{Ri} and static E (Section 2.2.2).

3.4 SUBBASE EFFECTS

3.4.1 Effect of a Granular Subbase

A layer of granular material is frequently used as a subbase in PCC pavement construction. The structural contribution of the granular material layer is generally acknowledged by assigning an increased design k to the granular layer-subgrade system (6,24).

TABLE 3.3

REGRESSION EQUATION PARAMETERS AND STATISTICS

Subgrade Type	A_1	A_2	A_3	A_4	A_5	D_Y	R*	SEE**	Coefficient of Variation, %
Very Soft	15.0	0.80	0.1680	0.62	11.9	0.0400	0.993	3.9	1.4
Soft	9.5	2.60	0.0594	10.25	33.7	0.0782	0.995	9.1	2.5
Medium	7.0	3.74	0.0377	28.10	53.1	0.0734	0.997	9.1	1.4
Stiff	5.0	5.30	0.0282	45.90	71.0	0.0707	0.995	13.9	1.5

* Correlation Coefficient

** SEE = Standard error of estimate (psi/in.)

$$K_R = \frac{A_1\left[1 - \exp\left\{-A_2\left(\frac{w}{D_y} - A_3\right)\right\}\right] + A_4\left(\frac{w}{D_y} - A_3\right) + 2}{w}$$

Plate load tests, employing a 30-in. diameter plate on a granular subbase-subgrade soil support system, were simulated using ILLI-PAVE. The properties of the granular subbase (gravel) are listed in Table 3.1. Three different granular subbase thicknesses (8, 16 and 24 in.) were considered. The applied plate pressure was 2c (c = subgrade cohesion). Figure 3.8 shows the effect of granular layer thickness on K_R for each of the four subgrades. It may be concluded that the introduction of a granular subbase up to 8-in. thick, has a pronounced beneficial effect on K_R. For higher thicknesses of subbase, the K_R-thickness effect decreases with an increase in the thickness of the granular subbase. Subbase thickness has only a slight effect within the 8 to 24-in. thickness range considered. The comments made in the previous section with regard to the seemingly high K_R-values, apply here as well.

Plate pressure effects were also evaluated for an 8-in. granular subbase layer thickness and a "soft" subgrade type. Plate pressures of c, 2c, and πc psi were considered. Comparative data for the no-subbase and subbase conditions are shown in Fig. 3.9. Plate pressure has only a nominal effect. The stress stiffening behavior of the granular material counteracts to some extent the stress softening behavior of the fine-grained subgrade.

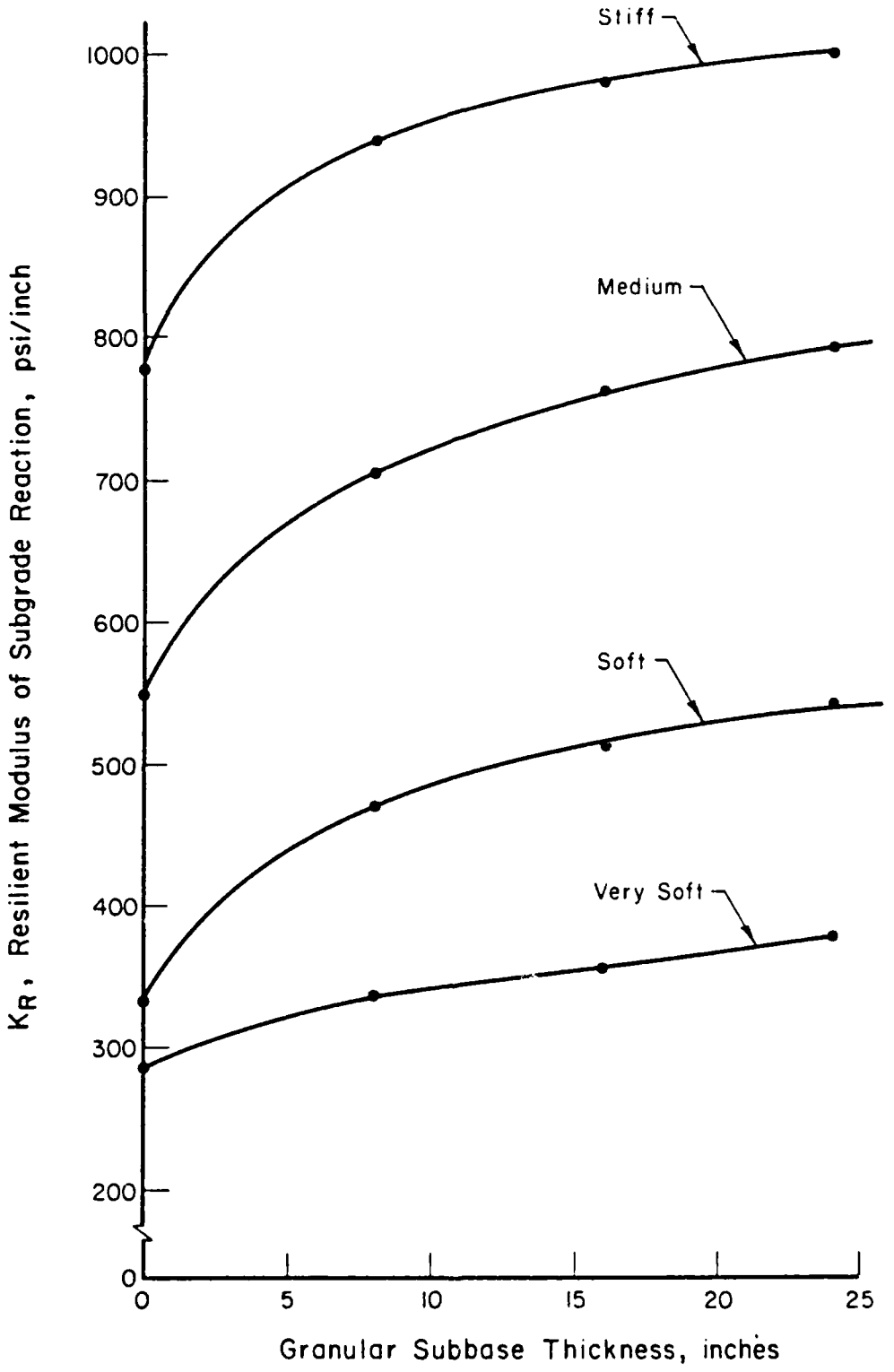

Fig. 3.8 K_R - Granular Subbase Thickness Effects

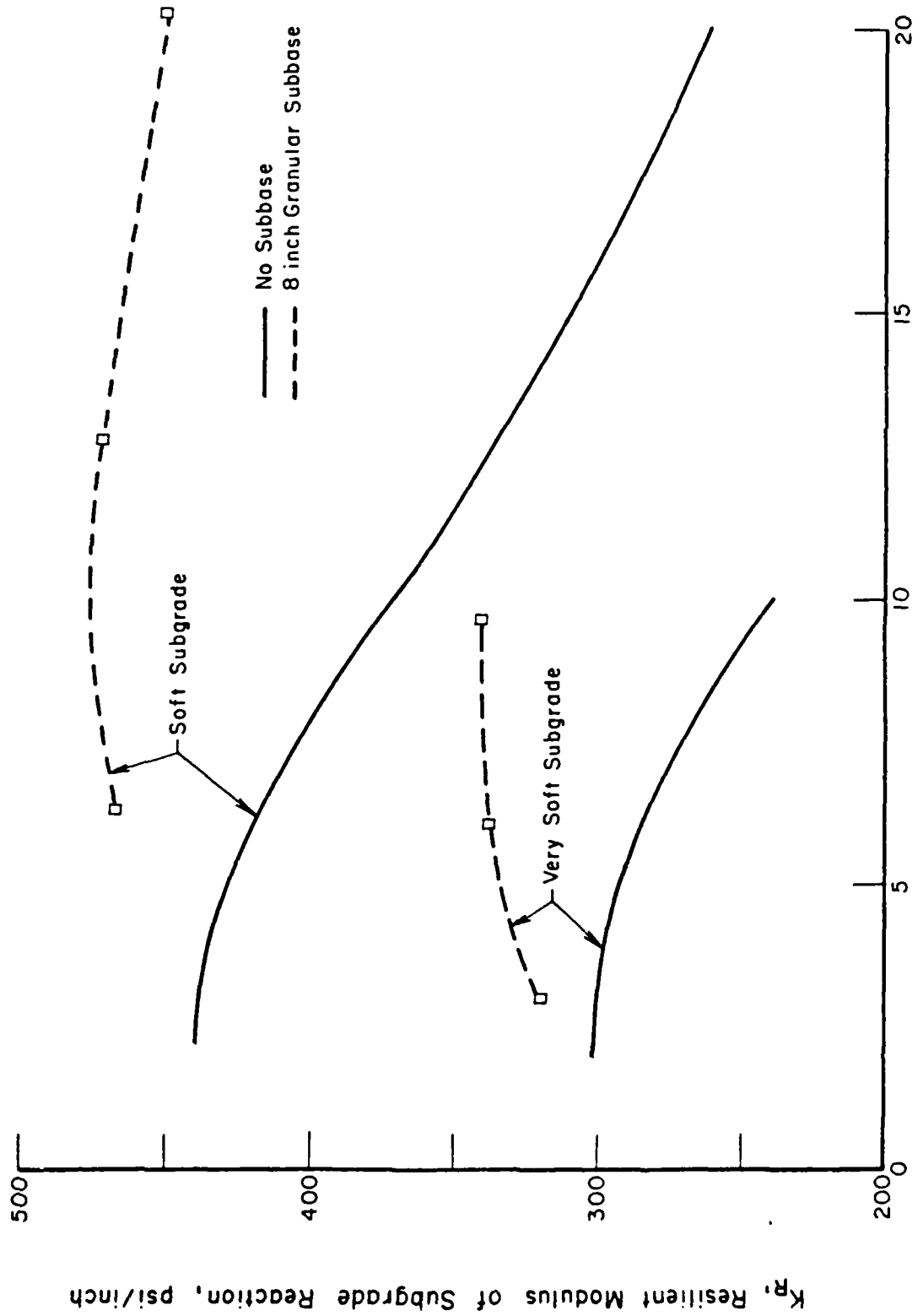

Fig. 3.9 K_R - Granular Subbase Effects for Variable Plate Pressures

3.4.2 Effect of a Stabilized Subbase

The effect of a high strength/modulus subbase for a PCC pavement can be considered by increasing k for the stabilized subbase-subgrade system. This procedure is recommended by the Portland Cement Association and the Federal Aviation Administration.

The ILLI-SLAB program considers the stabilized subbase as a flexural subbase beneath the PCC layer. This is a more desirable procedure than using an increased k, since the elastic properties of the subbase and its degree of bonding with the PCC slab can be considered.

CHAPTER 4

THE FINITE ELEMENT METHOD AS APPLIED TO SLAB-ON-GRADE DESIGN

4.1 GENERAL

The determination of stresses and deflections in slab-on-grade pavements with joints and/or cracks has been a subject of major concern for several years. For many pavement structures it has been virtually impossible to obtain analytical (closed form) solutions because of the complexity of geometry, boundary conditions, and material properties, unless certain simplifying assumptions are made. These, however, result in a modification of the characteristics of the problem. Since all the analytical (closed form) solutions are based on an infinitely large slab with no, or at most one discontinuity, they cannot be applied tc analysis of jointed or cracked slabs of finite dimensions, with or without load transfer systems at the joints and cracks.

With the advent of high speed digital computers, solution of these complex structural problems has been greatly facilitated. One of the most powerful methods that have evolved is the "Finite Element Method". This method of analysis is applicable to a wide range of complex, boundary value problems in engineering.

In the Finite Element Method the system to be analyzed is represented by an assemblage of subdivisions or discrete bodies called "finite elements". These elements are interconnected at specific locations called "nodes" or "nodal points". Functions are developed to approximate the distribution or variation of the actual displacements over each finite element. Such assumed functions are called "displacement functions" or "shape functions". Relationships are then established between these generalized displacements (usually denoted by {d}) and the generalized forces (usually denoted by {p}) applied at the nodes, using the principle of virtual work or some other variational principle. This element force-displacement relationship is expressed in the form of element stiffness matrices (usually denoted by [k]), each of which incorporates the material and geometrical properties of one element, viz.,

$$[k]\ \{d\} = \{p\}$$

The overall structural stiffness matrix, [K] is then formulated by superimposing the individual element stiffness matrices using the topological (element connectivity) properties of the structure. This "global" stiffness matrix is used to solve a set of simultaneous

equations of the form:

$$[K]\ \{D\} = \{P\}$$

where:

{P} = applied nodal forces for the whole system;

{D} = resulting nodal displacements for the whole system.

Various models have been developed for analyzing pavement systems using finite element (f.e.) techniques. A brief review of some of these follows.

4.2 THREE-DIMENSIONAL MODELS

All models reviewed in this study, except those described in the present section, are basically two-dimensional finite element models. The problem of a slab of finite dimensions on grade, however, involves processes that take place in three-dimensional space. Therefore, the response of the slab and the subgrade to loading, temperature and moisture changes etc., ideally requires a three-dimensional finite element model for accurate simulation. Nevertheless, there are several advantages to simulating the three-dimensional effects using two-dimensional finite element models. First, the difference in cost between a three-dimensional and two-dimensional calculation of the same mesh fineness can be several orders of magnitude depending on the size of the problem. In the three-dimensional case, there is a higher chance that any given mesh will exceed the memory core capacity of the computer. Second, due to its much lower cost, it is practical in a two-dimensional

analysis to increase the mesh fineness in selected zones, thereby increasing the accuracy with which the smaller scale phenomena can be observed. Even more important is the fact that three-dimensional analysis is beyond the state-of-the art of most engineering design groups. If three-dimensional finite element analysis were to be recommended as part of a standard pavement analysis procedure, it is doubtful that many designers would make use of the procedure.

On the other hand, theoretical analyses involving three-dimensional models are very desirable, not only in the investigation of those aspects that simply cannot be handled by a two-dimensional method, but also in providing helpful insight for the improvement and the better interpretation of the results of two-dimensional analyses. For example, the interaction between a loaded dowel and the surrounding concrete constitutes a three-dimensional state of stress. This interaction depends on the dimensions and elastic properties of the dowel bar and concrete slab, as well as any looseness between the dowel bar and the surrounding concrete. This makes the conventional dowel-concrete interaction model employed in the two-dimensional finite element programs not applicable. In the original development of ILLI-SLAB, Tabatabaie and Barenberg (25) performed a three-dimensional analysis of the concrete slab near the joint and around the dowel, in conjunction with the two-dimensional analysis of the jointed slab, to establish a realistic dowel-concrete interaction.

Such a two-stage analysis of the jointed pavement system provides a more reasonable engineering approach. A two-dimensional analysis is first performed, followed by a three-dimensional analysis of specific limited segments of the pavements. Results from the two-dimensional analysis are used as boundary conditions for the segments to be analyzed using the three-dimensional analysis.

In the original ILLI-SLAB study (1), the solid SAP finite element program developed by Wilson (26) was employed for the three-dimensional analysis. Figure 4.1 shows a typical finite element mesh used for the three-dimensional analysis of a small section of the concrete slab near the joint and around a dowel bar. Three-dimensional, 8-noded, isoparametric elements with three translational degrees-of-freedom (dof) per node, originally developed by Irons (27) were employed to represent the slab segment under study. The subgrade was idealized by spring elements. Dowel bars were modeled as beam elements with flexural and shear deformations. Either spring or elastic elements were used to represent the interaction between dowel bars and the surrounding concrete. In the regions where the dowel bar exerted pressure on the concrete, very stiff springs or very high elastic modulus elements were used to simulate this contact condition.

As a result of this and later analyses, the dowel bar is modeled in the two-dimensional ILLI-SLAB analysis by a bar element with one torsion and one deflection degree-of-freedom. This is preferable to both the original model, in which the bar element had one bending and one

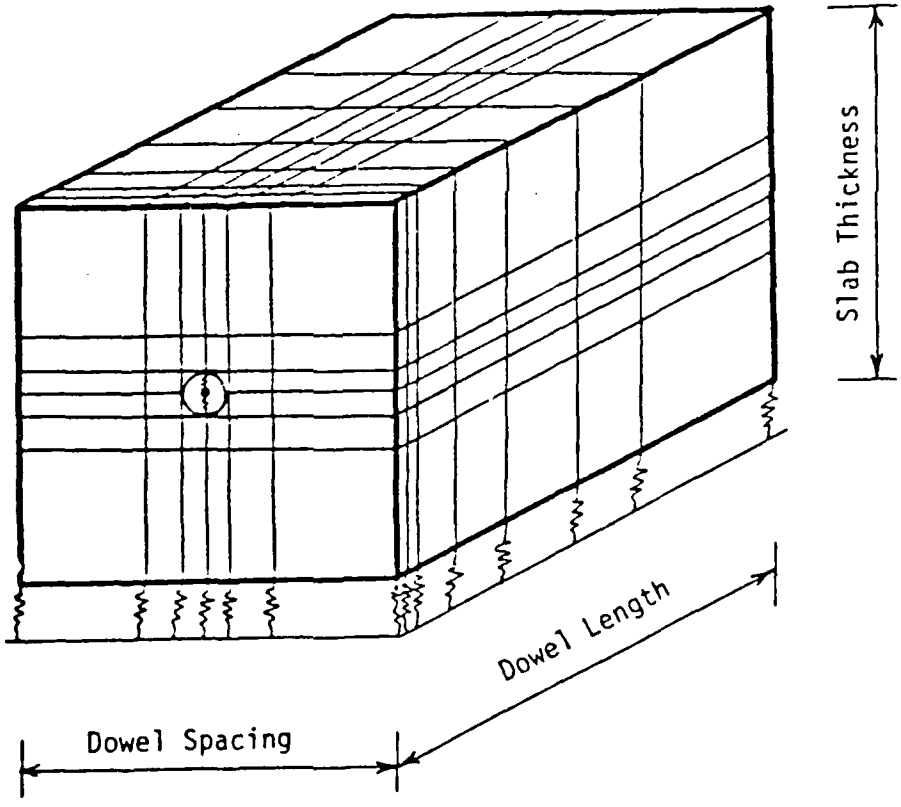

Fig. 4.1 A Typical F. E. Mesh Used for 3-Dimensional Analysis (After Tabatabaie, et al, 1979 - Ref. 1)

deflection degree-of-freedom, and to a third choice, that of a bar element with all three degrees-of-freedom.

Another three-dimensional finite element program was developed by Wilson and Pretorius (28) for the analysis of pavements. The program uses a constant strain prismatic solid element defined as a three-dimensional solid that has constant two-dimensional geometric shapes and infinite third dimension. Thus, the element properties can be varied at will in the transverse (x,z) plane, but are limited to 12 linearly elastic material types. These properties remain constant along the prisms in the longitudinal (y) direction. The system is essentially two-dimensional, with the third dimension introduced into the idealized structure by expressing the load as a Fourier series in this direction. Stresses and deformations caused by each Fourier term are summed, and the process is continued until further additions become insignificant. This program has been used to study the fatigue behavior of a cement-treated layer (29), reflection cracking through bituminous overlays (30), cracking in a treated pavement base layer (31), edge loading effects (32) and other problems. Execution times ran in the range of 30 to 35 minutes; a typical ILLI-SLAB run takes 5 to 10 seconds.

4.3 THE DISCRETE ELEMENT MODEL

This method is closer to a finite difference rather than a finite element solution to the problem of a medium-thick plate on a Winkler foundation. It was developed at the University of Texas (33,34,35) for the solution of problems involving discontinuous plates and slabs. The model is based on a physical representation of the slab as an assemblage of elastic springs, rigid bars and torsional bars grouped in a system of orthogonal beams (Fig. 4.2). The joints in the model are connected by rigid bars that are in turn interconnected by torsion bars representing the plate twisting stiffness, C. The flexible joint models the concentrated bending stiffness, D and the effects of Poisson's ratio, μ. The modulus of subgrade support, k is represented by independent elastic springs. The deflection at each joint is the unknown. The basic equilibrium equations are derived from the free body of a slab joint with all appropriate internal and external forces and reactions. These equations sum the vertical forces at each joint and the moments about each individual bar.

Computer programs developed at the University of Texas using the discrete element model are designated by the acronym SLAB. These programs can accommodate complex problems involving any combination of loads and boundary conditions, as well as a variety of discontinuities (cracks and joints) and support conditions. Thus, Hudson and Matlock (34) analyzed the case of partial subgrade support. The method was later extended for the elastic solid foundation (36,37). Ayyash et al (38)

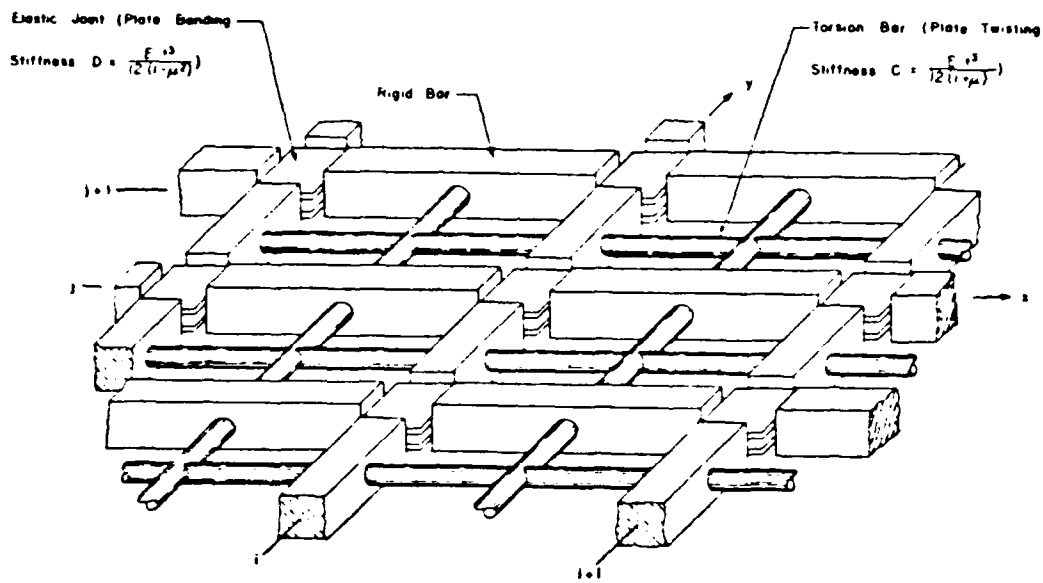

Fig. 4.2 Discrete Element Model of a Plate or Slab

used the program in a study of the effect of cracking on bending stiffness of a continuously reinforced concrete pavement (CRCP).

The discrete element model is helpful in visualizing the problem and forming the solution. It gives reasonable values for deflections but may be inaccurate in determining stresses along the edges. Furthermore, problems exist in the analysis of joints, cracks and gaps under the slab because of the nature of the method (39/1). The major advantages of the finite element over the discrete element method are that elements of various sizes can easily be incorporated in the analysis and no special treatment is needed at a free edge (40).

4.4 KENTUCKY

In this study, KENTUCKY denotes a finite element program developed at the University of Kentucky (40,41). The analysis is based on the classical theory of medium-thick plates and employs the 4-noded, 12-dof element, known as ACM or RPB12 in the finite element literature. The subgrade is modeled as a Winkler foundation by attaching four spring elements at the corners of each plate bending element. The program was developed for determining deflections and stresses in a system composed of a single-layer pavement arranged in series of up to three rectangular slabs, with or without load transfer at the transverse joints. The externally applied loads are converted to a system of statically equivalent nodal loads which often are not work equivalent to the applied loads.

The program can be used to investigate the effect of partial slab-subgrade contact. Problems involving partial contact are analyzed first by assuming the slab and subgrade are in full contact. If they are indeed in full contact, the problem is considered solved. Otherwise, an iterative procedure is employed. The reactive forces at the nodes out of contact are set to zero and the process is repeated until the assumed and the calculated contact patterns are the same. This procedure considers the self-weight of the slab, allowing for some 'precompression' of the subgrade springs produced by this weight.

Joints are modeled by equating the sum of the forces at each pair of nodes at a joint to the externally applied force(s) there, and by requiring that the deflections at these nodes be related according to the prescribed load transfer efficiency at the joint. This procedure destroys the symmetry of the stiffness matrix and results in an upper half band which is greater than the lower half. It is thus necessary to store both the upper and lower bands, at a considerable memory core expense. Bar elements are not used in modeling dowel bars because dowels are considered unable to transmit moments from one slab to the other over the very small joint width (39/1,25:Discussion).

4.5 WESLIQID

This program constitutes an enhanced version of KENTUCKY (39/1,2). Only the additions and/or changes to KENTUCKY made at Waterways Experiment Station in the preparation of WESLIQID will be described here.

WESLIQID can handle slab thicknesses and moduli of subgrade reaction which vary from node to node and any number of slabs arranged in any arbitrary pattern. The only restriction is the amount of memory core required. The pavement can consist up to two layers, bonded or unbonded. WESLIQID retains the KENTUCKY model in which the support springs are connected only at the nodal points.

Once the subgrade reactive forces at each mode are determined, stresses and strains in the soil are computed using Boussinesq's or Burmister's equations. An equivalent elastic modulus, E, corresponding to the subgrade modulus, k, is introduced for this purpose. Superposition is employed to compute the response to each of the nodal forces.

Four options are provided for specifying load transfer at the joints. Three involve shear transfer only while the fourth involves moment transfer. They are:

(a) Efficiency of Shear Transfer: The load transfer efficiency is specified as a ratio of the vertical deflections at two adjacent nodes on either side of the joint.

(b) Spring Constant: According to Chou (39/1), the use of imaginary shear transfer springs along the joint is more realistic than specifying a load transfer efficiency because the springs take into consideration the shear force at joint. The spring constant, defined as a force to cause unit deflection, is specified by the user.

(c) Diameter and spacing of dowels: Chou (39/1) considers this to be most straightforward and to yield results far superior to the other two options. This option applies only to cases where dowels are the only load transfer device. Dowel diameter, spacing and modulus of dowel support are specified by the user. The selection of the latter is a design decision depending upon the tightness with which the dowels are held in the concrete, the type of dowels, strength of concrete and method of construction.

(d) Efficiency of moment transfer: This is defined as a fraction of the full moment which is determined by assuming that the rotations on both sides are the same, rather than as the ratio of the rotations at two adjacent nodes on either side of the joint. A moment transfer efficiency of 100% implies equal rotations on both sides of the joint. A zero moment transfer efficiency requires that the moment of all nodal points along the joint is zero, although rotations may not be zero. Unless the efficiency is 0.0 or 1.0 at all joints it is necessary to analyze the problem twice. First, an efficiency of 1.0 is assumed for all joints where the real efficiency is not equal to

zero, to determine the 'full moments' along the cracks. These moments are multiplied by the real moment transfer efficiency and are applied as external moments during a second analysis.

4.6 FINITE

This is a general purpose computer system for the analysis of linear and nonlinear structures, developed at the Universities of Illinois and Kansas (42,43). FINITE supports a wide variety of elements, from the simplest one- and two-dimensional symmetric elements, to nonsymmetric elements, some types of hybrid elements and elements with varying degrees-of-freedom at each node.

For the purposes of this study, the term FINITE model refers to a representation of the slab on grade system using the RPB12 (or ACM) element for plate bending (44) with 4 supporting SPRING elements for the subgrade. This model is identical to that used in KENTUCKY and WESLIQID. In contrast to the latter two models --which use statically equivalent loads--, FINITE uses a work equivalent load vector (44) to convert applied external loads to nodal loads. The FINITE model is used to analyze a single slab with full contact and yields results identical to those obtained by the 'SPRINGS' option of revised ILLI-SLAB.

4.7 ILLI-SLAB

ILLI-SLAB was developed at the University of Illinois in 1977 for structural analysis of jointed, one- or two-layer concrete pavements with some load transfer system at the joints (1,2). The ILLI-SLAB model is based on the classical theory of a medium-thick plate on a Winkler foundation (49), and can evaluate the structural response of a concrete pavement system with joints and/or cracks. It employs the 4-noded, 12-dof plate bending (ACM or RPB12) element (44). The Winkler type subgrade is modeled as a uniform, distributed subgrade through an equivalent mass formulation (55). This is a much more realistic representation than the four concentrated spring elements in WESLIQID and FINITE. A work equivalent load vector is used (44), as in FINITE.

The assumptions regarding the concrete slab, stabilized base, overlay, subgrade, dowel bar, keyway, and aggregate interlock can be briefly summarized as follows:

(i) The small deformation theory of an elastic, homogeneous medium-thick plate is employed for the concrete slab, stabilized base and overlay. Such a plate is thick enough to carry transverse load by flexure, rather than in-plane force (as would be the case for a thin membrane), yet is not so thick that transverse shear deformation becomes important. In this theory, it is assumed that lines normal to the middle surface in the undeformed plate remain straight, unstretched and normal to the middle surface of the deformed plate, each lamina parallel to

the middle surface is in a state of plane stress, and no axia or in-plane shear stress develops due to loading.

(ii) The subgrade behaves as a Winkler foundation.

(iii) In case of a bonded stabilized base or overlay, full strain compatibility exists at the interface, or for the unbonded case shear stresses at the interface are neglected.

(iv) Dowel bars at joints are linearly elastic, and are located at the neutral axis of the slab.

(v) When aggregate interlock or a keyway is used for load transfer, load is transferred from one slab to an adjacent slab by shear. However, with dowel bars some moment as well as shear may be transferred across the joints.

Various types of load transfer systems, such as dowel bars, aggregate interlock, keyways, or a combination of these can be considered at the pavement joints. The model can also accommodate the effect of a stabilized base or an overlay (either with perfect bond or no bond). Thus, ILLI-SLAB provides several options, that can be used in analyzing the following problem types:

1. Jointed concrete pavements with load transfer systems at the joints.
2. Jointed reinforced concrete pavements with cracks having reinforcement steel at the cracks.
3. Continuously reinforced concrete pavements.
4. Concrete shoulders with or without tie bars.
5. Concrete pavements with a stabilized base or an overlay,

assuming either a perfect bond or no bond between the two layers.

6. Concrete slabs of varying thicknesses and moduli of elasticity, and subgrades with varying moduli of support.

The program inputs are:

(a) Geometry of the slab, including the type of base or overlay, load transfer system, subgrade, and slab dimensions.

(b) Elastic properties of the concrete, stabilized base or overlay, load transfer system, and subgrade.

(c) Loading.

The outputs given by the program are:

(a) Nodal stresses in the slab, stabilized base or overlay.

(b) Vertical surface stresses of the subgrade.

(c) Nodal deflections and rotations.

(d) Reactions on the dowel bars.

(e) Shear stresses at the joint for the aggregate interlock and keyed joint systems.

The model was verified by comparison with the available theoretical solutions and the results from experimental studies (1,25).

4.8 TYPICAL RESULTS AND COMPARISONS

4.8.1 Objectives

The purpose of the analyses described in this section is threefold:

(1) Recent modifications (described in Chapter 5) to essential features of ILLI-SLAB, viz. the subgrade stiffness matrix, as well as the addition of several higher-level routines (eg. free-form input, contouring, subgrade types, stress dependence, etc.) have created the need for a revalidation of the program. Such revalidations have been carried out in the past since the publication of Ref. 1 in 1979, by various graduate students as part of their studies and research at the University of Illinois. These, however, have been incomplete and remained scattered in the private files of each worker. As a result, no benefit could be derived from them by ILLI-SLAB users at large. Several of these unpublished studies are referenced in this section.

(2) In the preceding sections several available models were reviewed. Completeness demands that typical results be presented and comparisons made between ILLI-SLAB and other programs. The purpose of such comparisons is primarily to provide a further means for validating the ILLI-SLAB model, rather than to assert the superiority of one particular model. Different models may perform better than others depending on the problem considered. It is obvious that the restricted scope of the analyses presented in this report do not exhaust the

capabilities of each model.

(3) The most efficient utilization of the capabilities of ILLI-SLAB, as well as any of the other programs, greatly depends upon the extent of the user's familiarity with simple and yet very important factors affecting the program's performance. The analyses presented herein aim at providing some guidelines that can be applied by the user when ILLI-SLAB is employed in typical pavement design and analysis problems.

4.8.2 Problems Investigated

In the present study the following questions are addressed using a well-designed factorial of ILLI-SLAB and WESLIQID runs:

(i) How does the revised version of ILLI-SLAB compare to that used in the validation presented in Ref. 1? (As the reader may already know, the conclusion of this validation was that ILLI-SLAB agreed with Westergaard very well).

(ii) How should the circular loaded area assumed by Westergaard be modeled in ILLI-SLAB? What is the effect on response of different ways of loaded area representation?

(iii) Since ILLI-SLAB can accommodate partially loaded elements, what is the effect of load placement with respect to the finite element mesh? Is there any particular configuration which can be recommended to the general ILLI-SLAB user?

(iv) Finite element theory requires that in the limit of mesh refinement, the finite element solution should approach the

correct closed-form solution (if available). Is this true of ILLI-SLAB? If not, why not?

(v) How does slab size affect the manner in which ILLI-SLAB results approach the Westergaard solution? Are the empirically developed slab size criteria verified by the finite element method, or do they require redefinition?

(vi) What is the effect of element aspect ratio? How important is it to have square elements?

(vii) How is the relation between Westergaard and f.e. solutions affected by the extent of the loaded area?

To provide answers to these questions, the interior loading condition was chosen. This condition has been extensively studied and is well understood. Theoretical analyses are available and they have been found to be much closer to observed pavement behavior than for any other loading condition. This condition also lends itself for a factorial of simple runs using finite element programs at a relatively low cost. The conclusions drawn from the investigation of the interior condition are believed to be general enough to apply to other conditions as well.

4.8.3 Comparison of the Present Version of ILLI-SLAB to That Developed by A. Tabatabaie

The original ILLI-SLAB code contained several errors, notably in the formulation of the stiffness matrix for the subgrade. These have now been corrected (see Chapter 5), but this created a credibility problem for the excellent agreement with Westergaard theory reported in Ref. 1. In order to verify the results obtained during that study, the same factorial of ILLI-SLAB runs was performed using the updated version of the program and the results are compared to those reported by Tabatabaie et al (1) in Table 4.1a.

The original factorial (1) consisted of 3 slab thicknesses, 12, 16 and 20 in. and 3 moduli of subgrade reaction, 50, 200 and 500 psi/in. A 25-ft. square slab was used in the analysis. As will be shown in a later paragraph, this slab may be slightly smaller than the minimum requirement for the development of the Westergaard infinite slab condition, in view of a large radius of relative stiffness. The modulus of elasticity and Poisson's ratio of the concrete slab were assumed to be 5×10^6 psi and 0.15, respectively. A single load of 50 kips was modeled as a 15 in. x 15 in. area with a load intensity of 222.2 psi. The results were compared with the Westergaard solution in which the 50 kip load is distributed over a circular area 15 in. in diameter (WESI in Table 4.1a). Some results tabulated in Table 4.1a are also plotted in Fig. 4.3. The mesh used for these runs is shown in Fig. 4.4.

TABLE 4.1

(a) REVALIDATION OF ILLI-SLAB

RUN No.	k (psi/in.)	h (in.)	ℓ (in.)	DEFLECTION (mils)			BENDING STRESS (psi)		
				Ref. 1	Revised ILLI-SLAB	WESI	Ref. 1	Revised ILLI-SLAB	WESI
1	50		61.95	36.3	35.8	32.3	562.9	562.4	528.0
2	200	12	43.81	16.9	16.6	16.1	488.0	487.2	461.9
3	500		34.84	10.3	10.1	10.1	443.2	442.3	418.2
4	50		69.55	29.4	29.1	25.7	431.1	430.9	399.1
5	200	14	49.18	13.8	13.5	12.8	376.3	375.8	350.5
6	500		39.11	8.3	8.2	8.0	341.9	341.3	318.4
7	50		76.87	24.6	24.4	21.0	340.4	340.3	311.5
8	200	16	54.36	11.5	11.3	10.5	300.4	300.1	274.3
9	500		43.23	6.9	6.8	6.6	273.0	272.5	249.8
10	50		90.88	18.9	18.8	15.1	226.4	226.4	203.9
11	200	20	64.26	8.5	8.4	7.5	205.4	205.3	180.1
12	500		51.10	5.1	5.0	4.7	187.4	187.1	164.4

Notes:

Finite Element Solution

Slab: 25'x25' ($\frac{L}{\ell}$=3.3 to 8.6)

$E = 5 \times 10^6$ psi

$\mu = 0.15$

p = 222.2 psi

A = 15"x15" interior

Mesh: Fig. 4.4

Theoretical Solution (WESI)

P = 50,000 lb.

p = 282.94 psi

a = 7.5"

Equations used:

Special Theory - Infinite Slab-Circular Load

$$\sigma_i = 0.275\ (1 + \mu)\ \frac{P}{h^2}\ (4\log_{10}\frac{\ell}{b} + 1.069)$$

$$\delta_i = \frac{P}{8k\ell^2}\ [(1 - \frac{a^2}{\ell^2}\ (0.217 - 0.367\ \log_{10}\frac{a}{\ell})]$$

$$b = \sqrt{1.6a^2 + h^2} - 0.675h \quad \text{for } a < 1.724$$

$$= a \quad \text{for } a > 1.724$$

TABLE 4.1 (Cont'd)

(b) COMPARISON WITH WESTERGAARD SOLUTIONS

RUN No.	DEFLECTION (mils)			BENDING STRESS (psi)					
				WESI		WESII			Revised
	WESI	WESII	REVISED ILLI-SLAB	ORD. THEORY	SP. THEORY	ORD. THEORY	SP. THEORY	WESIII	ILLI-SLAB
1	32.3	32.2	35.8	520.3	528.1	497.3	508.4	495.2	562.4
2	16.1	16.0	16.6	454.5	462.3	431.6	442.7	429.5	487.2
3	10.1	10.0	10.1	411.1	418.9	388.3	399.4	386.2	442.3
4	25.7	25.6	29.1	398.4	399.1	381.5	386.4	379.9	430.9
5	12.8	12.7	13.5	350.0	350.7	333.2	338.0	331.6	375.8
6	8.0	8.0	8.2	318.1	318.8	301.3	306.1	299.8	341.3
7	21.0	21.0	24.4	315.7	311.5	302.8	303.0	301.6	340.3
8	10.5	10.4	11.3	278.7	274.5	265.8	265.9	264.6	300.1
9	6.6	6.6	6.8	254.2	250.0	241.3	241.5	240.2	272.5
10	15.1	15.1	18.8	213.5	203.9	205.3	199.7	204.5	226.4
11	7.5	7.5	8.4	189.8	180.1	181.5	175.9	180.8	205.3
12	4.7	4.7	5.0	174.1	164.5	165.9	160.3	165.1	187.1

Notes:

See Table 4.1(a) for values of k,h,ℓ and Notes on F. E. Solution and WESI.

Theoretical Solutions

WESII, WESIII

P = 50,000 lb.

p = 222.2 psi

a = 8.46" (WESII)

c = 15" (WESIII)

Equations Used:

WESI, WESII: $\sigma_i = \frac{3}{2\pi}(1+\mu)\frac{P}{h^2}\left[\left\{\ln\frac{2\ell}{a}\right\} - \gamma + \frac{1}{2} + \frac{\pi}{32}\left(\frac{a}{\ell}\right)^2\right]$

(Ordinary Theory Circular Load)

$$\delta_i = \frac{P}{8k\ell^2}\left[1 + \frac{1}{2\pi}\left(\left\{\ln\frac{a}{2\ell}\right\} + \gamma - \frac{5}{4}\right)\left(\frac{a}{\ell}\right)^2\right]$$

For Special Theory, substitute b for a in Equation for σ_i.

WESIII: Substitute c' for a in Equation for σ_i, where

(Ordinary Theory Square Load) $c' = \frac{e^{\frac{\pi}{4}} - 1}{\sqrt{2}}\,c$; c = side of square load

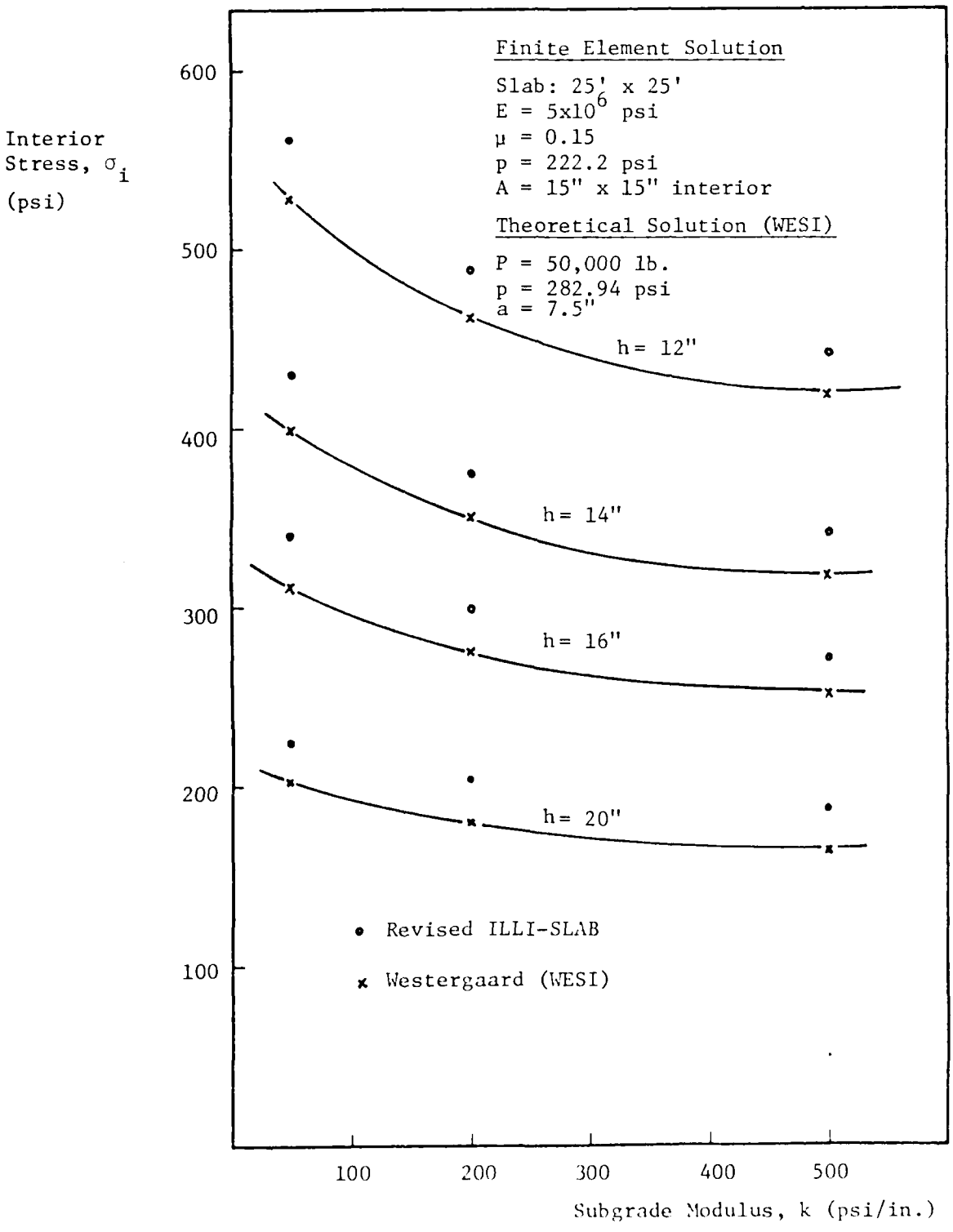

Fig. 4.3 Revalidation of ILLI-SLAB

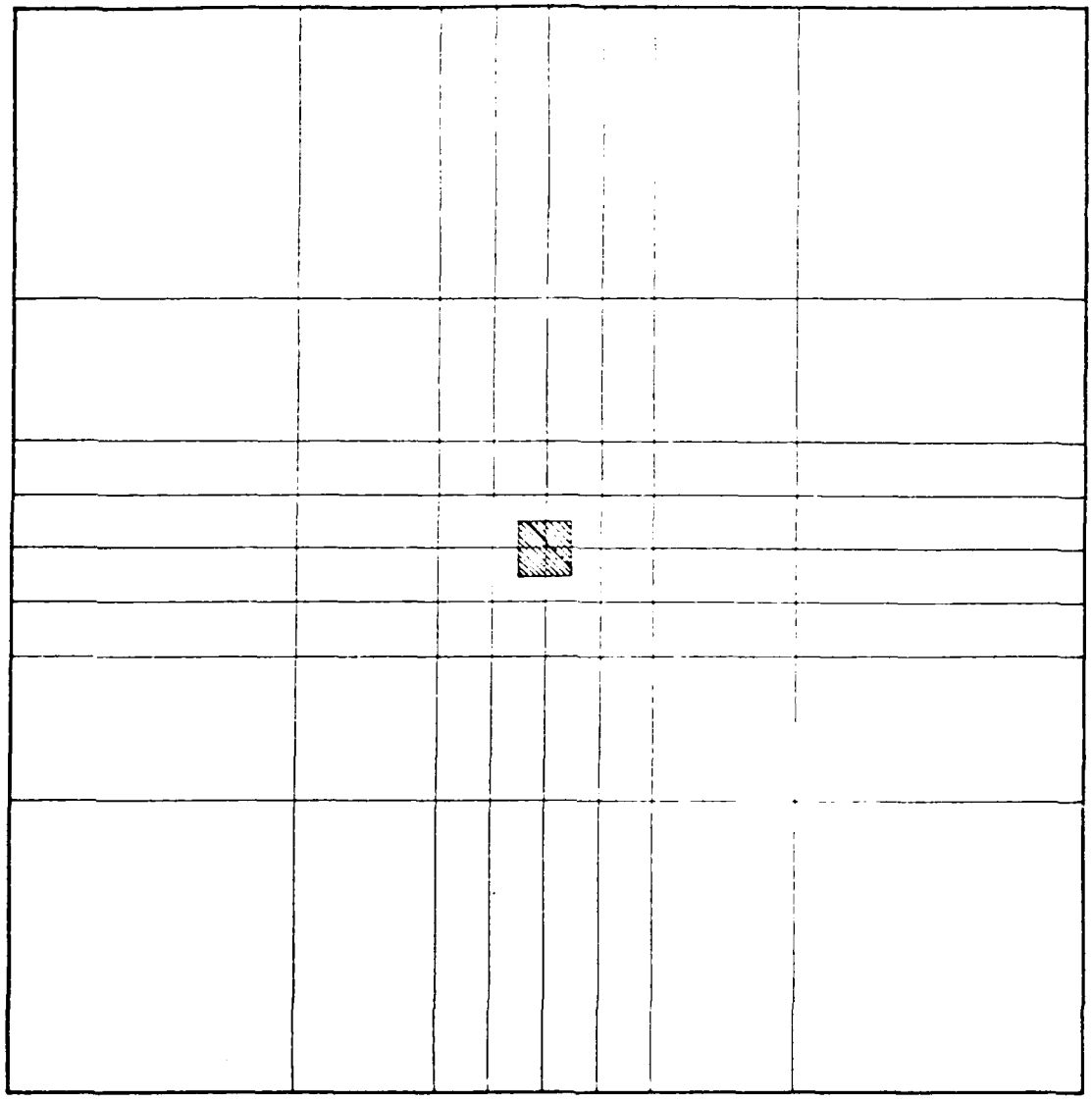

Fig. 4.4 F. E. Mesh Used for Revalidation of ILLI-SLAB (Mesh I)

For the cases considered the results of the updated version are slightly improved compared to those of the original version. The difference between the two versions is very small, from an engineering viewpoint. Any conclusions reached by previous studies using the original version are considered valid.

4.8.4 Effect of Load Representation

In Table 4.1b comparisons of the finite element solution are presented with three different Westergaard idealizations, WESI, WESII and WESIII. The difference is the way the square or rectangular loaded area in ILLI-SLAB is modeled for Westergaard's analysis. WESI is the same representation as used in Ref. 1 and was retained here for consistency. It essentially matches the total load, P and the diameter of the loaded area (which is assumed to be equal to the side of the square loaded area in the finite element solution). As a result, the load intensity used in the finite element solution (222.20 psi) is different from that in the Westergaard idealization (282.94 psi).

A more rigorous representation is attempted in WESII where the total load (P) and the load intensity (p) are matched, while the diameter of the equivalent circular load is chosen to retain the same area, despite the fact that this leads to a higher diameter than the side of the square element (16.92 in. cf. 15.0 in.).

Finally, in WESIII the load is treated as a square of the same side length and load intensity as in the f.e. analysis. Such a solution is only available for the maximum bending stress of the interior condition.

The following equations were used in Ref. 1 for the Westergaard solution:

$$\sigma_i = 0.275\ (1 + \mu)\ \frac{P}{h^2}\ \left(4 \log_{10} \frac{\ell}{b} + 1.069\right)$$

$$\delta_i = \frac{P}{8k\ell^2}\ \left[1 - \frac{a^2}{\ell^2}\ \left(0.217 - 0.367 \log_{10} \frac{a}{\ell}\right)\right]$$

$$b = \sqrt{1.6a^2 + h^2} - 0.675h \quad \text{for } a < 1.724h$$
$$= a \quad \text{for } a > 1.724h$$

(NB:- The equation for deflection is misquoted in Ref. 1 without the factor of 8, evidently due to a typographical error. Also, in the calculation of b, the factor 1.724h is wrongly stated as 1.74h).

In the expression for the interior stress, an equivalent radius, b was introduced by Westergaard (45) to account for the effect of shear stresses in the vicinity of the applied load. This effect is neglected in the "ordinary theory" of medium-thick plates, in which the true radius, a, is used. The validity of this semi-empirical adjustment and of the resulting "special theory" has been debated by various investigators [see, for example, Scott (10)], but a discussion of this issue would be beyond the scope of this report. It is considered, however, that the results of a f.e. solution as obtained from ILLI-SLAB, should be compared to Westergaard's "ordinary theory", because both ignore the effect of shear stresses. Such a comparison is much more

meaningful as will be shown below.

The following general form of the Westergaard equations was used in this study (WESII):

$$\sigma_i = \frac{3}{2\pi} (1 + \mu) \frac{P}{h^2} \left[\left\{ \ell n \frac{2\ell}{a} \right\} - \gamma + \frac{1}{2} + \frac{\pi}{32} \left(\frac{a}{\ell}\right)^2 \right]$$

$$\delta_i = \frac{P}{8k\ell^2} \left[1 + \frac{1}{2\pi} \left(\left\{ \ell n \frac{a}{2\ell} \right\} + \gamma - \frac{5}{4} \right) \left(\frac{a}{\ell}\right)^2 \right]$$

γ = Euler's Constant (= 0.577 215 664 901 532 860 61 ...)

These equations differ from those quoted above inasmuch as the former are a specialized and simplified (hence, not as rigorous) version of the latter. Furthermore, the general equation for interior stress includes Westergaard's "supplementary" σ_2 stress (46). Although this usually makes only a small contribution, it is included here for completeness.

To obtain the interior stress in the case of a square loaded area (WESIII), the radius of the circular load, a, in the equation above, is replaced by a constant c', related to the length of the side of the square, c, as follows:

$$c' = \frac{e^{\frac{\pi}{4}} - 1}{\sqrt{2}} c$$

The resulting expression is not stated explicitly by Westergaard, but follows directly from his theory (47,48). Timoshenko and Woinowsky-Krieger (49) provide a theoretical justification for this

solution by showing that, loaded by the same total load P, a square side c and a circle radius a, give the same maximum interior stress.

Table 4.1b shows that the WESII representation yields, in general, lower deflections and bending stresses than WESI (with deflections being much less sensitive). Furthermore, the discrepancy between the finite element responses and WESII is greater than that with WESI, indicating that using WESI may tend to conceal some of the differences between Westergaard and the finite element analysis. WESI appears to agree better with the finite element solution. It is shown below that this "improvement" is only apparent.

Note in Table 4.1b that both the finite element deflections and bending stresses are slightly higher than Westergaard's. Deflections are much less sensitive to changes in load representation and are closer to theory than bending stresses. This agrees with the observation that deflections are much less sensitive to changes in the finite element discretization and even formulation. Computer program validations which quote only comparisons of theoretical and calculated deflections (50) may be misleading.

As will be noted in subsequent paragraphs, the difference between calculated and theoretical responses may be attributed to:

1. The 25-ft. square slab may be too small to develop the Westergaard infinite slab condition thus leading to higher

calculated deflections. This should also lead to somewhat lower calculated stresses, however, a feature not observed in Table 4.1b;

2. The placement of the load on top of a single node (Fig. 4.4) leads to higher calculated stresses and deflections;
3. The use of elements with aspect ratios much different from unity. Note that the mesh in Fig. 4.4 was used in Ref. 1 and is retained here for consistency;
4. The relatively large size of the loaded area. This is deemed to be the most important factor in this case.

4.8.5 Effect of Load Placement with Respect to Finite Element Mesh

The effect of load placement with respect to the finite element mesh was investigated for one of the cases presented in Table 4.1 (k = 200 psi/in. and h = 14 in.). Three different mesh configurations were used:

- Mesh I (Fig. 4.4) is the one used for all runs in Table 4.1 and has the load placed on top of one central node, without any corner nodes;
- Mesh II (Fig. 4.5) introduces 4 corner nodes in addition to the central node, thus turning the 9x9 mesh in Fig. 4.4 into an 11x11 mesh, requiring 71% more memory spaces to execute. It is, however, considered a closer representation of reality;
- Mesh III (Fig. 4.6) has the 4 corner nodes but the central node is missing. It is thus a 10x10 mesh, requiring only 32% more memory spaces to execute than Mesh I.

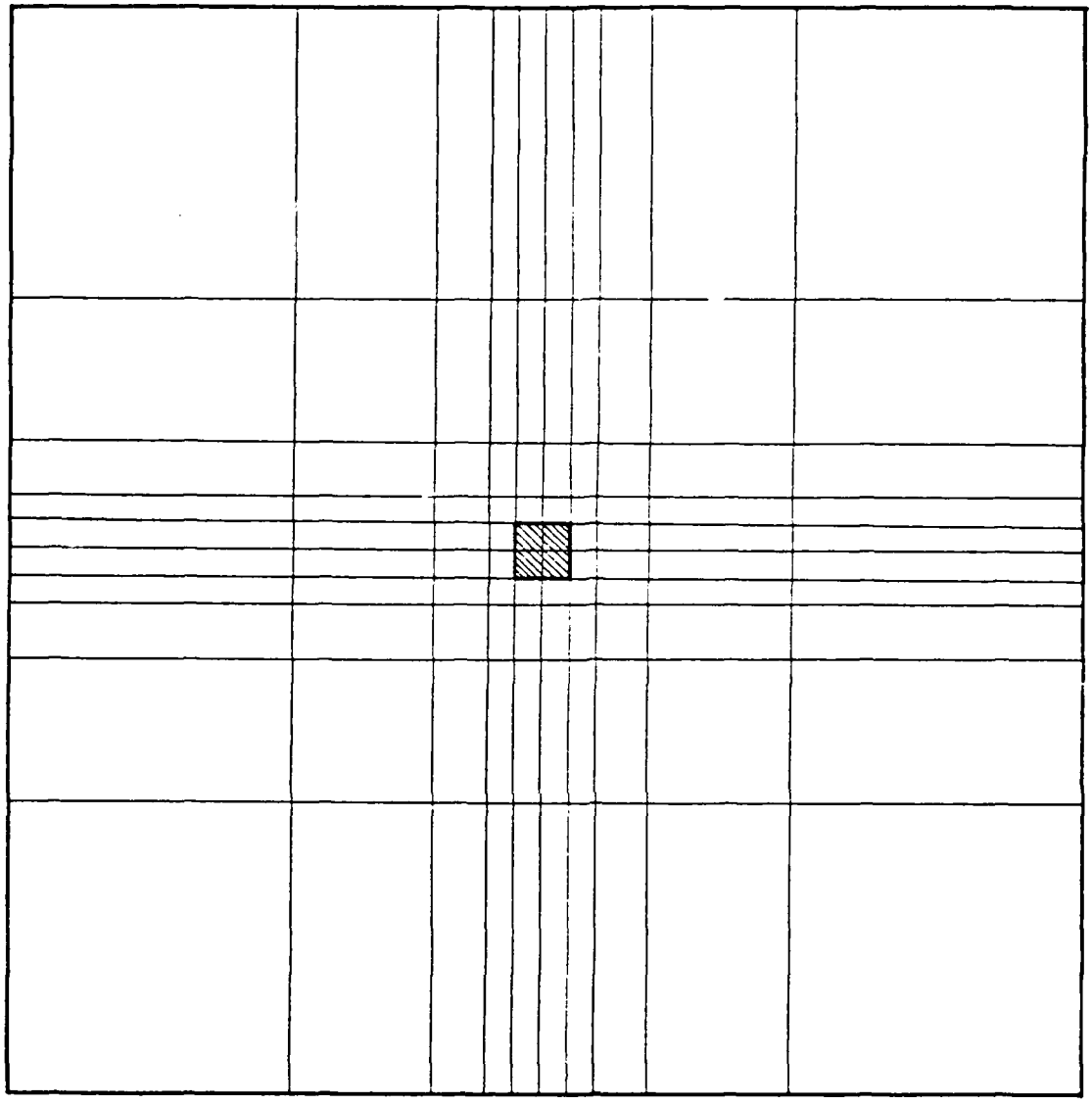

Fig. 4.5 Effect of Load Placement (Mesh II)

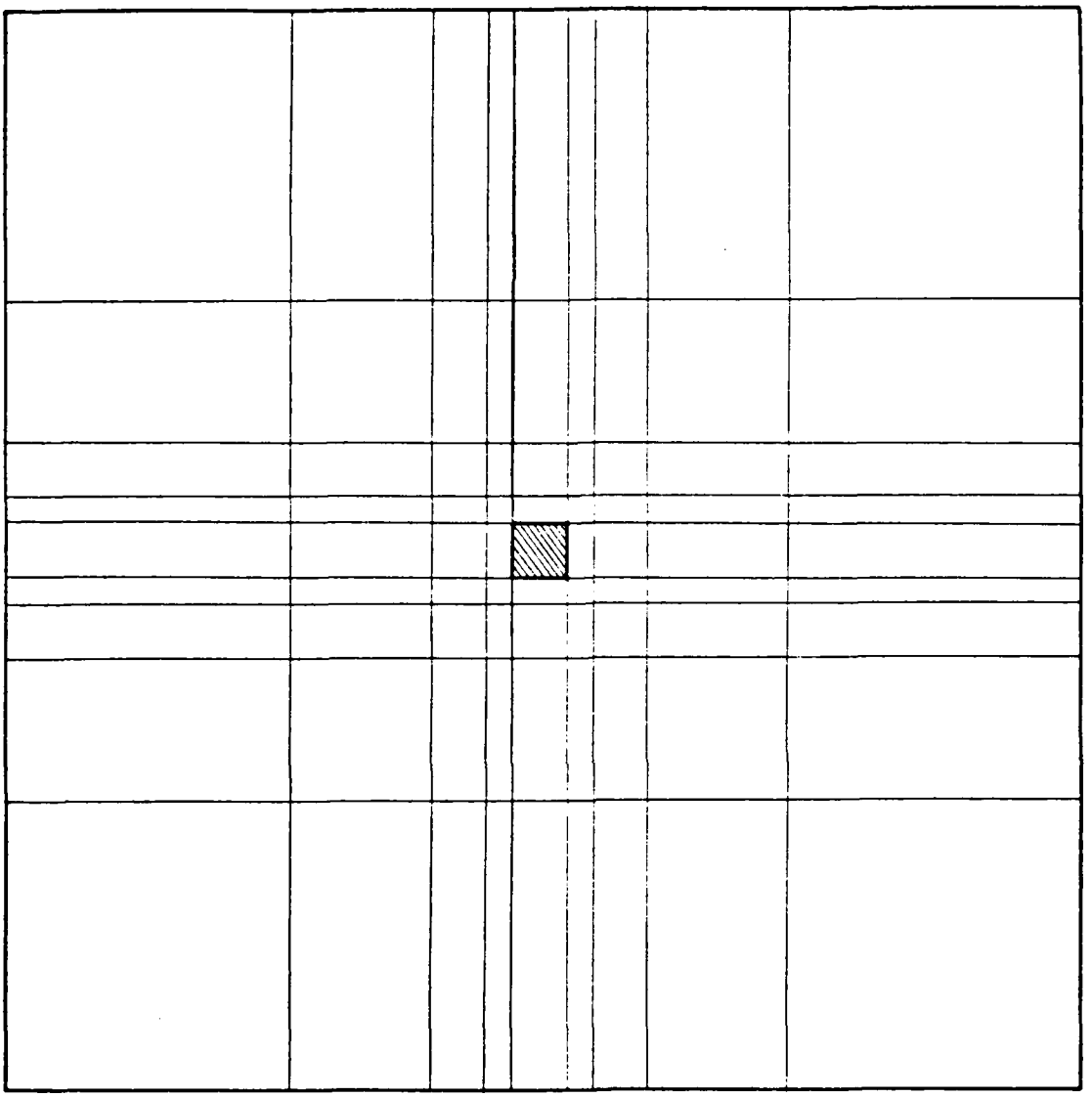

Fig. 4.6 Effect of Load Placement (Mesh III)

Comparisons among the results of these configurations and the results of the Westergaard idealizations WESI, WESII and WESIII are shown in Table 4.2. It is observed that the deflections are again largely insensitive to these changes, but they do follow the same pattern as calculated bending stresses. Of the three meshes, Mesh II yields the best results compared to Westergaard's (close and slightly conservative). Mesh I offers an attractive alternative, especially for those cases where a coarser mesh must be used. The results obtained with this mesh are slightly more conservative. Table 4.2 indicates that where possible, Configuration III must be avoided. Despite the extra effort involved in using this mesh as compared to Mesh I, the results are unconservative by a greater percentage.

In view of the above results, it is recommended that either Configuration I or Configuration II be used, the decision being a trade-off between extra computer core usage and accuracy. A similar recommendation was made by Costigan (51) who conducted a detailed investigation of this effect. At a future stage of this research, it is proposed to add an automatic mesh generator that will provide the user with an "optimum" mesh for the specified problem using the guidelines developed here.

TABLE 4.2

EFFECT OF LOAD PLACEMENT WITH RESPECT TO F.E. MESH

RUN No.	MESH USED	MEMORY SPACES	DEFLECTION		BENDING STRESS	
			mils	% WESII	psi	% WESIII
5	MESH I	20171	13.5	106	375.8	113
21	MESH II	34507	13.4	106	348.3	105
22	MESH III	26711	13.1	103	257.5	78
WESI	-	-	12.8	-	350.0	-
WESII	-	-	12.7	-	333.2	-
WESIII	-	-	unavailable	-	331.6	-

Notes:

(a) See also Table 4.1(b) for more details

(b) Mesh I: 9x9 mesh (Fig. 4.4)
Mesh II: 11x11 mesh (Fig. 4.5)
Mesh III: 10x10 mesh (Fig. 4.6)

(c) Finite Element Solution

Slab: 25'x25'

$E = 5 \times 10^6$ psi

$\mu = 0.15$

p = 222.2 psi

A = c"x" interior

c = 15"

k = 200 psi/in.

h = 14"

ℓ = 49.18"

$\frac{c}{\ell} = 0.305$

Theoretical Solutions

Ordinary Theory

WESI	WESII	WESIII
P = 50,000 lb.	P = 50,000 lb.	P = 50,000 lb.
p = 282.94 psi	p = 222.2 psi	p = 222.2 psi
a = 7.5" (circular)	a = 8.46" (circular)	c = 15" (square)

4.8.6 Convergence Characteristics of ILLI-SLAB upon Mesh Refinement

In its present as well as its original version, ILLI-SLAB employs the 12 degree-of-freedom plate element (44) which is referred to in the literature as the RPB12 or ACM element. The dimensions of this rectangular (or square) element are 2a by 2b. It is a 4-node, 3-dof per node plate bending element formulated using classical medium-thick plate theory. Deformations due to transverse shear are neglected in this formulation. Because all terms of a complete fourth order polynomial are not present in the assumed displacement shape (15 terms would be required), the element is non-conforming, ie. slopes normal to interelement boundaries are not continuous. However, the element is capable of correctly reproducing constant strain (curvature) states. Therefore, convergence to the exact solution is assumed as the element mesh is refined. What is not guaranteed is that convergence will be monotonic, ie. consistently from above or from below.

To check the convergence characteristics of ILLI-SLAB, a factorial of runs was designed which would permit the examination of the effect of mesh refinement without interference from limitations due to finite slab size and element aspect ratio. It will be noted in a subsection below that minimum slab size, L for the development of the Westergaard infinite slab condition with respect to stresses seems to be about 3.5 times the radius of relative stiffness, l of the slab. For the 12′x12′ slab used, parameters were chosen that gave l equal to 23.16 in. ie. an (L/l) ratio of 6.2. Thus no slab size problems can be expected, at least as

far as stresses are concerned.

The thickness, h of the slab was chosen as 15 in. despite the fact that this meant a higher radius of relative stiffness than would be obtained with a thinner slab. The objective here was to allow the investigation of element sizes smaller than h, since it had been pointed out by previous investigators that elements this small produced a stiffening effect. The other parameters used for this factorial are shown in Table 4.3a. Square elements were used to eliminate any aspect ratio effects, but their size varied from run to run depending on how many were available to fill the 12-ft.x12-ft. slab used. The ratio of element size, 2a to the thickness, h of the slab used varied between 4.8 when 4 elements were used, to 0.8 when 144 elements were used. The mesh used for the latter case is shown in Fig. 4.7. Also shown in Table 4.3a are the results from two Westergaard idealizations of the problem, one where P and p were matched using a circular load (WESII) and another for a square load (WESIII).

The results shown in Table 4.3a are presented graphically in Fig. 4.8. It is noted that for the cases studied, as the mesh is refined both deflection and bending stress converge monotonicaly from below to a theoretical value that would be obtained in the limit of refinement. In the case of deflection, this is slightly higher than the Westergaard value for the corresponding problem. This is probably due to the lack of an exact solution for a square load, as well as as the finite size of the slab (L/l=6.2; see below). In this study, deflections are compared to

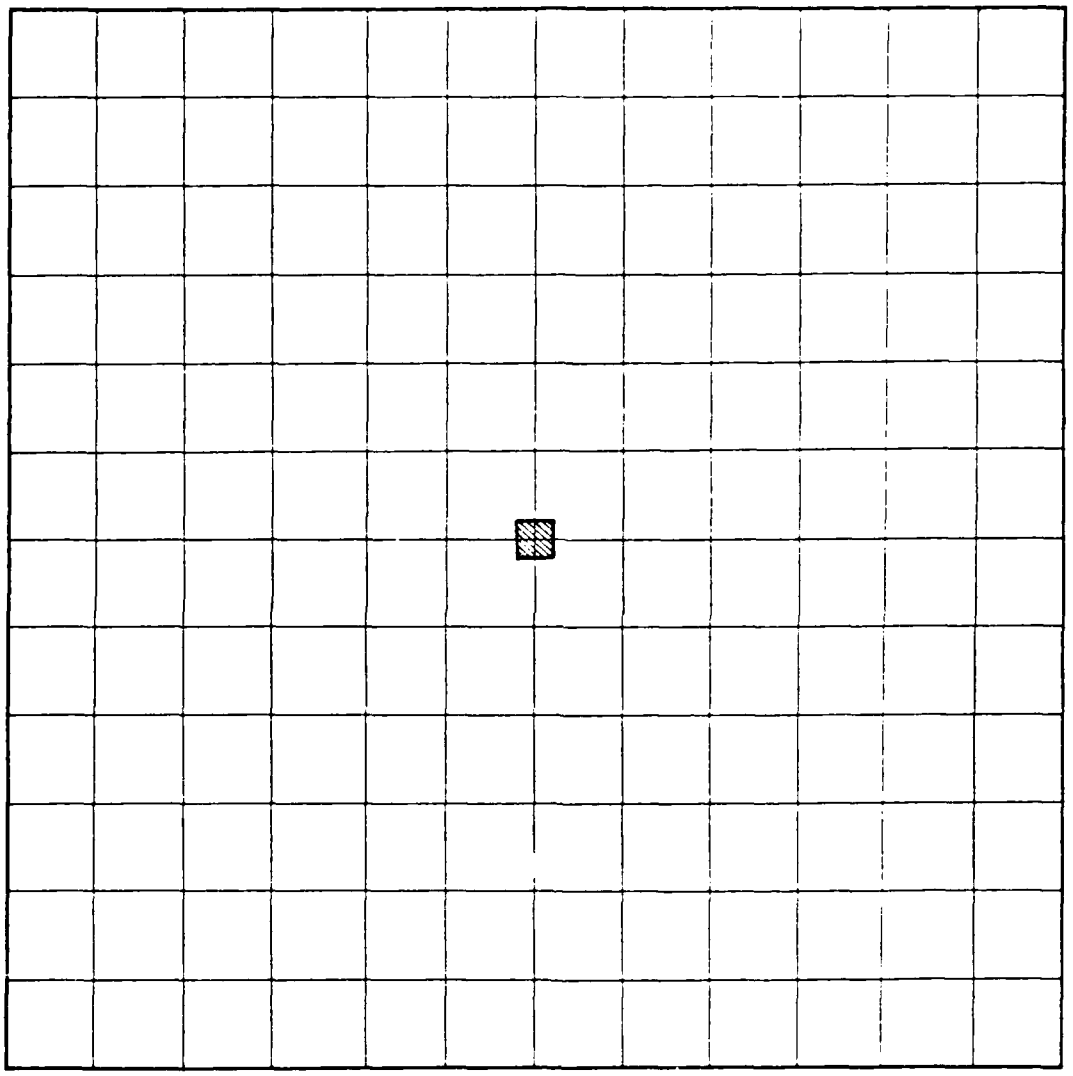

Fig. 4.7 Effect of Mesh Fineness: Number of Elements = 144

TABLE 4.3

(a) EFFECT OF F.E. MESH FINENESS

RUN No.	No. of Elements	$(\frac{2a}{h})$	DEFLECTION (mils)	% WESII	BENDING STRESS psi	% WESIII
32	4	4.8	1.06	91	4.53	27
33	16	2.4	1.23	106	9.68	59
34	64	1.2	1.25	108	14.22	86
35	144	0.8	1.24	107	16.34	99
WESII	-	-	1.16	-	16.61	-
WESIII	-	-	unavailable	-	16.54	-

Notes:

Finite Element Solution: Revised ILLI-SLAB

Slab: 12'x12' (= 6.2ℓ square)
Elements: 2ax2a

$E = 0.5 \times 10^6$ psi
$\mu = 0.15$
p = 100 psi
A = c"xc" interior
c = 5"
h = 15"
k = 500 psi/in.
ℓ = 23.16"
$\frac{c}{\ell} = 0.216$

Theoretical Solutions

See Table 4.1b for equations used.
Ordinary Theory

P = 2500 lb
p = 100 psi
a = 2.82" (circular: WESII)
c = 5" (square: WESIII)

TABLE 4.3 (Cont'd)

(b) COMPARISON BETWEEN ILLI-SLAB, 'SPRINGS' AND WESLIQID

RUN No.				DEFLECTION						BENDING STRESS					
ILLI-SLAB	SPRINGS	WESLIQID	No. of Elements	ILLI-SLAB		'SPRINGS'		WESLIQID		ILLI-SLAB		'SPRINGS'		WESLIQID	
				mils	% WESII	mils	% WESII	mils	% WESII	psi	% WESIII	psi	% WESIII	psi	% WESIII
32	62		4	1.06	91	0.82	71			4.53	27	2.06	12		
33	63	83	16	1.23	106	1.19	103	1.15	99	9.68	59	9.01	54	8.44	51
34	64		64	1.25	108	1.24	107			14.22	86	14.13	85		
35	65	85	144	1.24	107			1.21	104	16.34	99			14.71	89
		86	576					1.22	105					16.67	100
		87	784					1.22	105					16.69	100
WESII:						1.16						16.61			
WESIII						unavailable						16.54		-	

Note :

Slab and load characteristics as in Table 4.3(a).

AD-A135 836 DEVELOPMENT OF A STRESS-DEPENDENT FINITE ELEMENT SLAB MODEL(U) ILLINOIS UNIV AT URBANA DEPT OF CIVIL ENGINEERING M R THOMPSON ET AL. MAY 83 2/2

UNCLASSIFIED AFOSR-TR-83-1061 AFOSR-82-0143 F/G 13/2 NL

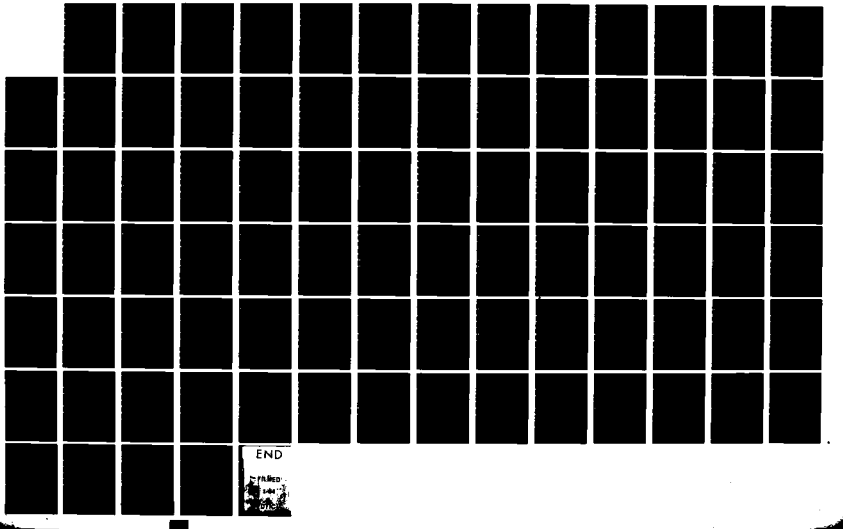

END

FILMED

DTIC

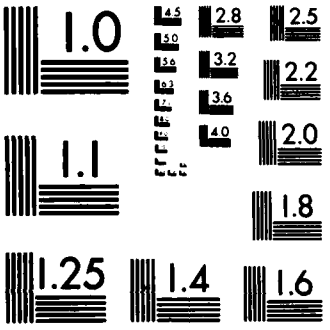

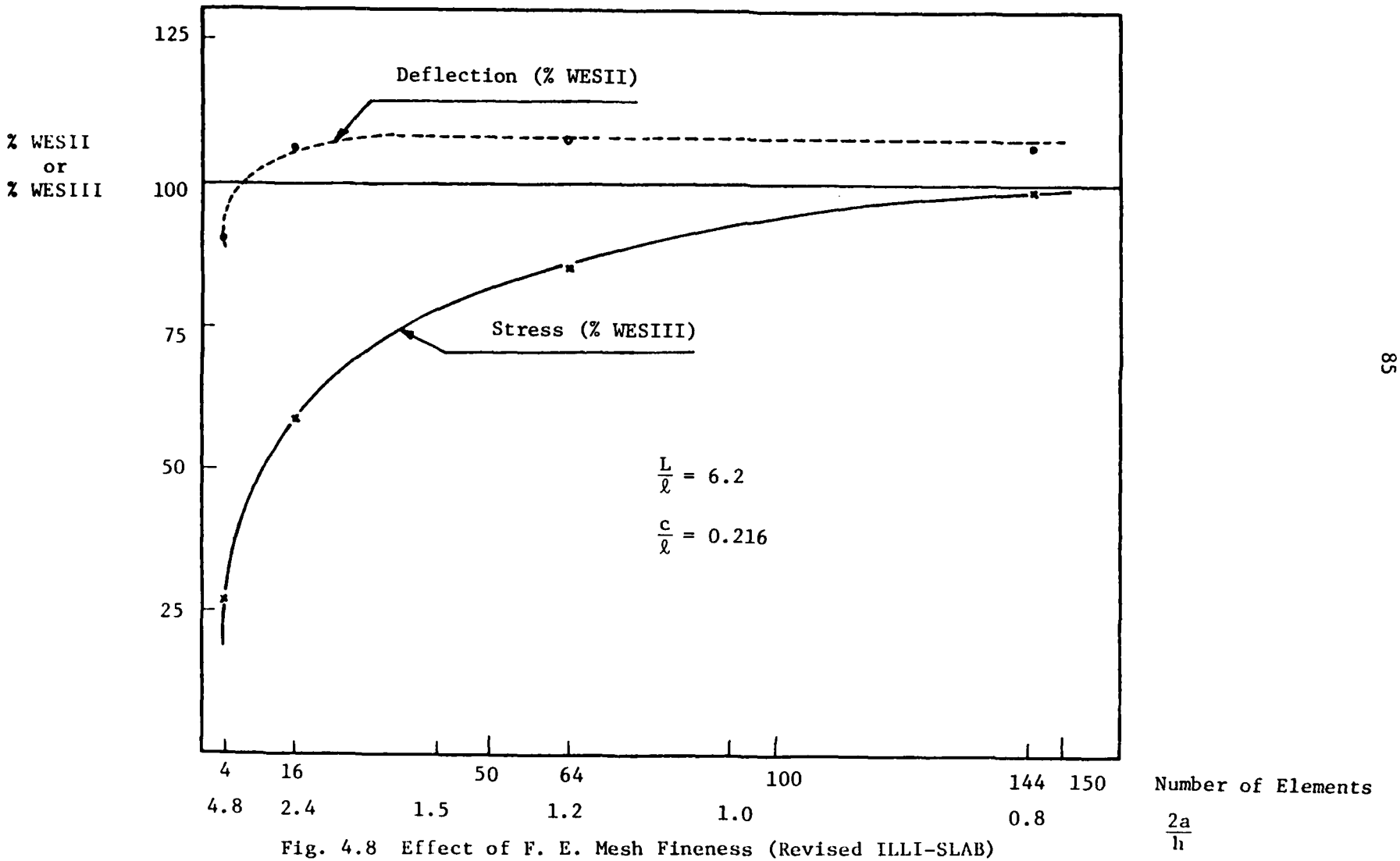

Fig. 4.8 Effect of F. E. Mesh Fineness (Revised ILLI-SLAB)

the theoretical values for an equivalent circular load of the same area as the square load (WESII). The observed discrepancy is very small. It is also noted that the convergence rate of deflection is much faster than that of bending stress, the limit solution being reached at values of (2a/h) as small as 2 to 3.

On the other hand, the bending stress converges to the corresponding Westergaard solution, but at a smaller value of 2a/h (=0.8). Note that this comparison is with Westergaard's ordinary theory for a square load (WESIII). The stress from a special theory analysis would be 12.8 psi and this could lead to unjustified conclusions with respect to the f.e. method. The true cause of this discrepancy is, of course, that the special theory and the f.e. method based on medium-thick plate theory are not directly comparable, since the first accounts (in some semi-empirical fashion) for the effect of shear stresses in the vicinity of the load, while the latter does not.

The problem was further investigated by using a similar factorial of WESLIQID runs, as well as runs using the 'SPRINGS' option in revised ILLI-SLAB. As mentioned previously, this option is identical to the FINITE model. In Table 4.3b, the results from these runs are compared to those from ILLI-SLAB.

It is observed that all three models exhibit basically the same behavior, ie. they monotonically converge from below to the same limit values. No "bending over" is observed with mesh refinement. The effect

of mesh refinement on the distribution of deflections and stresses is shown in Figs. 4.9 and 4.10, respectively. Deflections are fairly insensitive, especially outside a region of about twice the size of the loaded area. Stress differences persist relatively longer.

4.8.7 Convergence Characteristics of ILLI-SLAB upon Slab Size Expansion

As mentioned earlier, the closed-form Westergaard solution assumes a slab of infinite dimensions, although in practice empirical guidelines have been developed for the least slab dimension required to achieve the Westergaard "infinite slab" condition. These guidelines are summarized in Table 4.4. It is the purpose of this part of the present study to examine if and how ILLI-SLAB converges to the Westergaard solution as the slab size is increased and establish whether the empirical guidelines in Table 4.4 are verified by the finite element method.

The same parameters were used for this factorial of runs as in the study of mesh refinement, giving again a radius of relative stiffness, l of 23.16 in. The element size was kept at 18 in. (ie. 2a/h=1.2). The mesh used for these runs shown in part in Fig. 4.11. The pattern shown is repeated in all 4 directions to give the required slab size.

The results from this investigation are given in Table 4.5, where they are compared to the corresponding Westergaard values. The same results are presented graphically in Fig. 4.12. Both deflection and bending stress converge to a theoretical value for an infinite slab. The

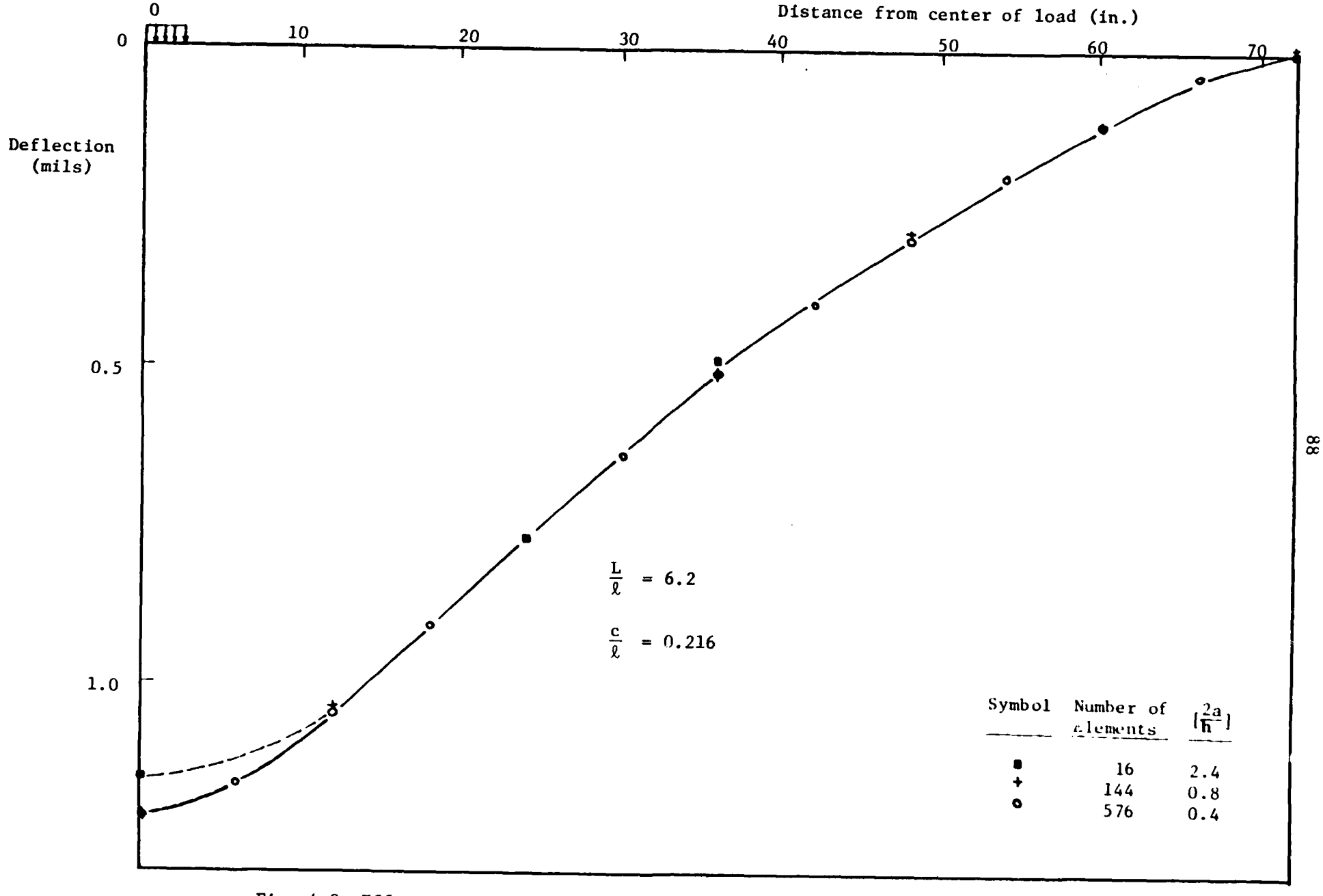

Fig. 4.9 Effect of F. E. Mesh Fineness on Deflection Bowl (WESLIQID)

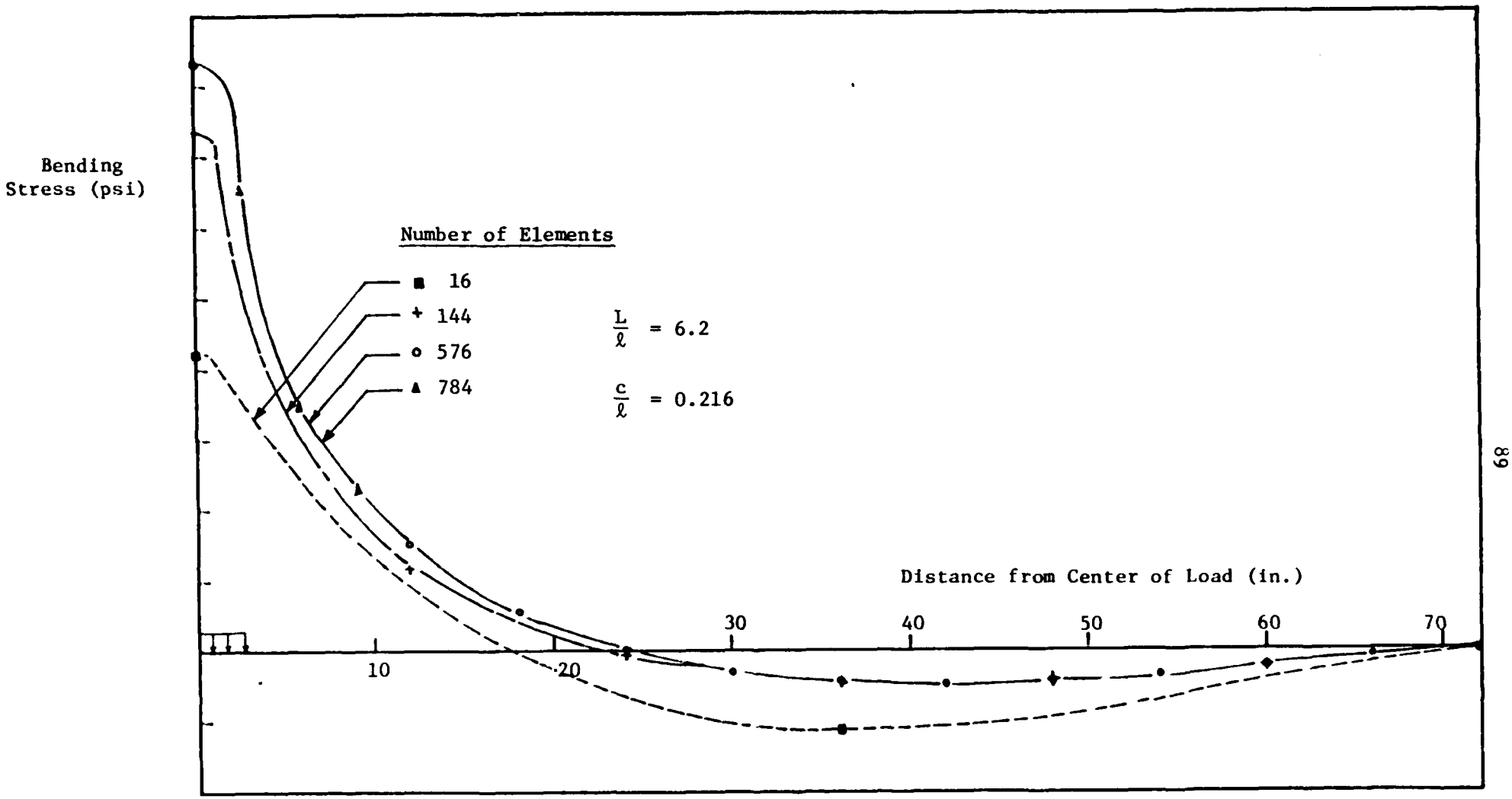

Fig. 4.10 Effect of F. E. Mesh Fineness on Stresses (WESLIQID)

TABLE 4.4

THEORETICAL AND EMPIRICAL SIZE LIMITATIONS FOR THE WESTERGAARD SOLUTION

Loading Condition	Minimum Side Length	
	Theoretical	Practical
Interior	11ℓ	6ℓ
Edge	11ℓ	6ℓ
Corner		Unavailable

ℓ = radius of relative stiffness

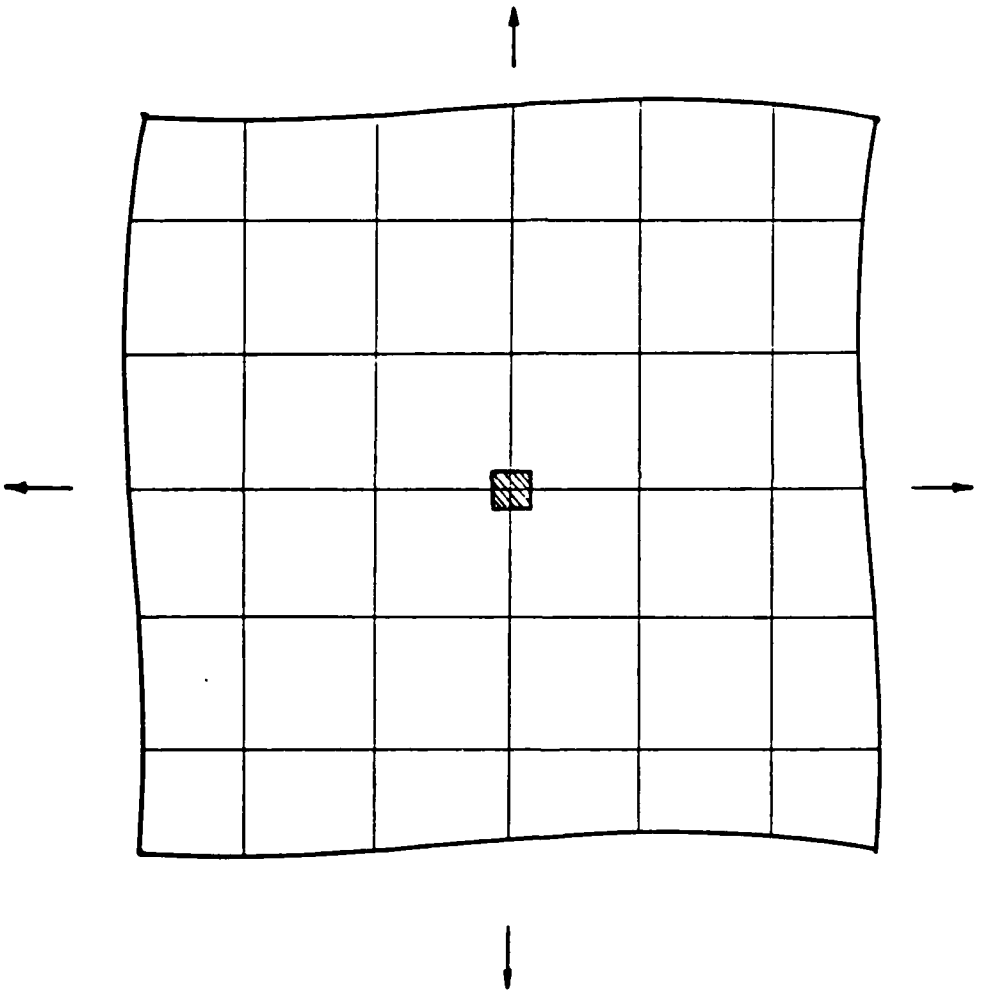

Fig. 4.11 Effect of Slab Size: F. E. Mesh

TABLE 4.5

EFFECT OF SLAB SIZE

RUN No. ILLI-SLAB	RUN No. SPRINGS	L (ft)	L/ℓ	DEFLECTION ILLI-SLAB mils	DEFLECTION ILLI-SLAB % WESII	DEFLECTION 'SPRINGS' mils	DEFLECTION 'SPRINGS' % WESII	BENDING STRESS ILLI-SLAB psi	BENDING STRESS ILLI-SLAB % WESIII	BENDING STRESS 'SPRINGS' psi	BENDING STRESS 'SPRINGS' % WESIII
41	71	3	1.6	4.01	346	4.09	353	9.88	60	11.09	67
42	72	6	3.1	1.52	131	1.56	134	14.13	85	14.14	85
43 or 34	73	12	6.2	1.25	108	1.24	107	14.22	86	14.13	85
44		18	9.3	1.18	102			14.10	85		
WESII					1.16				16.61		
WESIII					unavailable				16.54		

Notes:

Finite Element Solution

Revised ILLI-SLAB and 'SPRINGS'
Slab: L'xL'
Element Size: 18"x18" ($\frac{2a}{h}$ = 1.2)

$E = 0.5 \times 10^6$ psi
$\mu = 0.15$
p = 100 psi
A = c"xc"; interior
c = 5"
h = 15"
k = 500 psi/in.
ℓ = 23.16 in.
$\frac{c}{\ell}$ = 0.216

Theoretical Solutions

See Table 4.1b for equations used
Ordinary Theory

P = 2500 lb
p = 100 psi
a = 2.82" (circular: WESII)
c = 5" (square: WESIII)

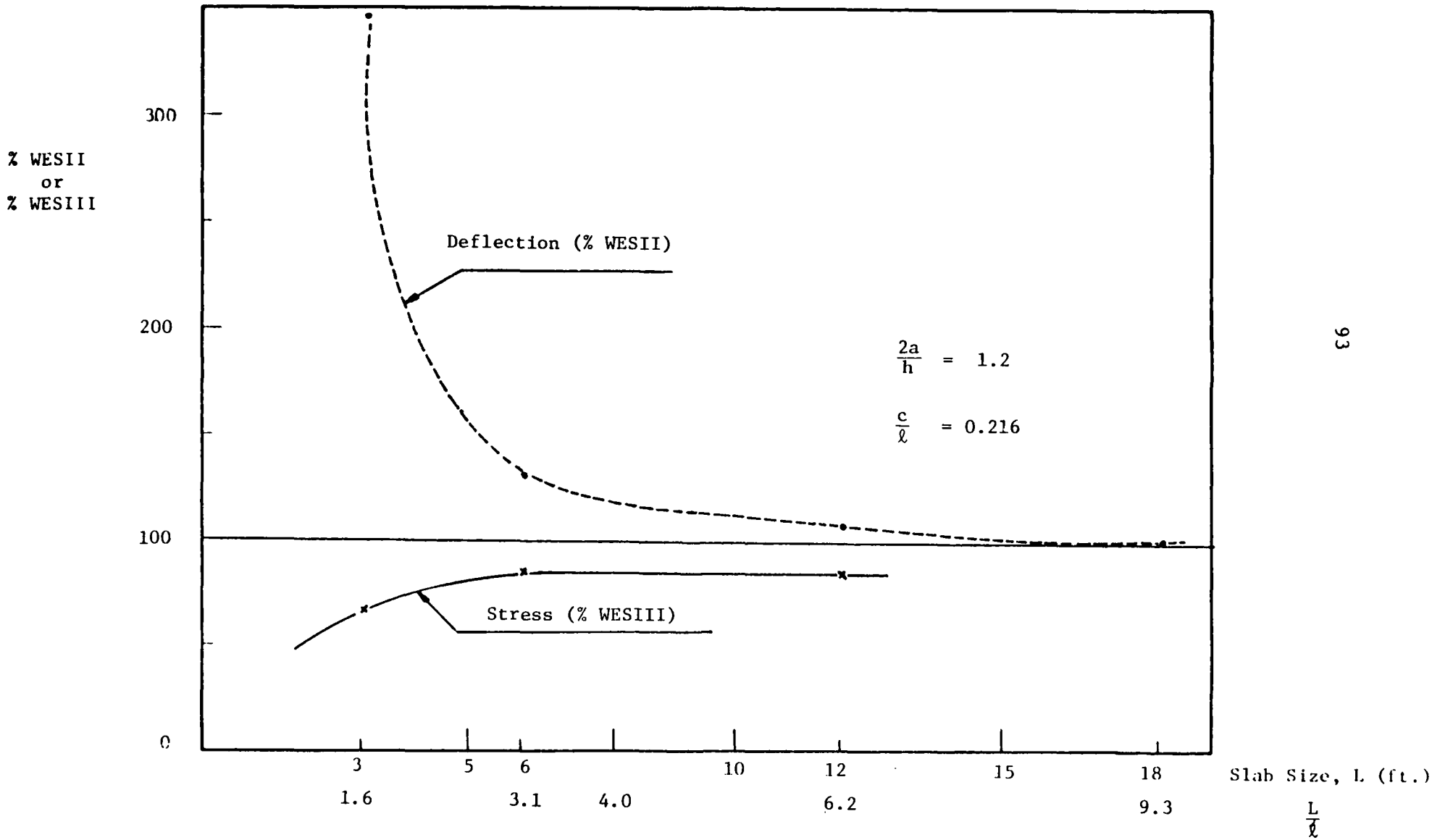

Fig. 4.12 Effect of Slab Size (ILLI-SLAB)

convergence of deflection is from above, indicating that a smaller slab settles more than a bigger one in a "punch-like" fashion. Bending stress converges from below, as expected. The rate of convergence, defined as the slab size at which the solution is essentially that for an infinite slab, is different for deflection (L/l=9.3) than for bending stress (L/l=3.5). Surprisingly, deflection appears to be much more sensitive to slab size changes for (L/l) values of less than 3, because of the above-mentioned "punch-like" effect. The limit value approached by the deflection is the Westergaard solution.

The value to which bending stress converges upon slab size expansion is exactly that which would be expected for the given mesh fineness (2a/h=1.2) as shown in Table 4.3a. This indicates that, fineness effects apart, stress converges to the theoretical value for L/l values of about 3.5. In Table 4.5, the stress is not expected to approach the Westergaard solution by any appreciable amount upon further slab expansion, simply because the discrepancy observed arises from mesh fineness effects, as shown in Table 4.3a.

It is interesting to note the similarity in behavior patterns between ILLI-SLAB and 'SPRINGS'. This reinforces the observations above.

4.8.8 Effect of Element Aspect Ratio

The effect of element aspect ratio was investigated by the factorial of runs with WESLIQID shown in Table 4.6. Theoretically, best results are obtained when the aspect ratio is kept close to unity, ie. the elements are as close to square as possible. This postulate is borne out in Table 4.6.

Figures 4.13 and 4.14 show how the aspect ratio affects deflection and stress distributions. It is observed that deflection is largely insensitive --as always-- to any changes. The bending stress distribution is also insensitive except in a small region surrounding the loaded area. The radius of this region is approximately twice the radius of the loaded area. Within this region, a departure of aspect ratio from unity may cause significant errors.

4.8.9 Effect of Size of Loaded Area

In his attempt to develop equations for a loaded area of finite size, Westergaard used an approach which essentially consists of first deriving a solution for a point load. Then, the loaded area is split into a number of small subareas, each subarea being replaced by a statically equivalent point load acting at its center. A summation is performed over these subareas. In the limit of refinement, this summation tends to an exact integration (52). Westergaard suggests that his equations are valid for any size of loaded area and that, in fact,

TABLE 4.6

EFFECT OF ELEMENT ASPECT RATIO

RUN NO.	ASPECT RATIO	DEFLECTION		BENDING STRESS	
		mils	% WESII	psi	% WESIII
91 or 86	1	1.22	105	16.67	100
92	2	1.21	104	16.07	97
93	3	1.21	104	15.19	92
94	4	1.20	103	14.29	86
96	6	1.18	102	12.65	76
WESII			1.16		16.61
WESIII			unavailable		16.54

Notes:

Finite Element Solution (WESLIQID)

Slab: 12'x12' (= 6.2ℓ square)
Elements: 2ax2b
$E = 0.5 \times 10^6$
$\mu = 0.15$
p = 100 psi
2a = 6"
2b = 2a x (Aspect Ratio)
A = c" x c" interior
c = 5"
h = 15"
k = 500 psi/in.
$\ell = 23.16"$

$\frac{c}{\ell} = 0.216$

$\frac{2a}{h} = 0.4$

Theoretical Solutions

See Table 4.1b for equations used.
Ordinary Theory
P = 2500 lb.
p = 100 psi
a = 2.82" (circular: WESII)
c = 5" (square: WESIII)

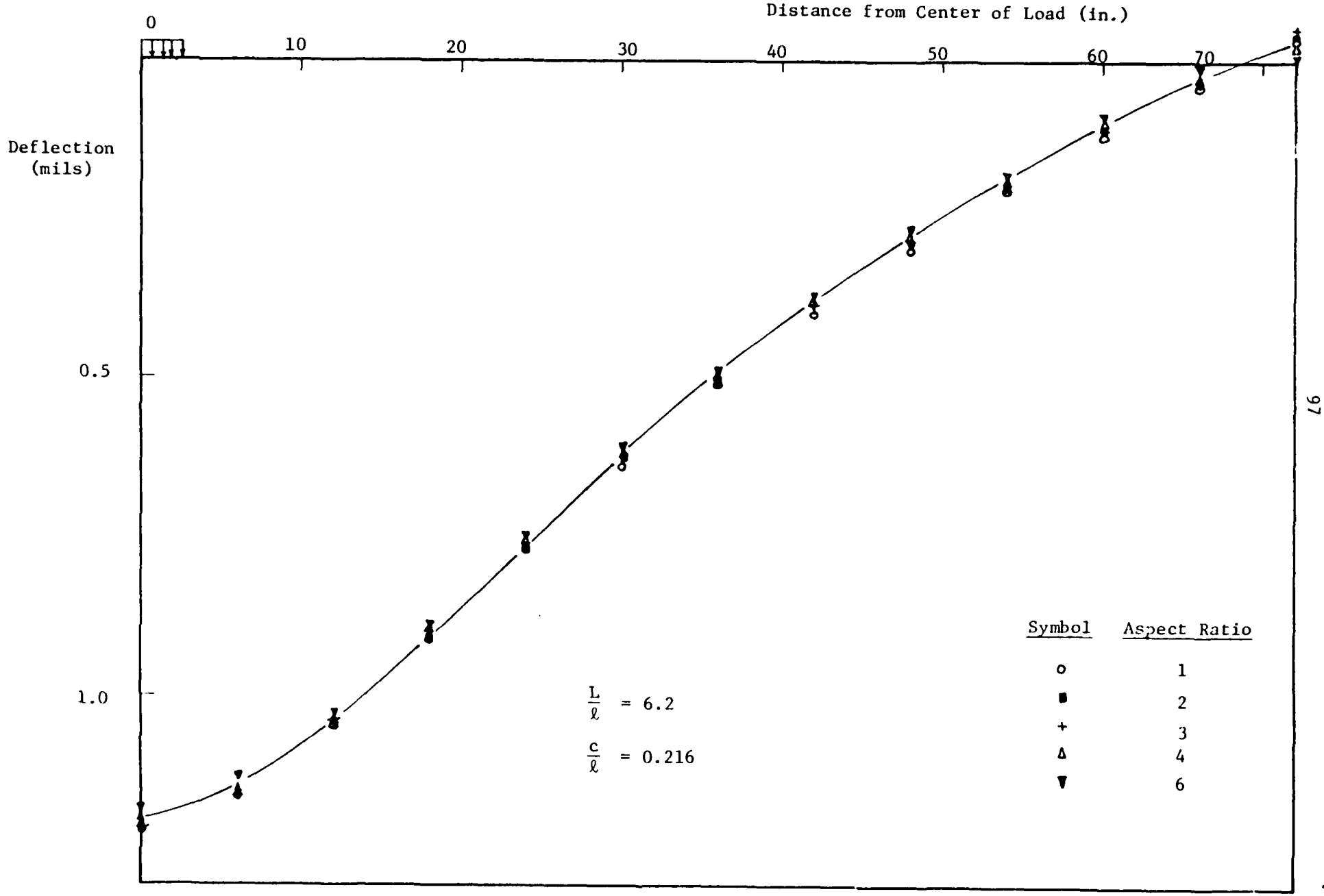

Fig. 4.13 Effect of Element Aspect Ratio on Deflection Bowl (WESLIQID)

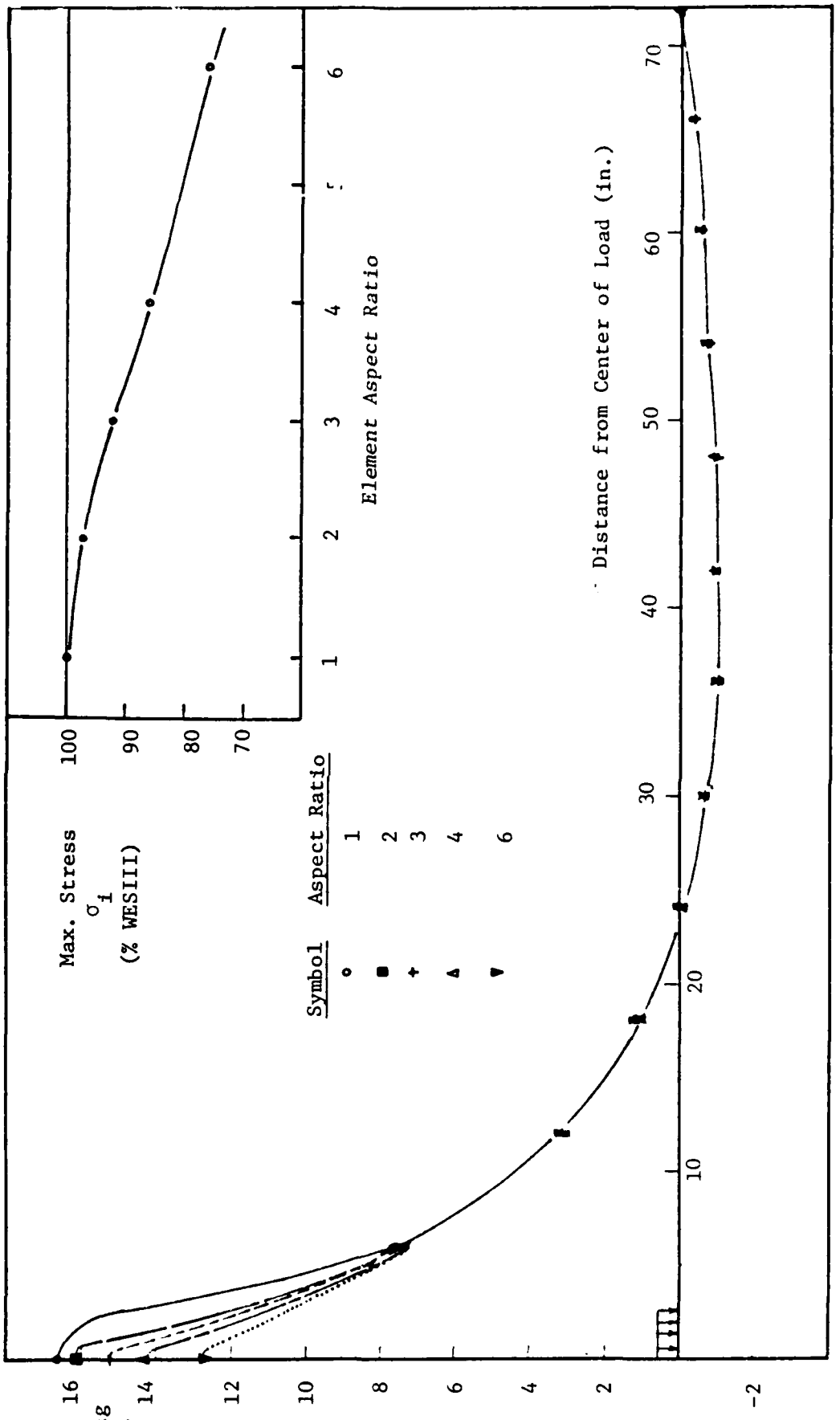

Fig. 4.14 Effect of Element Aspect Ratio on Stresses (WESLIQID)

his "New Formulas" (48) assume that "the average width and length of the footprint of the tire is greater than the thickness of the slab in all significant cases".

Losberg (53) showed that the stress and deflection equations presented by Westergaard and widely used in practice, are only the first one or two terms of a rapidly converging infinite series. Westergaard's supplementary stress, σ_2 mentioned above, for example, is an additional term of this series. The rate of convergence can be expected to vary depending, among other things, upon the size of the loaded area.

Timoshenko and Woinowsky-Krieger (49) state that the equations apply only when the radius of the loaded area is "small in comparison with 1". [Scott (10) attributes this restriction to the fact that "in the derivation of the equation a term of approximate value 0.1 c^2/l^2 was omitted". This cannot be the real cause of the restriction imposed by Timoshenko and Woinowsky-Krieger, since in most cases (even when the radius of the loaded area is not "small in comparison with 1") this term is, indeed, negligible.]

In this study, the effect of the size of the loaded area was investigated using the f.e. method. Table 4.7 shows a factorial of ILLI-SLAB runs and comparisons with Westergaard's ordinary theory solutions. To eliminate slab size, mesh fineness and aspect ratio effects, a large (L/l=9.33) and fine (2a/h=0.6) mesh was used, consisting of square elements (aspect ratio=1.0). The results in Table 4.7 are

TABLE 4.7

EFFECT OF SIZE OF LOADED AREA

RUN No.	p (psi)	c (in.)	c/ℓ	DEFLECTION mils	DEFLECTION % WESII	BENDING STRESS psi	BENDING STRESS % WESIII
108	200	3.54	0.153	1.18	102	18.12	97
107	175	3.78	0.163	1.17	101	18.01	99
106	150	4.08	0.176	1.17	101	17.87	100
105	125	4.47	0.193	1.17	101	17.68	103
101	100	5.00	0.216	1.17	101	17.40	105
102	75	5.77	0.249	1.17	102	16.96	108
103	50	7.07	0.305	1.16	101	16.17	112
104	25	10.00	0.432	1.15	102	14.23	115

Notes:

(a) The theoretical values WESII and WESIII (not explicitly given here) were obtained for a circular and a square load respectively using the equations given in Table 4.1b, for P = 2500 lb and p as shown above.

(b) Finite Element Solution

Slab: 18'x18' $(\frac{L}{\ell} = 9.33)$

Element Size: 9"x9" $(\frac{2a}{h} = 0.6)$

Number of Elements = 576

$E = 0.5 \times 10^6$ psi
$\mu = 0.15$
A = c" x c" interior
h = 15"
k = 500 psi/in.
$\ell = 23.16$"

plotted in Fig. 4.15.

It is observed that the Westergaard stress values apply for a loaded area whose side length, c (if square) is about 0.2 times the radius of relative stiffness, l; if the load is circular, its radius must be about 0.11. As (c/l) or (a/l) increases, f.e. stresses become progressively higher than Westergaard's.

4.8.10 Preliminary Recommendations

The following preliminary recommendations can be made at this stage:

1. The load(s) must be placed over the finite element mesh with at least one node at the anticipated location of maximum response. For example, in the case of interior loading, a central node must be provided. Otherwise, the results must be carefully interpreted. Any peaks in response missed by the finite element analysis because of node spacing, must be reconstructed.
2. The finest mesh practicable must be used. Accuracy of 99% can be expected if the element size, 2a, is about 0.8 times the thickness of the slab. A fine zone equal to twice the size of the loaded area(s) is recommended, with progressive decrease in fineness outside this area.
3. The convergence characteristics of the work equivalent uniform subgrade model (option IST = 6; 'WINKLER' in modified ILLI-SLAB) are slightly better than those of the 'SPRINGS' option (IST=7 in modified ILLI-SLAB).

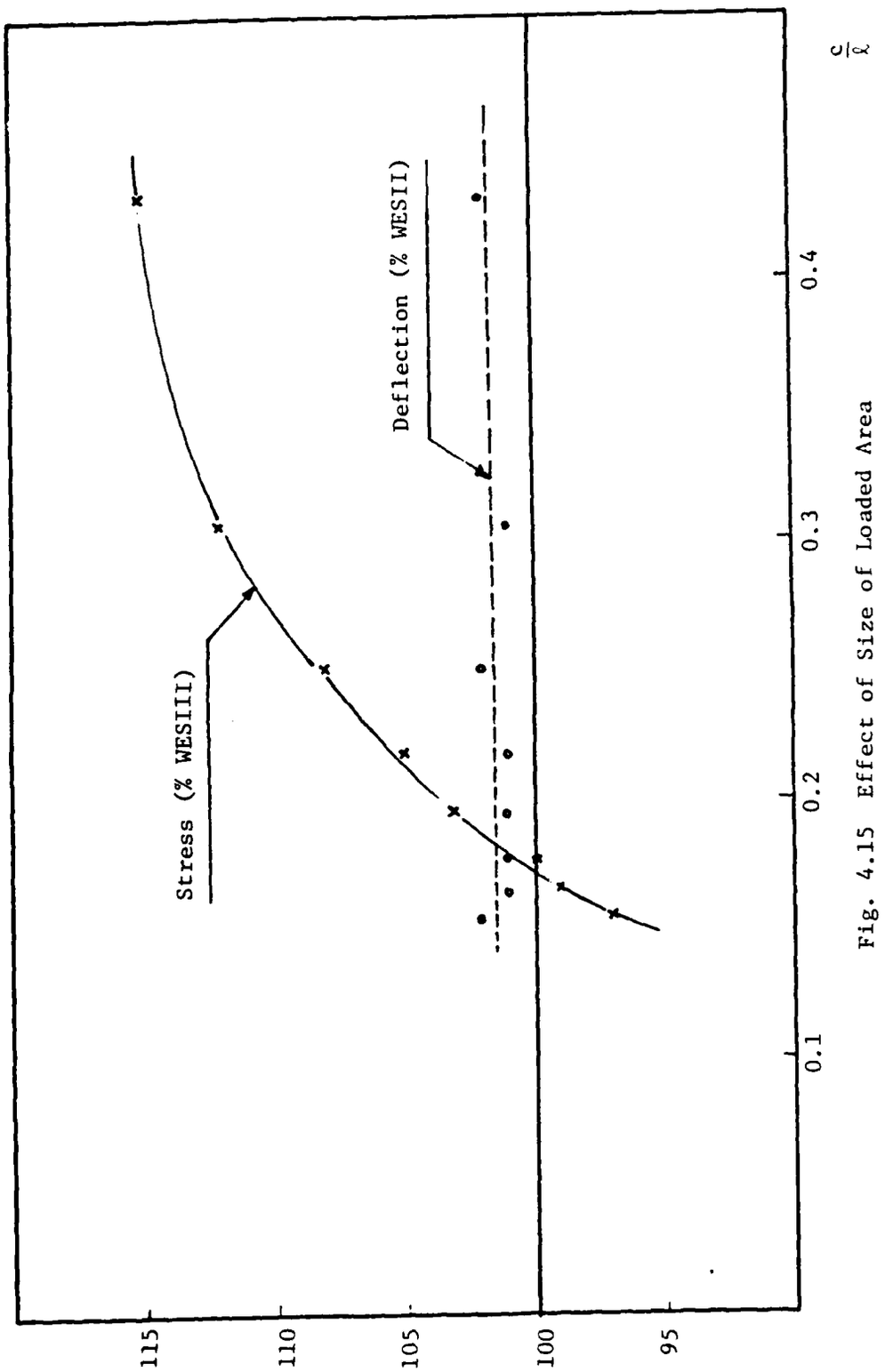

Fig. 4.15 Effect of Size of Loaded Area

4. Element aspect ratio should be kept close to unity, particularly in a region around the loaded area(s), extending to two radii of the loaded area. Within this region, this recommendation is a requirement.

CHAPTER 5

MODIFICATION OF ILLI-SLAB

5.1 AIMS OF MODIFICATIONS

For the benefits of the Finite Element Method to be fully realized, it is highly desirable that programs using this method:

(i) Accept easy to compile, user-oriented input data, restricted to the absolute minimum required and eliminating, where possible, potential pitfalls for the user;

(ii) Employ carefully selected default values that will reduce the amount of input data required;

(iii) Perform error checks, especially in the case of default values, so that errors that are concealed by the otherwise normal execution of the program will be avoided;

(iv) Be free of code errors;

(v) Organize the output so that it is neat, meaningful and user-oriented;

(vi) Incorporate skillful data-base management for the efficient utilization of available memory core;

(vii) Provide basic and higher-level routines; and

(viii) Present the results in a summary and a graphical form.

The modifications of ILLI-SLAB presented below aimed at providing these capabilities.

5.2 STRESS DEPENDENT SUBGRADE

The development of relationships between the resilient subgrade modulus, K_R and deflection, w is described in Chapter 3 of this report. It was desirable to incorporate these relationships into ILLI-SLAB through an iterative procedure which would compare support values (K_R) corresponding to calculated deflections with previously determined values. New support values would be assigned for a subsequent iteration until compatibility was achieved between support system stress and/or deflection and the user prescribed support relation/pattern. Furthermore, it was desirable to have the capability to assign variable support values to selected (or all) nodes according to a user prescribed relation/ pattern. These aims were achieved with the introduction of subroutine ITERATE.

The general expression for the relation between K_R and w as developed in this study (30-in. diameter plate) is:

$$K_R = (1/w)\{A_1 [1-\exp\{-A_2 ([w/D_y] - A_3)\}]+A_4 ([w/D_y] -A_3)+2\}$$

$$=A_5 /D_y \quad , \text{ if } [w/D_y] <A_3.$$

where A_1, A_2, A_3, A_4, A_5, D_y are regression parameters determined from plate load tests simulated using ILLI-PAVE. By specifying these

parameters, the user can define another stress dependent subgrade. During this study, parameter sets for the following broad subgrade types (Fig. 2.10) have been developed and are now a part of the revised version of ILLI-SLAB:

1. VERY SOFT (K_R = 300 psi/in.)
2. SOFT (K_R = 425 psi/in.)
3. MEDIUM (K_R = 725 psi/in.)
4. STIFF (K_R = 1000 psi/in.).

The figures in parentheses are recommended initial (small deflection) values, for fast convergence. As noted in Section 3.3, above, K_R is significantly higher than the corresponding static k-value, reflecting the increased subgrade stiffness in response to rapidly moving loads.

Other options available in modified ILLI-SLAB are:

5. OTHER : The user specifies the regression parameters individually to obtain a different K_R versus w relation.
6. WINKLER: This is the stress independent, uniform Winkler subgrade, available in the original version of ILLI-SLAB.
7. SPRINGS: Support is provided by 4 springs at the corner of the element (stress independent). This option allows direct comparison-validation with FINITE.

Option 0 specifies that support varies from node to node and requires that the user proceed to assign one of the above 7 options to each of the

nodes. In the case where most nodes have one type of support, the EXCEPT option in the free-form mode allows specification of exceptions only, rather than of each node.

Subroutine ITERATE is structured to allow easy modification of the regression equations and/or addition of other subgrade options.

When one of the stress dependent subgrade types are used, subroutine ITERATE provides a procedure for checking convergence, updating support values and proceeding with another iteration, if necessary. The user controls this procedure by three variables:

1. ITMAX: Specifies the maximum (total) number of iterations desired. Usually 3 iterations are sufficient; a value of ITMAX = 6 is recommended;
2. TOL1: Convergence tolerance for updated K_R compared with K_R from the previous iteration. A value of TOL1 = 0.05 ie. 5% is recommended;
3. TOL2: Convergence tolerance for the percentage of nodes at which TOL1 is not satisfied. Again, a value of TOL2 = 0.05 ie. 5% is recommended.

Through a fourth parameter (IOT), the user is allowed to specify the output type desired. Thus, he may opt to have only partial output during intermediate iterations (stresses not calculated or printed), reserving full output of deflections and stresses for the last iteration; or he may choose to have full output for each iteration.

5.3 CONTOURING CAPABILITY

During a study conducted in the Summer of 1981, Computer Program ILLI-SLAB was revised and the facility to generate contours of stresses and deflections was incorporated into it (54). This was done through subprogram CONT, which accepts as input data results from ILLI-SLAB. Subroutine CONTOUR in this subprogram passes these results to a number of NCAR subroutines. The software used in these subroutines has been developed at the National Center for Atmospheric Research (NCAR), and is made available with the restriction that NCAR be acknowledged as the source of the software in any resulting research or publications. For more information on the use of NCAR Contouring Software, the reader should refer to NCAR literature. Sample contour plots are shown in Fig. 5.1. A very brief outline of the Software, especially as used in the revised version of ILLI-SLAB is given below.

The NCAR Graphics Software consists of graphics utilities such as contour plotting, three-dimensional surface drawing, and world map projections. These utilities perform graphic output using low level graphics subroutines in the NCAR System Plot Package (SPP). This consists of subroutines to draw, move, plot characters, clear the plotting surface, and similar subroutines. The output of the SPP is not a plot, but a file (called "NCARMC") of 'metacode' which contains the plotter instructions. NCARMC, the Metacode File, is device independent - it contains instructions to drive an "ideal" plotter or graphics device. This file is interpreted by a Translator for a specific device. The

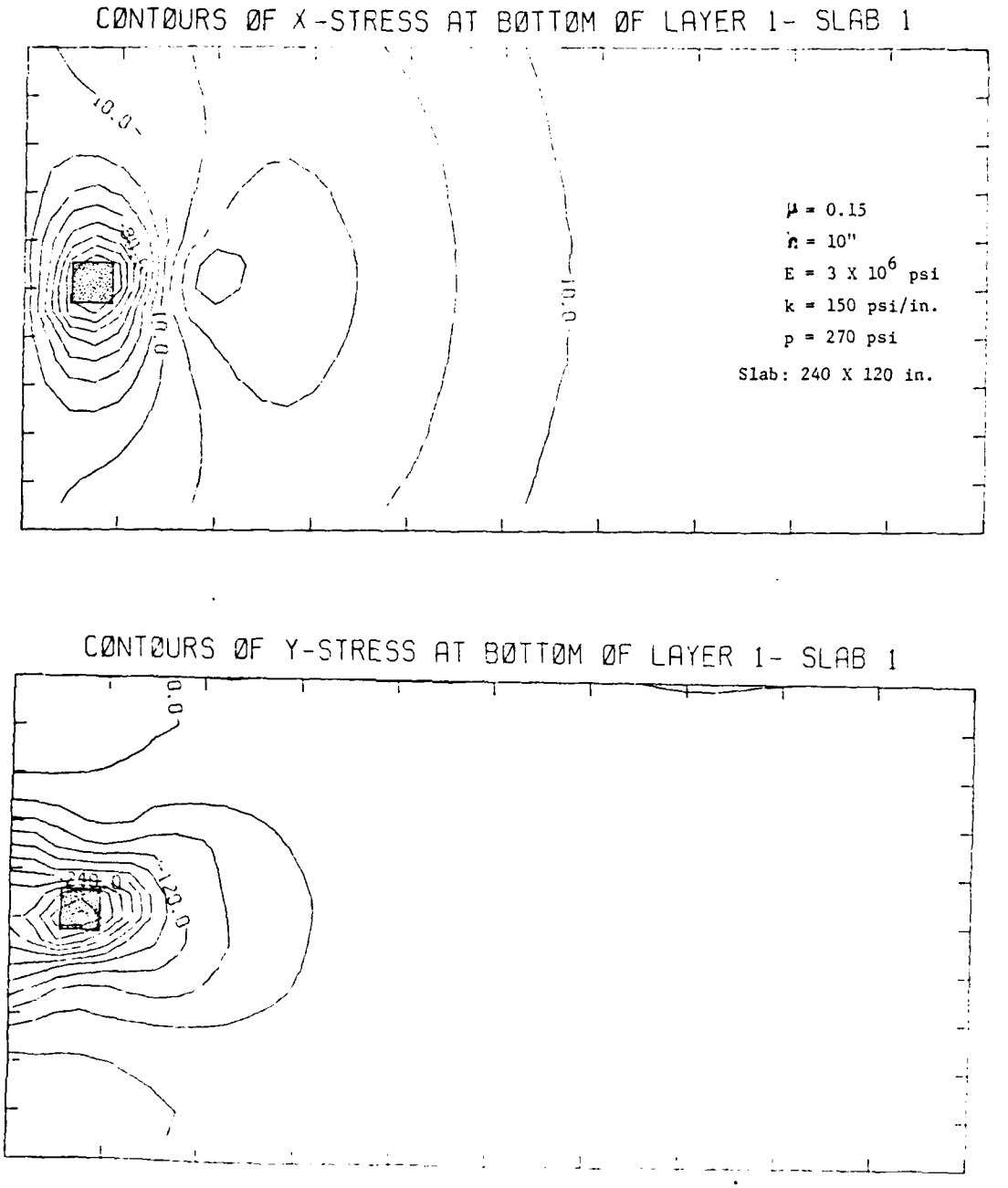

Fig. 5.1 Sample Contour Plots

Translator does the actual plotting.

The most important family of NCAR subroutines used in ILLI-SLAB is CONRAN. This is the name of a family of routines for the contouring of irregularly distributed data. The family consists of 4 versions: CONRAQ, CONRAN (used for two versions), and CONRAS. CONRAQ, the quick version, plots contours, perimeters, titles and messages. CONRAN, the standard version, adds line labeling, contour dash patterns, and plots relative highs and lows (this is the version in ILLI-SLAB). CONRAN, smooth version, adds splines under tension for smoothing of contour lines. CONRAS, super version, adds the elimination of contours when crowding with other contours or text occurs. CONRAQ is the fastest and smallest. The packages get progressively bigger and slower as features are added.

CONRAN plots contour lines using random, sparse or irregular data sets. The data is triangulated and then contoured. Contouring is performed using interpolation of the triangulated data.

5.4 TOWARD MORE EFFICIENT MEMORY CORE UTILIZATION

A major problem encountered by ILLI-SLAB users is that any attempt to refine the mesh used, especially when it is desired to investigate the stability and convergence of the numerical solution or when several slabs are used, faces the possibility of exceeding machine memory core capacity. This problem has been addressed by the introduction of the capability to take advantage of any symmetry lines that may exist. In

the modified ILLI-SLAB version, the user has the following options:

1. No lines of symmetry exist (ISYM=0);
2. The x-axis is a line of symmetry (ISYM=1);
3. The y-axis is a line of symmetry (ISYM=2);
4. The x- and y-axes are both axes of symmetry (ISYM=3).

Care was taken to introduce these options without imposing a burden on the user during the preparation of the input data. Particularly undesirable are requirements to include the node numbers for the nodes along the line(s) of symmetry. In the new version of ILLI-SLAB, the various options related with symmetry are specified by using a single input variable (ISYM), which may even be omitted if no symmetry exists.

Still on the issue of economizing memory core, several methods are continuously being investigated for better data-base management through the use of overlays. These are incorporated into ILLI-SLAB as they are developed. The possibility of breaking the program into two or more subprograms to be loaded and executed separately and sequentially is also investigated. Already the contouring subroutines have been separated from the main body of the program and placed in subprogram CONT with appreciable savings. Another group of routines offered for such a separation are those related to the free-form input capability. A subprogram could be easily created from these routines to read free-form input data and prepare them for the main body of ILLI-SLAB. A library of routines is envisaged at the end of this effort which will contain all necessary routines but only those needed for any given run will be loaded.

5.5 CORRECTION OF SUBGRADE STIFFNESS MATRIX

One of the major advantages of ILLI-SLAB, over other available programs, eg. WESLIQID or FINITE, is that the Winkler type foundation is no longer modeled by four concentrated springs at the corners of each slab element. Through an equivalent mass formulation, a uniform, distributed subgrade is provided. The formulation for the derivation of the stiffness matrix for this subgrade (1) follows the same steps as the one presented by Dawe, 1965 (55), who first derived this matrix. In Dawe's equivalent mass formulation, the product of mass per unit area and plate thickness (ρ h), replaces the subgrade modulus, k (or K_R). Similar derivations using different sign conventions are also presented by Przemieniecki (56) and Zienkiewicz (44).

The subgrade stiffness matrix used in ILLI-SLAB was compared to each of the matrices presented in these publications, which were further compared to each other, with due allowance for differences in sign convention. The result of this was the corrected formulation as included in the modified version of ILLI-SLAB. A typographical error in the matrix in Ref. 44 was also detected: element (3,1) should be +461, as also given in Ref. 57.

The corrections in the stiffness matrix are most obvious in the results of symmetric problems, where identical responses are obtained at corresponding points, as expected. Although the change in the results of a typical run may only range from 3% to 5%, it is important to have a

balanced formulation, to ensure the good behavior and convergence of the numerical solution.

5.6 SPECIFICATION OF LOADED AREAS IN TERMS OF GLOBAL COORDINATES

In its original version, ILLI-SLAB required that input data for loaded areas be specified in terms of local (element) coordinates. In this system, the origin is set at the lower left corner of each element and the axes extend from 0 to 2a in the x-direction and 2b in the y-direction, for a typical element of dimensions 2ax2b. The implication of this was that the user had to go through the following steps when specifying the loaded areas for his problem:

1. Determine the element numbers of the loaded elements, adhering to a fixed numbering sequence, ie. from bottom to top from left to right. It should be noted that depending on the fineness of the mesh used, each loaded area (such as a wheel imprint) might apply a load on 4 or more elements. Thus, a large number of partially or fully loaded elements might be needed to define the loading pattern in all but the simplest situations;
2. For each of the loaded elements, determine the extend of the loaded subarea in terms of the local element coordinate system. These coordinates should then be specified, one subarea per card, together with the load intensity in each case;
3. In case of a change in the f.e. mesh used, such as when making the mesh finer, the process must be repeated.

As a result of the complexity of this process, especially when used, as it was, with the fixed form input format, a large portion of all problems encountered by ILLI-SLAB users was related to specifying loading pattern data. To overcome these difficulties, Subroutine SUBAREA was coded to allow input data specification in terms of the global coordinate system. In this system, the origin is located at the lower left corner of the slab arrangement and the axes extend to the extreme corners of the arrangement in both the x- and y- directions. The advantages of this system are obvious:

1. Element numbering, although retained internally, does not enter into input data preparation;
2. Only as many loaded areas as actually exist need be specified. The global coordinates of the extent of each now acquires an improved physical meaning for the user;
3. The global coordinate system is independent of the mesh used, being solely determined by the arrangement of slab(s) analyzed.

The output from ILLI-SLAB now includes both the loaded areas as specified and the loaded subareas generated by Subroutine SUBAREA. The user familiar with the original version of ILLI-SLAB will recognize that the latter are identical to the input data the user would have had to prepare for the original version. A comparison of the two sets of information illustrates the significant improvement in input data specification achieved by Subroutine SUBAREA.

5.7 FREE-FORM INPUT CAPABILITY

With the addition of several new subroutines, ILLI-SLAB can now accept free-form input data using a Problem Oriented Language (POL) consisting of simple, easy-to-remember English-like statements. This has been made possible by accessing the SCAN Library of routines developed at the Civil Engineering Systems Laboratory (CESL), Department of Civil Engineering, University of Illinois at Urbana-Champaign (58,59,60). SCAN has been used as a teaching and research tool for a number of years at the University of Illinois. It is also the front end of the POLO System, including FINITE, and is used in a number of production systems at CESL.

Free-form input data for ILLI-SLAB are classified into 9 Groups, each defined by a Key-Word. Three of these Groups belong to Block 1 and the remainder to Block 2. Data in Block 1 must be read in first since they determine the amount of memory core required for a given run. Apart from this restriction in sequence, data can be read in any order desired by the user. Listed in Table 5.1 are the Key-Words defining each Data Group and a brief explanation of these.

Only those parameters that are different from the default values need be provided when using the free-form input capability. This will save time in preparing the input data file and executing the program. The free-form subroutines are set up to issue diagnostic error messages before execution in the event of improper input data. These greatly facilitate debugging the input data file and are particularly useful to

TABLE 5.1

FREE-FORM DATA GROUPS AND KEY WORDS

	GROUP	KEY-WORD	EXPLANATION
	1	TITLE	The title for a given problem; this will appear on the first page of the output.
BLOCK 1	2	NUMBER	Declaration of number of nodes, slabs, layers, and loaded areas.
	3	CONTOUR	Specification of contouring requests, if any, and of pertinent variables.
	4	COORDINATES	Specification of nodal coordinates along the x- and y-axes.
	5	PROPERTIES	Specification of properties of top and bottom layers (if any) and of the subgrade.
BLOCK 2	6	LOADED	Specification of loaded area limits and of load intensity.
	7	LOAD	Specification of load transfer type (if any), of direction and of pertinent variables.
	8	ITERATIVE	Specification of iterative scheme to be used (if any), including number of iterations, convergence tolerances and output type.
	9	SYMMETRY	Specification of lines of symmetry (if any)

the new user of ILLI-SLAB.

Use of the free-form input capability will be described in complete detail in an updated User's Manual. Figure 5.2 shows a comparison between the fixed-form and the free-form input data files for a typical run.

5.8 MISCELLANEOUS CHANGES

In addition to providing a user-oriented input data capability, it is desirable to have a user-oriented presentation of the results from a given run. The presentation of results in a graphical form as achieved by using the contouring subroutines is a major step in this direction. A lot can be done, however, with the actual printed output of ILLI-SLAB. Early in this study, particular attention was directed toward improving the output format by the introduction of appropriate carriage control characters, elimination of unnecessary lines of output (such as stresses in layer 2 when only one layer is used!) and replacement of these by other meaningful output information. The changes incorporated in the revised version of ILLI-SLAB aim at providing a well-organized, clear echo of the input file--so that the parameters and loading conditions used can be checked--, as well as giving the user a neat, usable output. Thus the appearance of the title page was enhanced (the date of the last update of the program is also shown on this page). The output now includes a listing of nodal coordinates as generated by the program. Of most interest to the user, however, is the summary of maximum values of

```
0
TITLE "**** RUN DR003: COMPARISON OF TWO TYPES OF INPUT FORMAT ****"
NUMBER OF NODES IN X DIRECTION SLABS 1  11
NUMBER OF NODES IN X DIRECTION SLABS 2  11
NUMBER OF NODES IN Y DIRECTION SLABS 1   8
NUMBER OF SLABS 2
NUMBER OF LOADED AREAS 1
NUMBER OF LAYERS 1
COORDINATES OF NODES IN X DIRECTION  0   80 140 170
190 210 220 225 230 235 240 240 245 250 255 260 270
290 310 340 400 480
IN Y DIRECTION 0 5 10 15 20 30 60 120
PROPERTIES OF TOP LAYER
THICKNESS 10
TOP LAYER ELASTIC MODULUS 4000000
POISSON RATIO 0.15
OF SUBGRADE MODULUS 430.9
TYPE SOFT
LOADED AREAS
1 IN X DIRECTION FROM 230 TO 240 AND IN Y DIRECTION FROM 0  TO 5
WITH PRESSURE 270
SYMMETRY X
LOAD TRANSFER IN X DIRECTION TYPE AGGREGATE INTERLOCK AGGREGATE
INTERLOCK FACTOR 1000000
NUMBER OF ITERATIONS 6
TOLERANCE FOR SUBGRADE MODULUS 0.05
TOLERANCE FOR NUMBER OF NODES 0.05
OUTPUT TYPE FULL
```

(a) Free-form Input Data

```
1
**** RUN DR003: COMPARISON OF TWO TYPES OF INPUT FORMAT ****
   11   11    0    8    0    1    1
000000   50
       0.0      80.0     140.0     170.0     190.0     210.0     220.0     225.0
     230.0     235.0     240.0     240.0     245.0     250.0     255.0     260.0
     270.0     290.0     310.0     340.0     400.0     480.0
       0.0       5.0      10.0      15.0      20.0      30.0      60.0     120.0
    2    1    0     430.9
      10.0 4.000E+06     0.150
   0
   1.0E+06
     270.0     230.0     240.0       0.0       5.0
    2    6 0.05 0.05    1
000000
```

(b) Fixed-form Input Data

Fig. 5.2 Comparison of Free-form and Fixed-form Input Data Files for Run DR003 (See Table 6.2; Fig. 6.1)

deflection and stresses and the nodal numbers at which these occur given at the end of the output. The output from ILLI-SLAB is now particularly suited for the Page Printer System (PPS), which produces good quality printouts on 8.5 x 11-in. forms, punched for a standard 3-ring binder. Such printouts may be directly included in a report.

A second group of changes involved the elimination of several code errors ("bugs") that were revealed during this study. Comparisons with FINITE show that at least the major routines of ILLI-SLAB, such as stiffness matrix assembly, inversion, solution and determination of stresses and deflections are probably free of any code errors.

CHAPTER 6

TYPICAL EFFECTS USING MODIFIED ILLI-SLAB

6.1 CASES CONSIDERED

To illustrate the capabilities of ILLI-SLAB and the impact of the modifications described in Chapter 5, a number of demonstration runs were performed. The results obtained from these runs are presented and discussed in this Chapter.

Two typical pavement cross-sections are considered in this investigation (Table 6.1). The first is a 10-in. Portland Cement Concrete (PCC) Pavement, consisting of 20-ft. square panels, with or without load transfer between adjacent slabs. The second pavement section is a 12-in. pavement incorporating a stabilized base layer with a modulus (E) of 1.5×10^6 psi. This pavement consists of 15-ft. by 12-ft. panels and is typical of pavements proposed for the USAF Alternate Launch and Recovery Surfaces (ALRS) Program.

TABLE 6.1

PARAMETERS FOR DEMONSTRATION RUNS

(a) PCC Pavement Section

Slab: 20' x 20' panels

h = 10"

$E = 4 \times 10^6$ psi

$\mu = 0.15$

k = 150 psi/in. or 'SOFT'

(b) ALRS Pavement Section

Slab: 12' x 15'

h = 12"

$E = 1.5 \times 10^6$ psi

$\mu = 0.15$

k = 120 psi/in. or 'SOFT'

(c) Loading Patterns

(i)	F - 4:		10-in.	x	10-in.	@	270 psi
(ii)	C-130:	2	21-in.	x	21-in.	@	100 psi
(iii)	F-111:		20.2-in.	x	15.5-in.	@	150 psi

The two pavement sections are loaded by three typical USAF aircraft loading patterns: the F-4, the C-130 and the F-111. A typical soft subgrade is assumed using two alternative ways of characterization. The first is the conventional static subgrade modulus, k, which was assigned a value of 120 to 150 psi/in. using the 'WINKLER' option in ILLI-SLAB. The second is the proposed resilient modulus, K_R, which was set at 425 psi/in. using the 'SOFT' option. Associated with the latter option, is stress dependence, provided by the iterative scheme in ILLI-SLAB.

The f.e. meshes used for the demonstration runs are shown in Figures 6.1 through 6.9. For the cases involving load transfer, a second "mirror image" panel was added to the right of the panels showed in these figures. Note that the ALRS runs involving load transfer are of academic interest only, since load transfer systems are not recommended for such sections.

The major results from the demonstration runs are summarized in Table 6.2. In an effort to clarify the picture presented by these results, three distinct effects are identified:

(a) Effect of Load Transfer;

(b) Effect of Resilient Modulus; and

(c) Effect of Stress Dependence--Iterative Scheme.

These effects are discussed separately below.

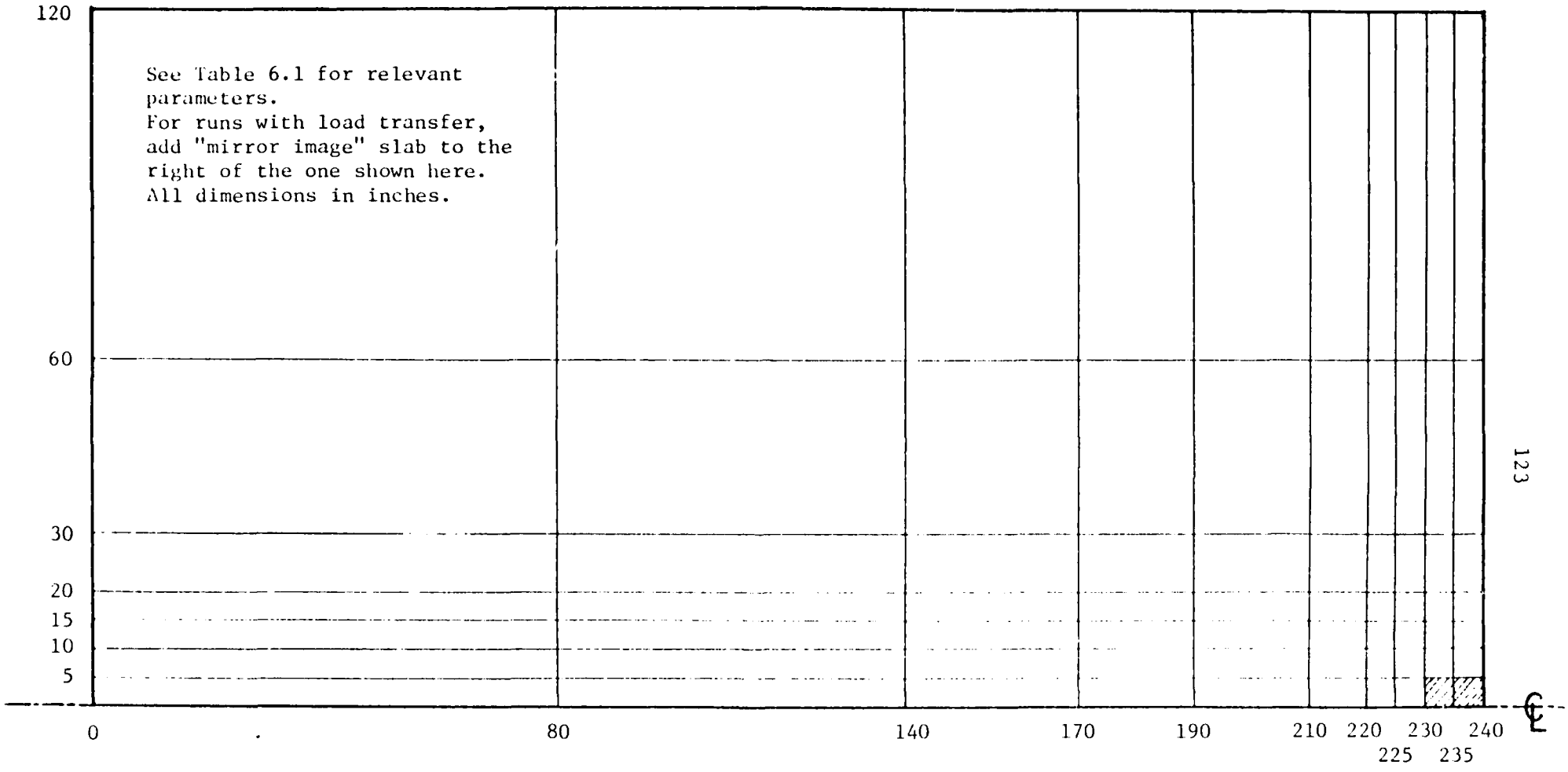

Fig. 6.1 F. E. Mesh for F-4 at Edge of PCC Pavement

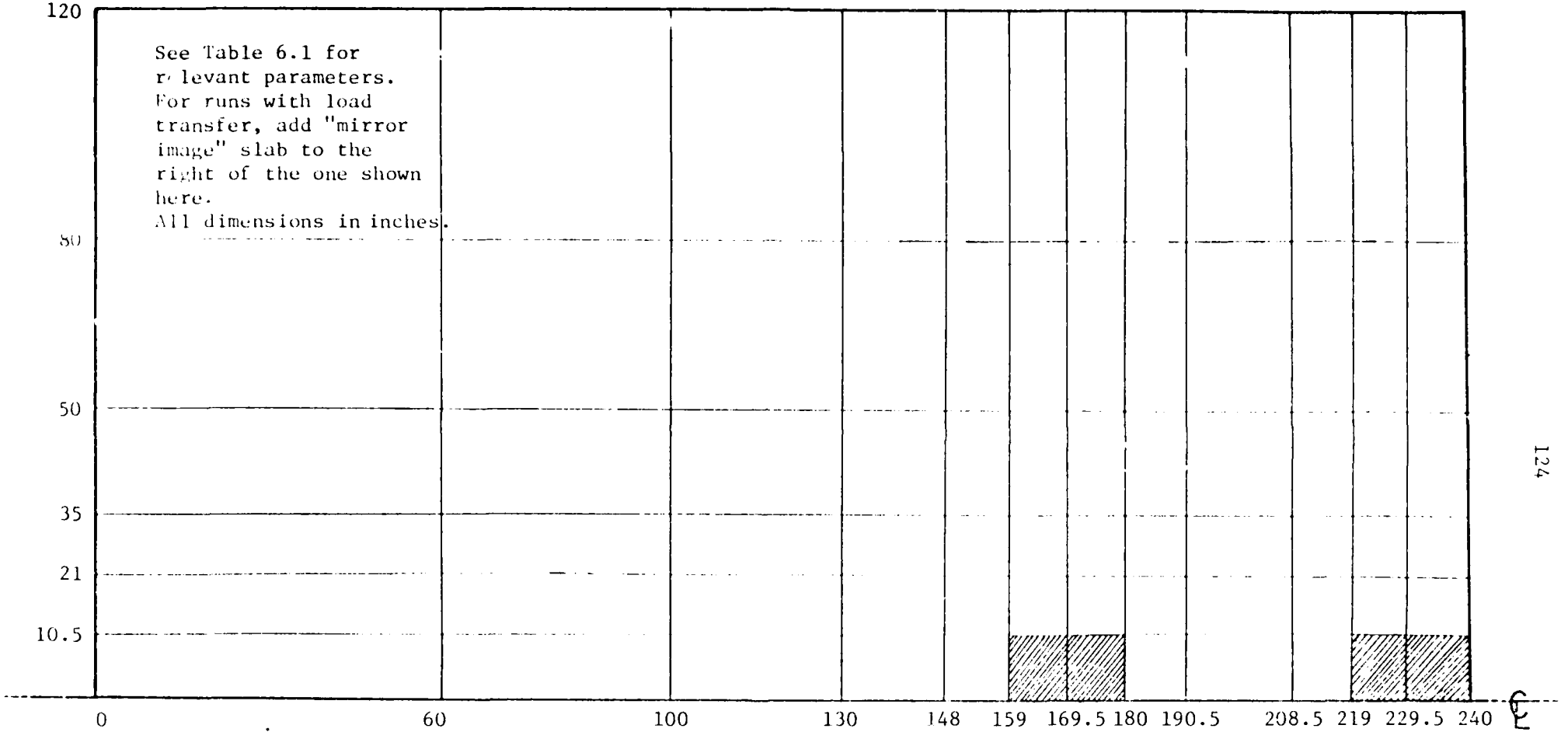

Fig. 6.2 F. E. Mesh for C-130 at Edge of PCC Pavement

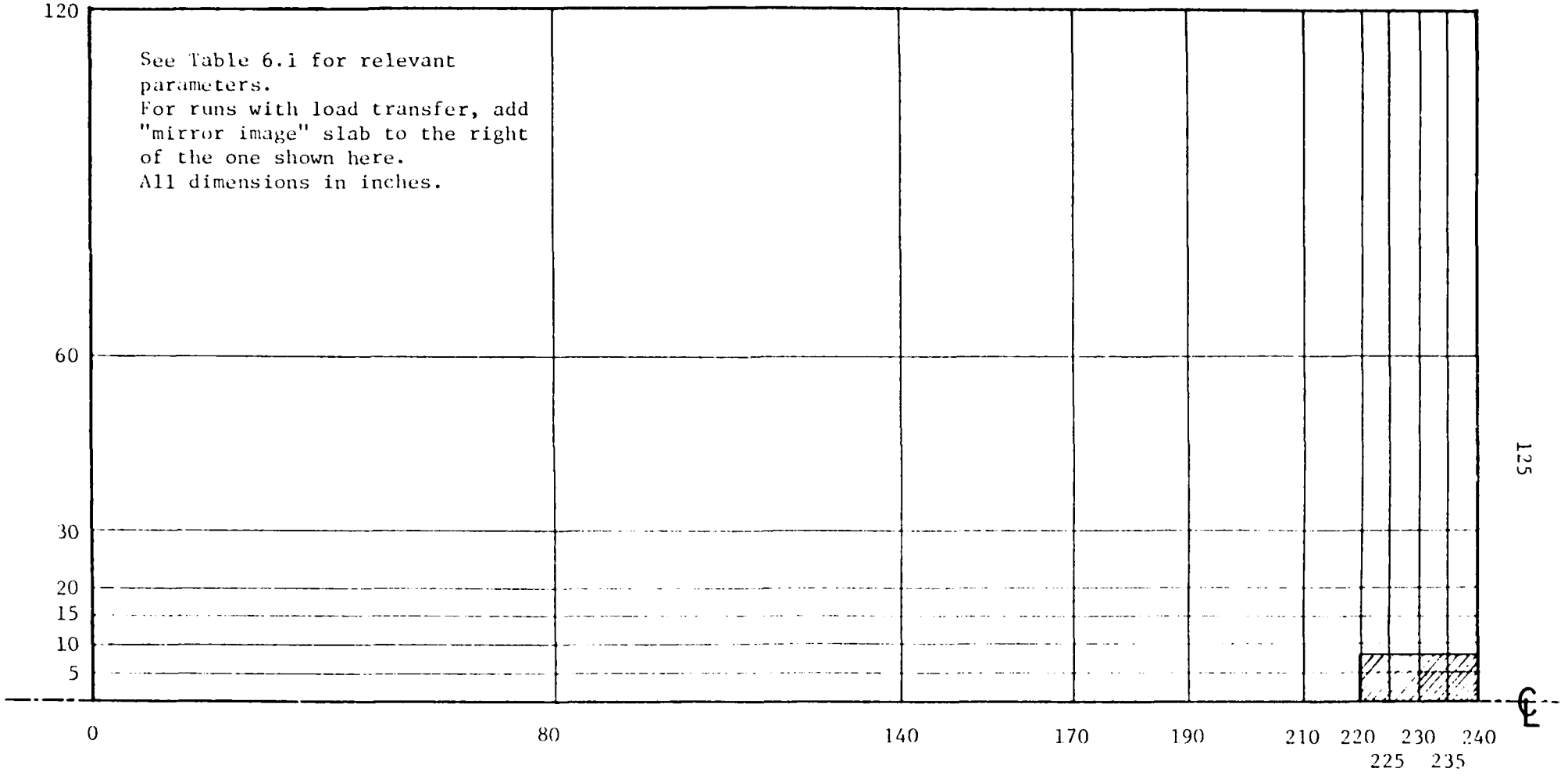

Fig. 5.3 F. E. Mesh for F-111 at Edge of PCC Pavement

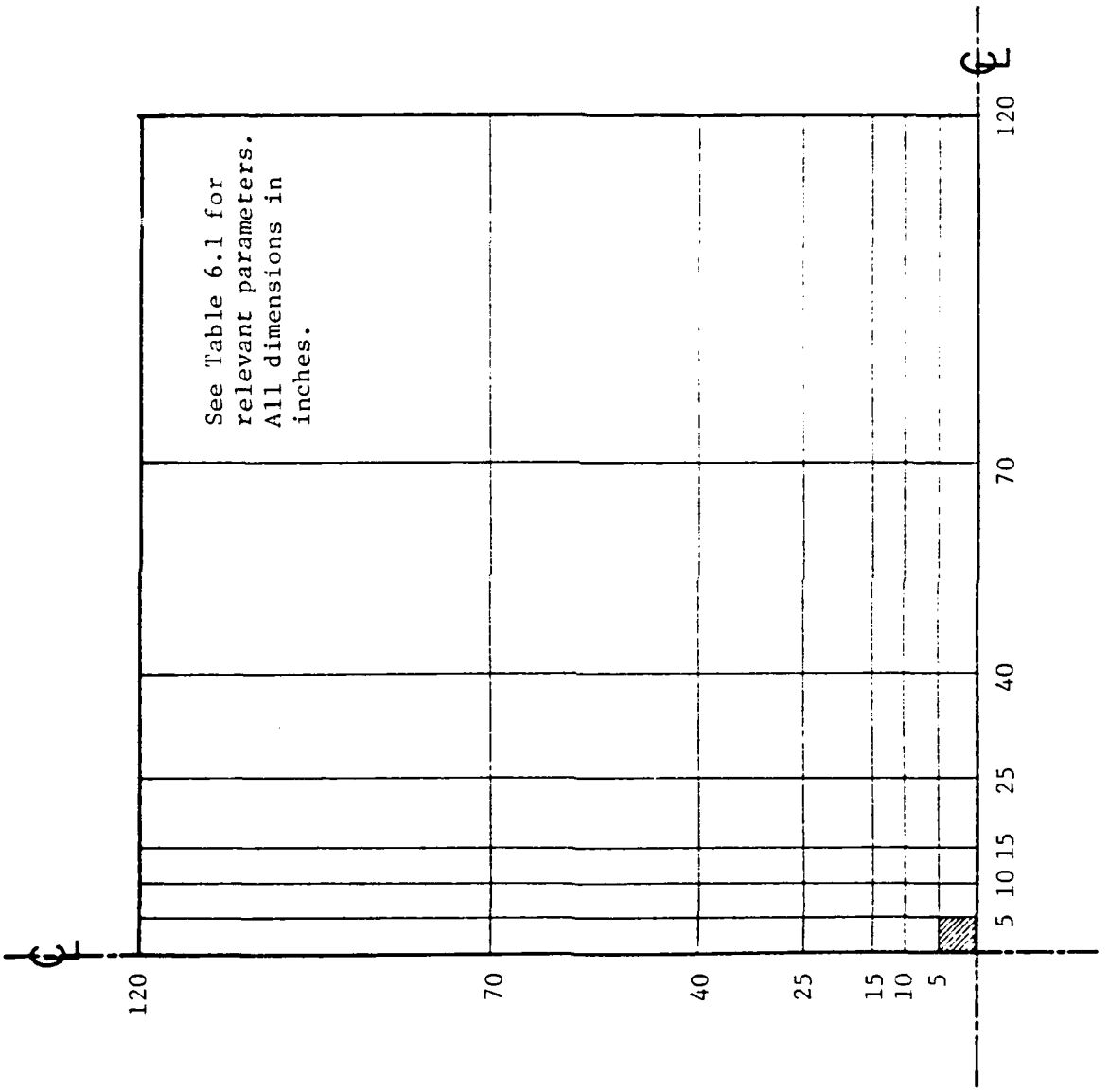

Fig. 6.4 F. E. Mesh for F-4 at Interior of PCC Pavement

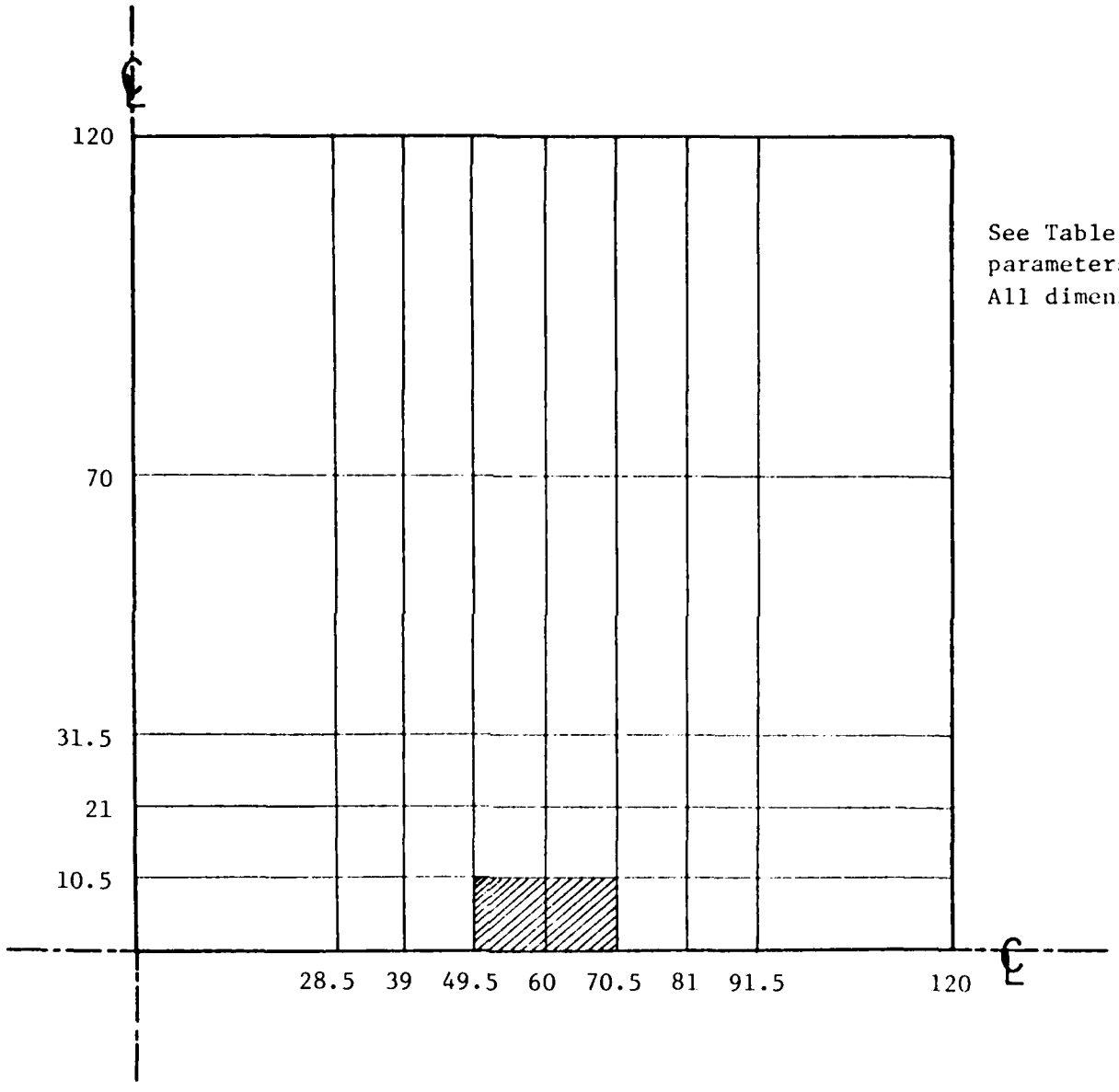

See Table 6.1 for relevant parameters.
All dimensions in inches.

Fig. 6.5 F. E. Mesh for C-130 at Interior of PCC Pavement

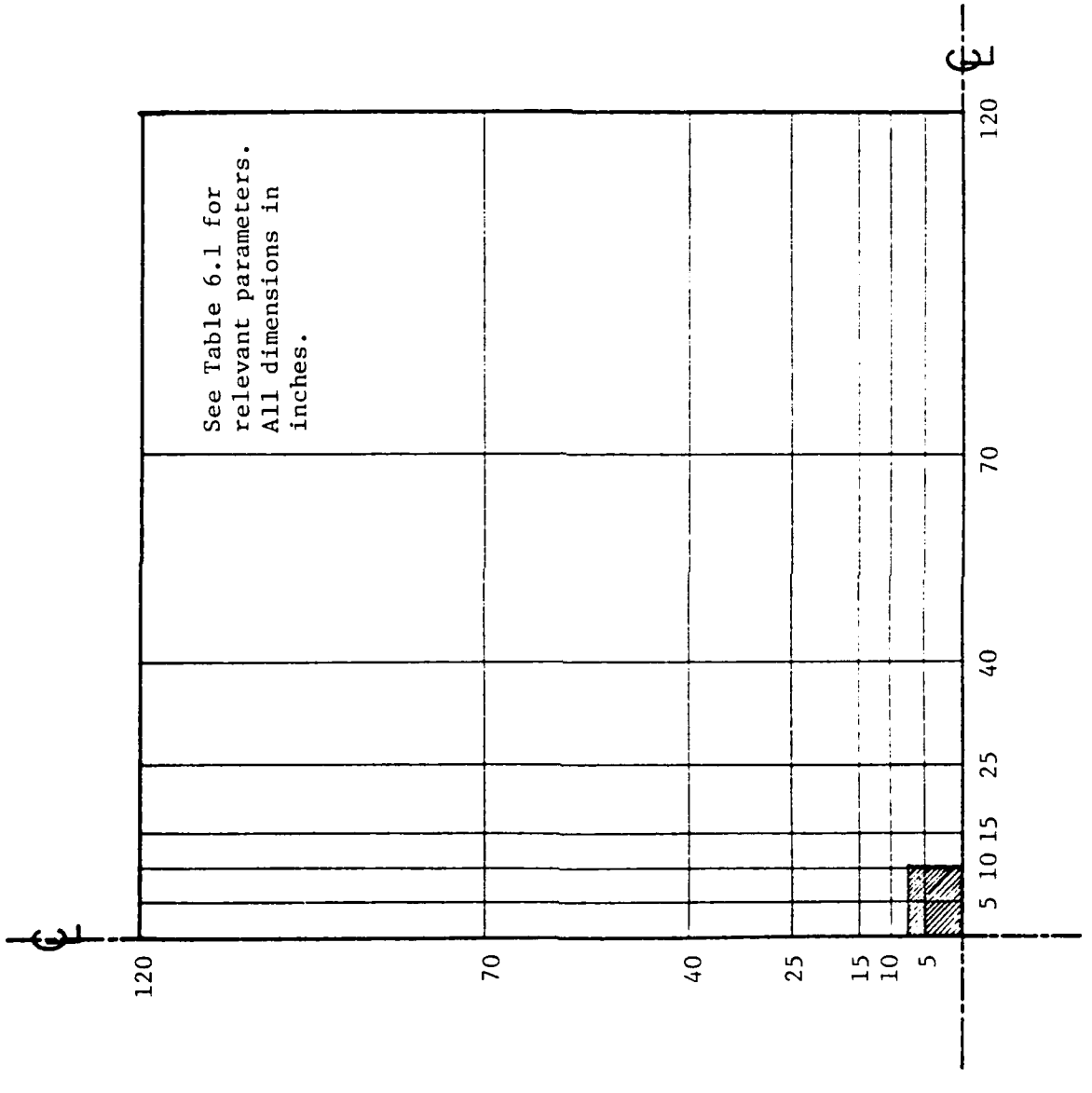

Fig. 6.6 F. E. Mesh for F-111 at Interior of PCC Pavement

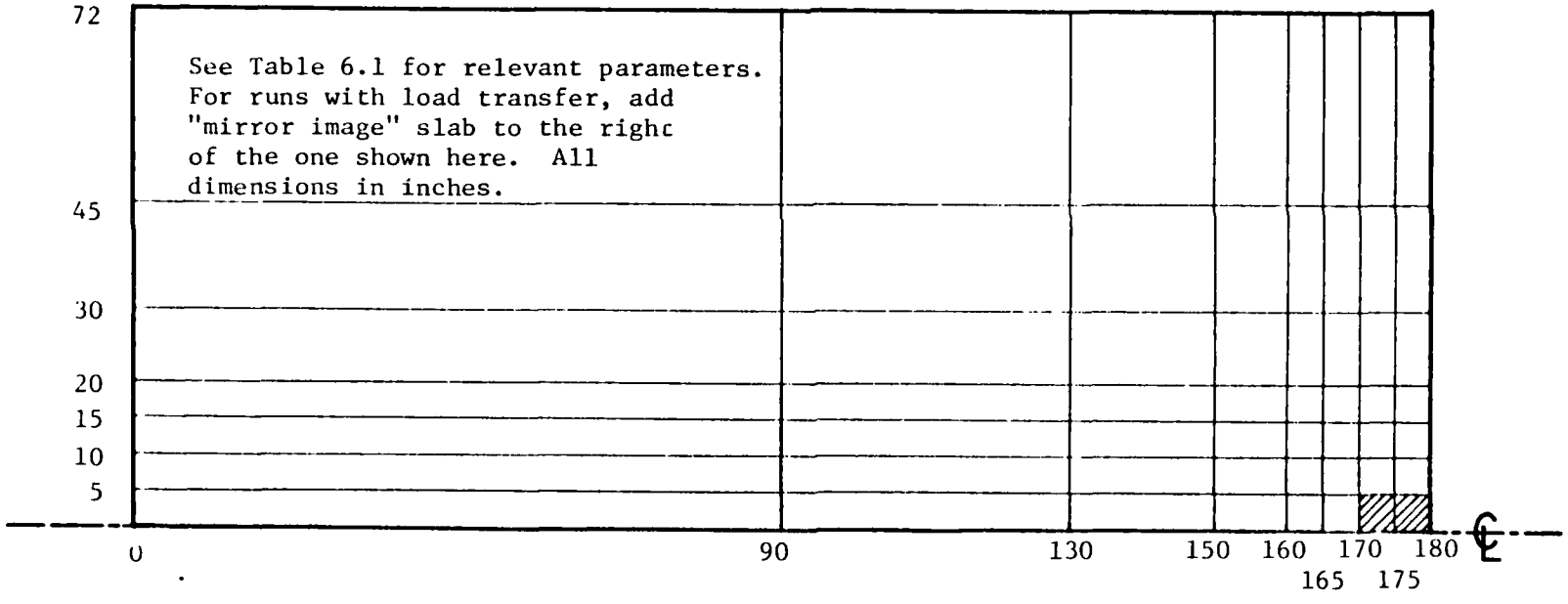

Fig. 6.7 F. E. Mesh for F-4 at Edge of ALRS Pavement

See Table 6.1 for relevant parameters.
For runs with load tranfer, add "mirror image"
slab to the right of the one shown here.
All dimensions in inces.

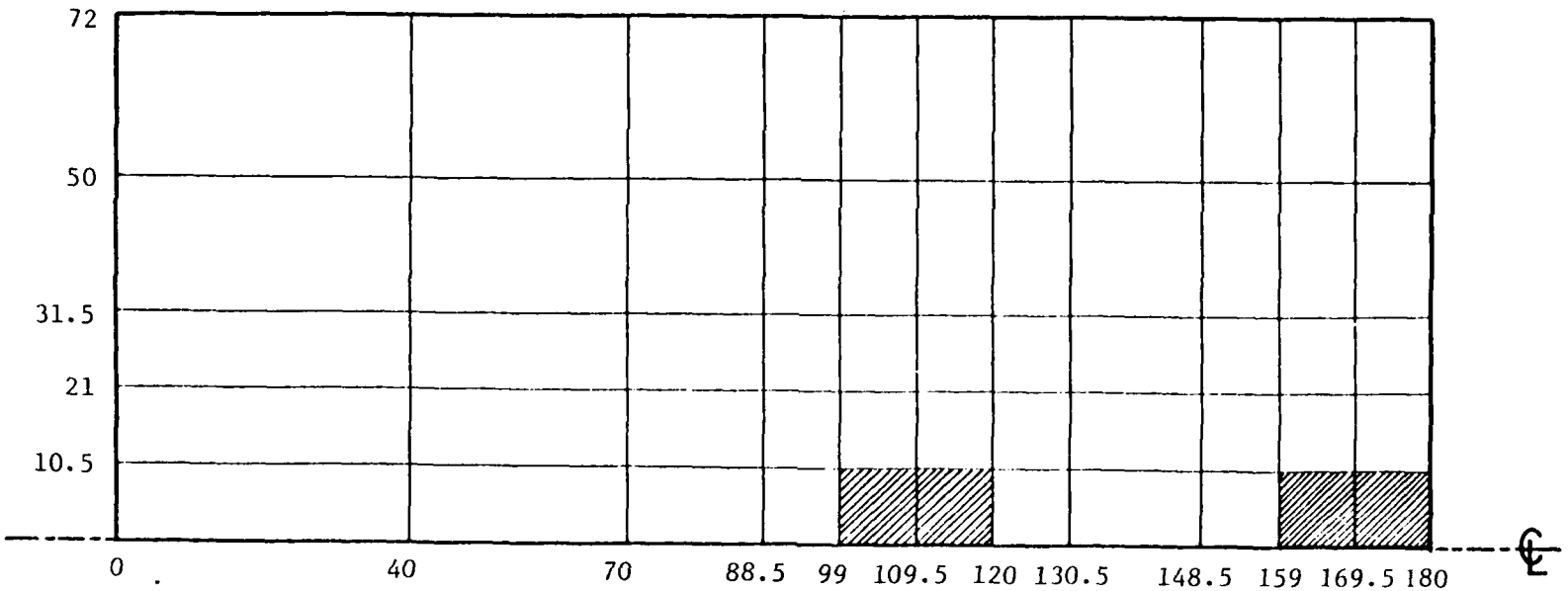

Fig. 6.8 F. E. Mesh for C-130 at Edge of ALRS Pavement

See Table 6.1 for relevant parameters.
For runs with load transfer, add "mirror image"
slab to the right of the one shown here.
All dimensions in inches.

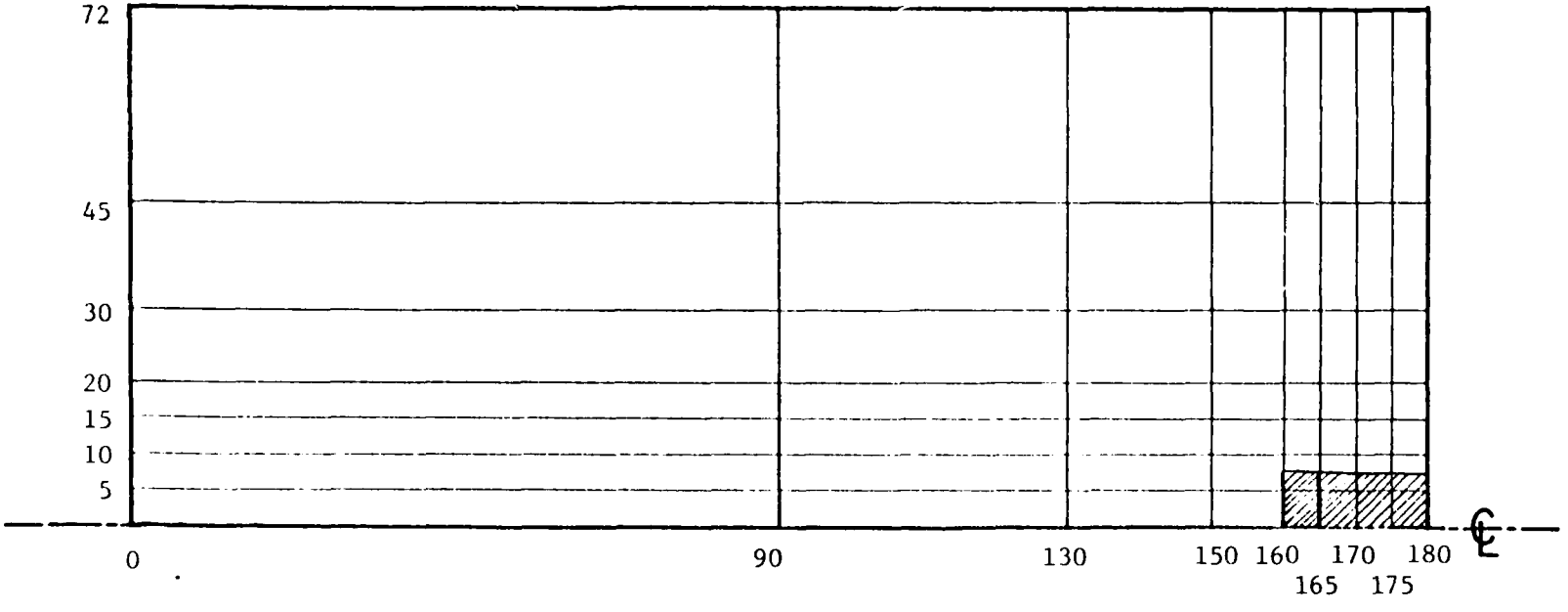

Fig. 6.9 F. E. Mesh for F-111 at Edge of ALRS Pavement

TABLE 6.2

DEMONSTRATION RUNS RESULTS

RUN	PAVEMENT	AIRCRAFT	SUBGRADE	LOAD POSITION	SPECIFIED AIF	ACTUAL LTE	MAX. DEFLECTION (mils/node) NIT=1	NIT=2	NIT=3	MAX. STRESS (psi/node) NIT=1	NIT=2	NIT=3
DR001	PCC	F-4	k=150 psi/in.	Edge	10^6	98	24.1/81	--	--	470/81	--	--
DR002	PCC	F-4	k=150 psi/in.	Edge	0	--	47.7/81	--	--	773/81	--	--
DR003	PCC	F-4	'SOFT'	Edge	10^6	96	13.5/81	x	x	423/81	x	x
DR004	PCC	F-4	'SOFT'	Edge	0	--	26.4/81	27.3/81	x	680/81	690/81	x
DR005	PCC	C-130	k=150 psi/in.	Edge	10^6	98	40.4/85	--	--	561/78	--	--
DR006	PCC	C-130	'SOFT'	Edge	0	--	38.6/85	42.3/85	x	740/85	776/85	x
DR007	PCC	C-130	'SOFT'	Edge	10^6	97	19.7/78	20.3/78	x	456/78	464/78	x
DR008	PCC	F-111	'SOFT'	Edge	0	--	39.6/81	42.6/81	x	806/81	834/81	x
DR009	ALRS	F-4	k=120 psi/in.	Edge	10^6	98	37.1/65	--	--	302/65	--	--
DR010	ALRS	F-4	k=120 psi/in.	Edge	0	--	73.6/65	--	--	509/65	--	--
DR011	ALRS	F-4	'SOFT'	Edge	10^6	97	17.3/65	17.5/65	x	270/65	272/65	x
DR012	ALRS	F-4	'SOFT'	Edge	0	--	34.1/65	36.0/65	x	446/65	455/65	x
DR013	ALRS	C-130	k-120 psi/in.	Edge	10^6	99	59.1/67	--	--	366/61	--	--
DR014	ALRS	C-130	'SOFT'	Edge	10^6	98	23.9/67	25.1/61	x	294/61	301/61	x
DR015	ALRS	C-130	'SOFT'	Edge	0	--	47.2/67	53.6/67	x	475/67	507/67	x
DR016	ALRS	F-111	'SOFT'	Edge	0	--	50.3/65	56.1/65	x	518/65	545/65	x
DR017	PCC	F-4	'SOFT'	Interior	0	--	8.8/1	x	x	356/1	x	x
DR018	PCC	C-130	'SOFT'	Interior	0	--	14.1 /25	x	x	408 /25	x	x
DR019	PCC	F-111	'SOFT'	Interior	0	--	14.8/1	x	x	462/1	x	x

Notes: (a) For f.e. meshes, see Figs. 6.1 through 6.9.

(b) For relevant parameters, see Table 6.1.

(c) Parameters for option 'SOFT':

ITMAX = 6
TOL1 = 5%
TOL2 = 5%

(d) Actual LTE's calculated after first iteration.

(e) NIT: Iteration Number
x : Convergence achieved at an earlier iteration.

6.2 DISCUSSION OF RESULTS

6.2.1 Effect of Load Transfer

To investigate the impact of load transfer systems, load transfer by aggregate interlock was provided in some runs and these are compared to those in which only one panel was used. It was intended to investigate the two extreme cases, that of no load transfer (LTE = 0%) and that of full load transfer (LTE = 100%). For the latter, an aggregate interlock factor (AIF) of 1×10^6 was specified, producing load transfer efficiencies (LTE) between 97% and 99% (see Table 6.2).

Under conditions of full load transfer, maximum deflection is reduced to half its value for the condition of no load transfer. The effect of load transfer on maximum bending stress is shown as a stress ratio in Table 6.3. The Table indicates that full load transfer stress is about 0.6 times the no load transfer value. It is also observed that the proposed change to a resilient modulus subgrade characterization has only a minor effect in this respect. As expected, the load transfer effect is more pronounced (albeit only very slightly) in the case of the less stiff ALRS pavement.

TABLE 6.3

EFFECT OF LOAD TRANSFER

PAVEMENT	AIRCRAFT	SUBGRADE	STRESS RATIO
PCC	F-4	k=150 psi/in.	0.61
		'SOFT'	0.62
	C-130	'SOFT'	0.62
ALRS	F-4	k=120 psi/in.	0.59
		'SOFT'	0.61
	C-130	'SOFT'	0.62

Notes: (a) All runs for edge loading condition

(b) $$\text{STRESS RATIO} = \frac{\sigma_{max.} \text{ for LTE } 100\%}{\sigma_{max.} \text{ for LTE} = 0}$$

where LTE = load transfer efficiency

$$= \frac{\text{Deflection across joint on unloaded side}}{\text{Max. Deflection along joint on loaded side}}$$

(c) The corresponding DEFLECTION RATIO is 0.50 for LTE = 100%.

(d) All comparisons for first iteration.

6.2.2 Effect of Resilient Modulus Characterization

As explained in Chapter 3, it is considered that a resilient modulus subgrade characterization would be more appropriate for airfield pavement systems under transient loads, than the conventional static plate load test subgrade modulus. The k-value used to characterize the subgrade in f.e. programs like ILLI-SLAB should be replaced by a stress dependent K_R-value, which at low stress levels is substantially greater than k. In the cases analyzed in this report, the subgrade was assumed to have a static k value of 120 to 150 psi/in. This is considered equivalent to the stress dependent 'SOFT' subgrade option in ILLI-SLAB. The low stress level K_R-value for this subgrade is 425 psi/in., according to the algorithms proposed in Chapter 3.

The effect of this change is shown in Table 6.4 in the form of "before" and "after" deflection and stress ratios. The former are seen to vary between 0.40 and 0.56, while the latter have values between 0.80 and 0.90. Thus, the proposed resilient modulus subgrade characterization leads to smaller calculated deflections and stresses, with stresses being affected to a smaller extent than deflection. Table 6.4 also shows that the impact of the proposed change is more significant as the load becomes more severe (C-130 instead of F-4) and/or the pavement system is less stiff (ALRS rather than PCC pavement).

TABLE 6.4

EFFECT OF RESILIENT MODULUS

PAVEMENT	AIRCRAFT	SPECIFIED LTE (%)	DEFLECTION RATIO	STRESS RATIO
PCC	F-4	0	0.55	0.88
		100	0.56	0.90
	C-130	100	0.49	0.81
ALRS	F-4	0	0.46	0.87
		100	0.47	0.89
	C-130	100	0.40	0.80

Notes: (a) All runs for edge loading condition

(b) DEFLECTION RATIO $= \frac{\text{Max. deflection for 'SOFT'}}{\text{Max. deflection for 'WINKLER'}}$

(c) STRESS RATIO $= \frac{\text{Max. stress for 'SOFT'}}{\text{Max. stress for 'WINKLER'}}$

(d) All comparisons for first iteration.

6.2.3 Effect of Stress Dependence -- Iterative Scheme

Associated with the stress dependent options in ILLI-SLAB, including 'SOFT' employed in these demonstration runs, is an iterative scheme. In this scheme, at the end of each iteration a check is performed for the compatibility of calculated deflections and assumed support pattern (i.e. K_R-values). A new iteration is performed after updating the support pattern until specified convergence tolerances are achieved. As seen in Table 6.2, no more than two iterations were required to achieve convergence in these runs. This may indicate that the tolerances TOL1 and TOL2 of 5% used are fairly liberal.

Table 6.5 is an attempt to filter out the effect of the iterative scheme, by presenting in terms of deflection and stress ratios, the responses after the first and after the last iterations. Deflection ratios range between 1.00 and 1.14 while stress ratios fall between 1.00 and 1.07. Thus the effect of the iterative scheme is to increase the maximum deflections and stresses obtained after the first iteration, thereby counterbalancing some of the change produced by the resilient modulus described in Section 6.2.2, above.

Since the application of the iterative scheme increases execution time, it is important to draw some conclusions as to when such an increased expense is justified by the changes in response produced. Table 6.5 shows that the iterative scheme effect becomes substantial (ie. in the region of 10% or more) for the more severe loading patterns (edge

TABLE 6.5

EFFECT OF STRESS DEPENDENCE

LOAD POSITION	PAVEMENT	AIRCRAFT	SPECIFIED LTE (%)	DEFLECTION RATIO	STRESS RATIO
Edge	PCC	F-4	0	1.03	1.01
			100	1.00	1.00
		C-130	0	1.10	1.05
			100	1.03	1.02
		F-111	0	1.04	1.07
	ALRS	F-4	0	1.06	1.02
			100	1.01	1.00
		C-130	0	1.14	1.07
			100	1.05	1.03
		F-111	0	1.12	1.05
Interior	PCC	F-4	0	1.00	1.00
		C-130	0	1.00	1.00
		F-111	0	1.00	1.00

Notes: (a) All runs for 'SOFT' subgrade

(b) DEFLECTION RATIO = $\frac{\text{Max. deflection for last iteration}}{\text{Max. deflection for first iteration}}$

(c) STRESS RATIO = $\frac{\text{Max. stress for last iteration}}{\text{Max. stress for first iteration}}$

(d) Convergence Tolerances: TOL1 = 5%
TOL2 = 5%

rather than interior; F-111, C-130 rather than F-4), on the less competent pavement systems (ALRS rather than PCC section; LTE = 0% rather than LTE = 100%).

In general, the effect of the iterative scheme is not dramatic. This may be attributed to the fact that the algorithms used in the present version of ILLI-SLAB were developed by simulating rigid plate load tests using ILLI-PAVE. The plates used in these tests are much stiffer than any ordinary pavement slabs, and their radius of relative stiffness, l, is much higher than the values encountered in pavement slabs. Westergaard (46) as well as other investigators have pointed out the effect of the radius of relative stiffness on subgrade--pavement system response.

Finally, Table 6.6 presents the combined effects of the resilient modulus and of the iterative scheme. The deflection ratios range between 0.42 and 0.57 and are, in general, substantially lower than the corresponding stress ratios, which lie between 0.82 and 0.90. This indicates that the impact of the proposed changes is much more significant with respect to deflection rather than stresses. Furthermore, the effects are more pronounced in the case of the more severe load patterns and/or the less competent pavement systems.

TABLE 6.6

COMBINED EFFECT OF PROPOSED CHANGES

PAVEMENT	AIRCRAFT	SPECIFIED LTE (%)	DEFLECTION RATIO	STRESS RATIO
PCC	F-4	0	0.57	0.89
		100	0.56	0.90
	C-130	100	0.50	0.83
ALRS	F-4	0	0.49	0.89
		100	0.47	0.90
	C-130	100	0.42	0.82

Notes: (a) All runs for edge loading condition.

(b) DEFLECTION RATIO = $\frac{\text{Max. deflection after changes}}{\text{Max. deflection before changes}}$

(c) STRESS RATIO = $\frac{\text{Max. stress after changes}}{\text{Max. stress before changes}}$

(d) Changes consist of:

(i) Subgrade Characterization by resilient modulus, K_R (= 425 psi/in.: 'SOFT'), instead of static subgrade modulus k (= 120 or 150 psi/in);

(ii) Stress dependence-iterative scheme.

CHAPTER 7

CONCLUDING REMARKS

The U.S. Air Force is continuously confronted with problems concerning:

1. The ability of an existing pavement to accommodate current and/or different types of aircraft loading;
2. The development of rehabilitation/reconstruction recommendations for existing pavements;
3. The design of new pavements;
4. The advantages/disadvantages of various aircraft gear configurations and wheel loadings; and
5. The effectiveness of new materials and pavement cross-sections.

Classical slab-on-grade pavement analysis procedures (such as those proposed by Westergaard), cannot accommodate nonlinear subgrade support conditions, complex loading patterns, cracked sections with varying load transfer efficiencies, and subbase effects. The modified ILLI-SLAB model

developed in this study alleviates many of these inadequacies.

Computer program ILLI-SLAB (1), originally developed at the University of Illinois, offers great flexibility in modeling loading conditions [i.e. position, size and intensity of loaded area(s)] and load transfer systems. The objective of this study was to modify the subgrade model in ILLI-SLAB from a simple, linear spring (Winkler) type, to a stress dependent (more accurately, a deflection dependent) model, in which the resilient subgrade modulus, K_R, decreases with increasing deflection, w.

In the first stage of the investigation, K_R was defined as a function of w for the four subgrade types (very soft, soft, medium, and stiff) characterized by Thompson and his co-workers (13) and used in computer program ILLI-PAVE. By simulating repeated plate load tests using ILLI-PAVE, a relationship of the following form was obtained between K_R and w:

$$K_R = \frac{A_1 \left[1 - \exp\left\{-A_2 \left(\frac{w}{D_y} - A_3\right)\right\}\right] + A_4 \left(\frac{w}{D_y} - A_3\right) + 2}{w}$$

in which:

A1,...A5: Constants, functions of subgrade type;

D_y:Constant, function of plate size;

K_R: Resilient subgrade modulus, in psi/in.;

w: Deflection in inches.

This model was incorporated into ILLI-SLAB using an iterative scheme. According to this, a selected initial value of K_R (dependent on subgrade type) is corrected after each iteration. After a number of iterations, the values of K_R before and after the last iteration differ by only a specified small percentage. The impact of the iterative K_R model was investigated for several typical pavement systems subjected to interior and edge loading. Some of the sections included load transfer systems.

The effect of a granular subbase on K_R was also examined. It was found that K_R is increased by the introduction of a 4- to 6-in. granular layer. However, in the subbase thickness range of 8 to 24 in., this effect is not pronounced.

The major effect of the proposed K_R model stems the difference between the value of the resilient subgrade modulus (initial K_R value assigned in the iterative procedure) and the static k typically utilized. The effect of iterative analysis is limited, and becomes more pronounced for conditions producing more severe pavement responses (thin structural sections, traffic overloads, edge loading, no load transfer).

Future phases of the investigation will be directed toward further verifying the proposed model. Pavement response data from well-documented laboratory or field studies will be analyzed with the modified ILLI-SLAB program. Such data are available in the literature, from State and/or Federal agencies, or, if necessary, can be collected in

a test program conducted by the investigators.

Further analytical verification of the model will be provided by comparisons with other existing computer programs such as GEOSYS, FINITE, BISAR, VESYS, KENTUCKY, CHEVRON, etc.. The comparative data thus collected will facilitate a reconsideration of current design practice which is primarily based on Westergaard theory. There is a need to understand, for example, the discrepancies between Westergaard and ILLI-SLAB results, especially for edge and corner conditions and to determine whether, indeed, some of Westergaard's analyses are "erroneous from a theoretical standpoint" (53).

REFERENCES

1. Tabatabaie, A. M., Barenberg, E. J., and Smith, R. E., "Longitudinal Joint Systems in Slip-Formed Rigid Pavements, Volume II -- Analysis of Load Transfer Systems for Concrete Pavements," U.S. Department of Transportation, Report No. FAA-RD-79-4, II, November, 1979.

2. Tabatabaie, A. M., and Barenberg, E. J., "Longitudinal Joint Systems in Slip-Formed Rigid Pavements, Volume III -- User's Manual," U.S. Department of Transportation, Report No. FAA-RD-79-4, III, November, 1979.

3. Kerr, A. D., "Elastic and Viscoelastic Foundation Models," Journal of Applied Mechanics, Transactions, ASME, Vol. 31, No. 3, 1964.

4. American Society for Testing and Materials, "Soil and Rock: Building Stones," Annual Book of ASTM Standards, 1982.

5. Departments of the Army, the Navy, and the Air Force, "Materials Testing," Technical Manual No. 5-530/Navy Publication NAVFAC MO-330/Air Force Manual No. 89-3, 1971.

6. Packard, R. G., "Design of Concrete Airport Pavement," Portland Cement Association, Engineering Bulletin EB050.03P, 1973.

7. Desai, C. S., and Christian, J. T., "Numerical Methods in Geotechnical Engineering," McGraw-Hill, 1977.

8. Butterfield, R., and Georgiadis, M., "New Interpretation of Plate-Bearing Tests," Transportation Research Record No. 810, Transportation Research Board, 1981.

9. Burland, J. B., and Lord, J. A., "The Load-Deformation Behavior of Middle Chalk at Mundford, Norfold: A Comparison Between Full Scale

Performance and In-situ and Laboratory Measurements," In-situ Investigation of Soils and Rocks, British Geological Society, 1970.

10. Scott, R. F., "Foundation Analysis," Prentice-Hall, 1981.
11. Engesser, F., "Zur Theorie des Baugraundes, Zentralblatt der Bauverwaltung," Berlin, Germany, 1893.
12. Butterfield, R. and Georgiadis, M., "Cyclic Plate Bearing Tests," Journal of Terramechanics, Vol. 17, No. 3, 1980.
13. Thompson, M. R. and Robnett, Q. L., "Resilient Properties of Subgrade Soils," Transportation Engineering Journal, ASCE, Vol. 105, No. TE1, January, 1979.
14. Rada, G., and Witczak, M. W., "Comprehensive Evaluation of Laboratory Resilient Moduli Results for Granular Material," Transportation Research Record No. 810, Transportation Research Board, 1981.
15. Figueroa, J. L., "Resilient Based Flexible Pavement Design Procedure for Secondary Roads," Ph.D. Thesis, University of Illinois, Urbana, 1979.
16. Raad, L. and Figueroa, J. L., "Load Response of Transportation Support Systems," Transportation Engineering Journal, ASCE, Vol. 106, No. TE1, January, 1980.
17. Hoffman, M. S., and Thompson, M. R., "Mechanistic Interpretation of Nondestructive Pavement Testing Deflections," Civil Engineering Studies, Trasportation Engineering Series No. 32, Illinois Cooperative Highway and Transportation Research Program Series No. 190, University of Illinois at Urbana-Champaign, June, 1981.
18. Suddath, L. P. and Thompson, M. R., "Load-Deflection Behavior of

Lime-Stabilized Layers," Technical Report M-118, Construction Engineering Research Laboratory, 1975.

19. Traylor, M. R., "Nondestructive Testing of Flexible Pavements," Ph.D. Thesis, Department of Civil Engineering, University of Illinois, Urbana, 1979.

20. Hoffman, M. S. and Thompson, M. R., "Nondestructive Testing of Flexible Pavements-Field Testing Program Summary," Civil Engineering Studies, Trasportation Engineering Series No. 31, Illinois Cooperative Highway and Transportation Research Program Series No. 188, University of Illinois at Urbana-Champaign, June, 1981.

21. Thompson, M. R., "Concepts for Developing a Nondestructive Based Asphalt Concrete Overlay Thickness Design Procedure," Civil Engineering Studies, Transportation Engineering Series No. 34, Illinois Cooperative Highway and Transportation Series No. 194, University of Illinois at Urbana-Champaign, June, 1982.

22. Figueroa, J. L. and Thompson, M. R., "Simplified ILLI-PAVE Based Structural Analyses of Flexible Pavement for Secondary Roads," Transportation Research Record No. 766, Transportation Research Board, 1980.

23. Thompson, M. R. and Figueroa, J. L., "Mechanistic Thickness Design Procedure for Soil-Lime Layers," Transportation Research Record No. 754, Transportation Research Board, 1980.

24. "Airport Pavement Design and Evaluation," Advisory Circular 150/5320-60, Federal Aviation Administration, December 7, 1978.

25. Tabatabaie, A. M., and Barenberg, E. J., "Finite-Element Analysis of Jointed or Cracked Concrete Pavements," Transportation Research

Record No. 671, Transportation Research Board, 1978.

26. Wilson, E. L., "Solid SAP, A Static Analysis Program for Three-Dimensional Solid Structures," UC-SESM Report 71-19, Structural Engineering Laboratory, University of California, Berkeley, CA, 1969.

27. Irons, B. M., "Engineering Application of Numerical Integration in Stiffness Methods," Journal of American Institute of Aeronautics and Astronautics, Vol. 4, No. 11, 1966.

28. Wilson, E. L., and Pretorius, P. C., "A Computer Program for the Analysis of Prismatic Solids," UC-SESM Report 70-21, Structural Engineering Laboratory, University of California, Berkeley, CA, 1970.

29. Pretorius, P. C., "Design Considerations for Pavements Containing Soil-Cement Bases," Ph. D. Dissertation, University of California, Berkeley, CA, 1970.

30. Luther, M. S., Majidzadeh, K., and Chang, C. W., "A Mechanistic Investigation of Reflection Cracking," Proceedings, 2nd Conference on Asphaltic Pavements for South Africa (CAPSA 1974), Durban, South Africa, 1974.

31. Otte, E., "Analysis of a Cracked Pavement Base Layer," Transportation Research Record No. 725, Transportation Research Board, 1979.

32. Fossberg, P. E., Mitchell, J. K., and Monismith, C. L., "Cracking and Edge-Loading Effects on Stresses and Deflections in a Soil-Cement Pavement," Transportation Research Record No. 379, Transportation Research Board, 1972.

33. Hudson, W. R., and Matlock, H., "Discontinuous Orthotropic Plates and Pavement Slabs," Research Report 56-6, Center for Highway Research, University of Texas at Austin, 1965.

34. Hudson, W. R., and Matlock, H., "Analysis of Discontinuous Orthotropic Pavement Slabs Subjected to Combined Loads," Highway Research Record No. 131, Highway Research Board, 1966.

35. Stelzer, C. F., Jr., and Hudson, W. R., "A Direct Computer Solution for Plates and Pavement Slabs," Research Report 56-9, Center for Highway Research, University of Texas at Austin, 1967.

36. Vesic, A. S., and Saxena, K., "Analysis of Structural Behavior of AASHO Road Test Rigid Pavements," NCHRP Report No. 97, Highway Research Board, 1970.

37. Saxena, S. K., and Vesic, A. S., "Experimental Study of Slabs Resting on a Silty Clay Subgrade," Proceedings, 52nd Annual Meeting, Highway Research Board, Washington, D. C., 1973.

38. Ayyash, A. A., Hudson, W. R., and Treybig, H. J., "Effects of Cracks on Bending Stiffness in Continuous Pavements," Highway Research Record No. 407, Highway Research Board, 1972.

39. Chou, Y. T., "Structural Analysis Computer Programs for Rigid Multicomponent Pavement Structures with Discontinuities--WESLIQID and WESLAYER; Report 1: Program Development and Numerical Presentations; Report 2: Manual for the WESLIQID Finite Element Program; Report 3: Manual for the WESLAYER Finite Element Program," Technical Report GL-81-6, U. S. Army Engineer Waterways Experiment Station, May, 1981.

40. Huang, Y. H., and Wang, S. T., "Finite-Element Analysis of

Concrete Slabs and its Implications for Rigid Pavement Design," Highway Research Record No. 466, Highway Research Board, 1973.

41. Huang, Y. H., and Wang, S. T., "Finite-Element Analysis of Rigid Pavements with Partial Subgrade Contact," Highway Research Record No. 485, Highway Research Board,1974.

42. Lopez, L. A., "FINITE: An Approach to Structural Mechanics Systems," International Journal for Numerical Methods in Engineering, Vol. 11, 1977.

43. Lopez, L. A., Dodds, R. H., Jr., Rehak, D. R., and Urzua, J., "POLO-FINITE: A Structural Mechanics System for Linear and Nonlinear Analysis," Technical Report, University of Illinois at Urbana-Champaign, and University of Kansas, Lawrence, (no date).

44. Zienkiewicz, O. C., "The Finite Element Method," 3rd Edition, McGraw-Hill, 1977.

45. Westergaard, H. M., "Stresses in Concrete Pavements Computed by Theoretical Analysis," Public Roads, Vol. 7, No. 2, April, 1926. Also in Highway Research Board, Proceedings, 5th Annual Meeting (1925 published 1926), Part I, under title "Computation of Stresses in Concrete Roads."

46. Westergaard, H. M., "Analytical Tools for Judging Results of Structural Tests of Concrete Pavements," Public Roads, Vol. 14, No. 10, December, 1933.

47. Westergaard, H. M., "Stress Concentrations in Plates Loaded over Small Areas," ASCE Transactions, Vol. 108, 1943. Also in ASCE Proceedings, Vol. 68, No. 4, April, 1942.

48. Westergaard, H. M., "New Formulas for Stresses in Concrete

Pavements of Airfields," ASCE, Transactions, Vol. 113, 1948. Also in ASCE Proceedings, Vol. 73, No. 5, May, 1947.

49. Timoshenko, S., and Woinowsky-Krieger, S., "Theory of Plates and Shells," 2nd Edition, McGraw-Hill, 1959.

50. Cheung, Y. K., and Zienkiewicz, O. C., "Plates and Tanks on Elastic Foundations: An Application of Finite Element Method," International Journal of Solids and Structures, Vol. 1, 1965.

51. Costigan, R., Unpublished Data, University of Illinois at Urbana-Champaign, 1982.

52. Pickett, G., Raville, M. E., Janes, W. C., and McCormick, F. J., "Deflections, Moments and Reactive Pressures for Concrete Pavements," Bulletin No. 65, Engineering Experiment Station, Kansas State College, October, 1951.

53. Losberg, A., "Structurally Reinforced Concrete Pavements," Doktorsavhandlingar Vid Chalmers Tekniska Hogskola, Gotesborg, Sweden, 1960.

54. Ioannides, A. M., "ILLI-SLAB Study," Vols. 1-4, University of Illinois, July, 1981.

55. Dawe, D. J., "A Finite Element Approach to Plate Vibration Problems," Journal of Mechanical of Engineering Science, Vol. 7, No. 1, 1965.

56. Przemieniecki, J. S., "Theory of Matrix Structural Analysis," McGraw-Hill, 1968.

57. Zienkiewicz, O. C., and Cheung, Y. K., "The Finite Element Method in Structural and Continuum Mechanics," McGraw-Hill, 1967.

58. Lopez, L. A., "POLO--Problem Oriented Language Organizer," Journal

of Computers and Structures, Vol. 2, 1972.

59. Rehak, D. R., and Lopez, L. A., "SCAN: A Tool for Translating Problem Oriented Languages," University of Illinois, CESL, February, 1982.

60. University of Illinois, CESL, "SCAN: User's Manual," September, 1976.

61. Ranck, F., and Barenberg, E.J., "MWELP: Multiple Wheel Elastic Layer Program," University of Illinois, November, 1972 (Unpublished).

62. SHELL OIL Co., "BISAR: Bitumen Structures Analysis in Roads, User's Manual," Koninklijke/Shell-Laboratorium, Amsterdam, Shell Research N.V., 1982.

63. Teller, L.W., and Sutherland, E.C., "The Structural Design of Concrete Pavements -- Part 5: An Experimental Study of the Westergaard Analysis of Stress Condition in Concrete Pavement Slabs of Uniform Thickness," Public Roads, Vol. 23, No. 8, April-May-June, 1943.

APPENDIX

INPUT GUIDE FOR ILLI-SLAB

(REVISED VERSION: FEB. 1983)

Finite element program ILLI-SLAB provides solution for deflections and stresses due to traffic loading in concrete pavements with joints and/or cracks. Longitudinal and transverse joints may have any one or a combination of load transfer systems such as dowel bars, aggregate interlock, and keyways. ILLI-SLAB is also capable of handling a stabilized base or an overlay, by assuming either perfect bond or no bond between the two layers. Thickness of the slab, concrete modulus of elasticity and modulus of subgrade reaction can be varied from node to node.

The concrete pavement can consist of 1, 2, 3, 4, or 6 slabs separated by one longitudinal and two transverse joints. The slabs are numbered from 1 to 6, beginning from left to right in the direction of the x-axis, and from bottom to top in the direction of the y-axis. Each slab is divided into rectangular elements of various sizes. The elements and

nodes are numbered consecutively from bottom to top along the y-axis and from left to right along the x-axis. Joints are treated as rectangular elements having zero width.

The wheel loads may be applied to any of the slabs, and stresses and deflections at all nodes in the slab, stresses in the stabilized base or overlay, vertical stresses in the subgrade, and transferred loads by the dowel bars are computed.

This revised version incorporates the facility to generate contours of stresses and deflections. Cards No. 3 and No. 24 contain relevant directions.

The program can accept either fixed-form or free-form type of input. The guide detailed below is for fixed-form input.

Card No. 0.

IFORM
I1

IFORM = A numeric flag indicating type of input data type used;
= 0, for free-form input;
= 1, for fixed-form input.

Card No. 1.

TITLE
20A4

TITLE = An 80-column label of alphameric characters used to identify the problem. This label will appear on the first page of the output.

Card No. 2.

N1X	N2X	N3X	N1Y	N2Y	NFOR	ISYM
I5	I5	I5	I5	I5	I5	I5

N1X = Number of nodes in x-direction in slabs 1 and 4.

N2X = Number of nodes in x-direction in slabs 2 and 5.

N3X = Number of nodes in x-direction in slabs 3 and 6.

N1Y = Number of nodes in y-direction in slabs 1, 2, and 3.

N2Y = Number of nodes in y-direction in slabs 4, 5, and 6.

NFOR = Number of loaded areas.

ISYM = Numeric flag indicating whether symmetry lines are used;

=0, if no symmetry lines are used;

=1, if x-axis is a line of symmetry;

=2, if y-axis is a line of symmetry;

=3, if x-axis and y-axis are lines of symmetry.

Card No. 3.

ICON(I), I=1,6	ISTEP
6I1	I4

ICON(I) = A numeric flag indicating which contour plots, if any, are desired;

ICON(1) = 1, if contours of deflection are wanted;
= 0, if not.

ICON(2) = 1, if contours of subgrade stress are wanted;
= 0, if not.

ICON(3) = 1, if contours of x-stress at bottom of Layer 1 are wanted;
= 0, if not.

ICON(4) = 1, if contours of y-stress at bottom of Layer 1 are wanted;
= 0, if not.

ICON(5) = 1, if contours of x-stress at bottom of Layer 2 are wanted;
= 0, if not.

ICON(6) = 1, if contours of y-stress at bottom of Layer 2 are wanted;
= 0, if not.

NB: ICON(5) and ICON(6) must be set to 0, if

NLAYER=1 (see Card No. 6).

ISTEP = An integer specifying the density of the Virtual Grid in the contouring routines. The value of 40 produces pleasing contours. For coarser but quicker lower the value. For smoother but longer time raise the value. ISTEP should be less than 200.

Card No. 4 (Use as many as needed).

XC(I), I=1,N1X+N2X+N3X
8F10.3

XC(I) = x-coordinate of node I.

Card No. 5 (Use as many as needed).

YC(I), I=1,N1Y+N2Y
8F10.3

YC(I) = y-coordinate of node I.

Card No. 6.

NSLAB	NLAYER	COMP	CK
I5	I5	I5	F10.3

NSLAB = Number of slabs: 1, 2, 3, 4, or 6.

NLAYER = Number of layers: 1 or 2.

COMP = Composite action factor;

= 0, if no bond exists between the slab and stabilized base or overlay;

= 1, if complete bond.

CK = Subgrade modulus, if subgrade modulus at all points is the same;

= 0.0, if not.

Card No. 7.

CT1	CE1	V(1)
F10.3	E10.3	F10.3

CT1 = Top layer thickness, if this is the same at all nodes;

= 0.0, if not.

CE1 = Modulus of Elasticity for top layer, if this is the same at all nodes;

= 0.0, if not.

V(1) = Poisson's ratio of top layer.

Card No. 8 (Read only if CT1=0.0; use as many as needed).

T1(I), I=1,((N1X+N2X+N3X)*(N1Y+N2Y))
8F10.3

T1(I) = Thickness of the top layer at node I.

Card No. 9 (Read only if CE1=0.0; use as many as needed).

E1(I), I=1,((N1X+N2X+N3X)*(N1Y+N2Y))
8F10.3

E1(I) = Modulus of Elasticity of the top layer at node I.

Card No. 10 (Read only if NLAYER=2).

CT2	CE2	V(2)
F10.3	E10.3	F10.3

CT2 = Bottom layer thickness, if this is the same at all nodes;
= 0.0, if not.

CE2 = Modulus of Elasticity for bottom layer, if this is the same at all nodes;
= 0.0, if not.

V(2) = Poisson's ratio of bottom layer.

Card No. 11 (Read only if CT2=0.0; use as many as needed).

T2(I), I=1,((N1X+N2X+N3X)*(N1Y+N2Y))
8F10.3

T2(I) = Thickness of the bottom layer at node I.

Card No. 12 (Read only if CE2=0.0; use as many as needed).

E2(I), I=1,((N1X+N2X+N3X)*(N1Y+N2Y))
8F10.3

E2(I) = Modulus of Elasticity of the bottom layer at node I.

Card No. 13 (Read only if CK=0.0; use as many as needed).

SUB(I), I=1,((N1X+N2X+N3X)*(N1Y+N2Y))
8F10.3

SUB(I) = Modulus of subgrade reaction at node I.

Card No. 14 (Read only if N2X or N3X are not equal to 0).

LTDX
I5

LTDX = Type of load transfer in x-direction;

= 0, if aggregate intelock or keyway;

= 1, if dowel bars;

= 2, if a combination of dowel bars and aggregate interlock or dowel bars and keyway.

Card No. 15 (Read only if LTDX=1 or 2).

DIN	DOUT	DE	DS	DL	DJW	DPR	DCI
F10.3	F10.3	E10.3	F10.3	F10.3	F10.3	F10.3	E10.3

DIN = Inside diameter of the dowel bars;

= 0.0 for solid round bars.

DOUT = Outside diameter of the dowel bars.

DE = Modulus of elasticity of the dowel bars.

DS = Spacing of the dowel bars.

DL = Length of the dowel bars.

DJW = Joint width.

DPR = Poisson's Ratio of the dowel bars.

DCI = Dowel-Concrete Interaction.

DCI for a round steel dowel bar may be determined from either Friberg's dowel analysis or from the relation developed based upon a three-dimensional dowel analysis:

(a) Friberg's Analysis:

```
DCI={K**0.75*D**2.5}/{0.041*D**0.75+0.0004*K**0.25*w}
```

(b) Three-dimensional Analysis:

```
DCI={E**0.75}/{(0.057-0.010*D)*(0.810+0.013*h)*(1+0.414*w)}
```

where

E = Concrete modulus of Elasticity, psi;

D = Dowel diameter, in.;

h = Slab thickness, in.;

w = Joint width, in.;

K = Modulus of dowel support, psi/in.

Card No. 16 (Read only if LTDX=0 or 2).

AGGX
E10.3

AGGX = Aggregate Intelock Factor in x-direction.
(Use a large value, eg. AGGX=1.000E+08, for keyways).

Card No. 17 (Read only if N2Y is not equal to 0).

LTDY
I5

LTDY = Type of load transfer in y-direction;

= 0, if aggregate intelock or keyway;

= 1, if dowel bars;

= 2, if a combination of dowel bars and aggregate interlock or dowel bars and keyway.

Card No. 18 (Read only if LTDY=1 or 2).

DIN	DOUT	DE	DS	DL	DJW	DPR	DCI
F10.3	F10.3	E10.3	F10.3	F10.3	F10.3	F10.3	E10.3

See Card No.15 for notations.

Card No. 19 (Read only if LTDY=0 or 2).

AGGY
E10.3

AGGY = Aggregate Intelock Factor in y-direction.
(Use a large value, eg. AGGY=1.000E+08, for keyway).

Card No. 20 (Read NFOR times).

PRS	XX1	XX2	YY1	YY2
F10.3	F10.3	F10.3	F10.3	F10.3

PRS = Tire pressure.

XX1, XX2 = Lower and upper limits of the loaded area in x-direction, in global coordinate system.

YY1, YY2 = Lower and upper limits of the loaded area in y-direction, in global coordinate system.

Note: The changes in this card are necessary after the addition of SUBROUTINE SUBAREA which generates loaded subareas with respect to specified mesh and local coordinate system.

Card No. 21.

IST	ITMAX	TOL1	TOL2	IOT
I5	I5	F5.3	F5.3	I5

IST = A numeric flag for subgrade type:

= 0, if support varies from node to node (See Card No. 22);

= 1, for VERY SOFT subgrade;

= 2, for SOFT subgrade;

= 3, for MEDIUM subgrade;

= 4, for STIFF subgrade;

= 5, for OTHER subgrade (see Card No. 23.);

= 6, for WINKLER energy consistent, uniform subgrade (not stress dependent);

= 7, for SPRINGS subgrade (not stress dependent).

Recommended values for k in first iteration:

VERY SOFT: K_R= 300 psi/in.

SOFT: K_R= 425 psi/in.

MEDIUM: K_R= 725 psi/in.

STIFF: K_R= 1000 psi/in.

OTHER: K_R= A5/DY psi/in.

ITMAX = Maximum number of iterations desired.

TOL1 = Tolerance for K_R (Recommended value= 0.05, ie.

5%)

TOL2 = Tolerance for % points exceeding TOL1 (Recommended value= 0.05, ie. 5%).

IOT = Numeric flag for output type:

= 0, for partial output during intermediate iterations.

= 1, for full output during intermediate iterations.

(Note: A new iteration is performed if the ratio of the number of nodes at which the updated K_R is more than TOL1 (%) off the previous K_R, to the total number of nodes, exceeds TOL2 (%)).

Card No. 22 (Read only if IST=0; use as many as needed)..

NST(I), I=1,((N1X+N2X+N3X)*(N1Y+N2Y))
8I5

NST(I) = Subgrade Type (IST) under node I.

Card No. 23 (Read only if IST=5).

A1	A2	A3	A4	A5	DY
F10.5	F10.5	F10.5	F10.5	F10.5	F10.5

A1, A2, A3, A4, A5, DY = Parameters for the regression equation defining K_R as as function of w, for 30" plate.

General form of the equation:

$K_R = \{A1[1-\exp\{-A2(w/DY-A3)\}]+A4(w/DY-A3)+\ldots\}/w$

$K_R = A5/DY$. if $w/DY<A3$.

where

w: deflection, in inches;

K_R: resilient subgrade modulus, in psi/in. .

Card No. 24 (Read only if contours are to be plotted).

JCON(I), I=1,6	RATIO
6I1	F10.7

JCON(I) = A numeric flag indicating over which slabs the contours requested in Card No.3, are to be plotted;

JCON(1) = 1, if contours over Slab 1 are to be plotted;
= 0, if not.

JCON(2) = 1, if contours over Slab 2 are to be plotted;
= 0, if not.

JCON(3) = 1, if contours over Slab 3 are to be plotted;
= 0, if not.

JCON(4) = 1, if contours over Slab 4 are to be plotted;
= 0, if not.

JCON(5) = 1, if contours over Slab 5 are to be plotted;
= 0, if not.

JCON(6) = 1, if contours over Slab 6 are to be plotted;
= 0, if not.

RATIO = A factor by which the y-scale is multiplied; RATIO=1.0 specifies x- and y-scales are equal.


FILM